Quality assured estimates of forest gross primary production

Integration of flux tower data and a process-based simulator

BIOME-BGC process

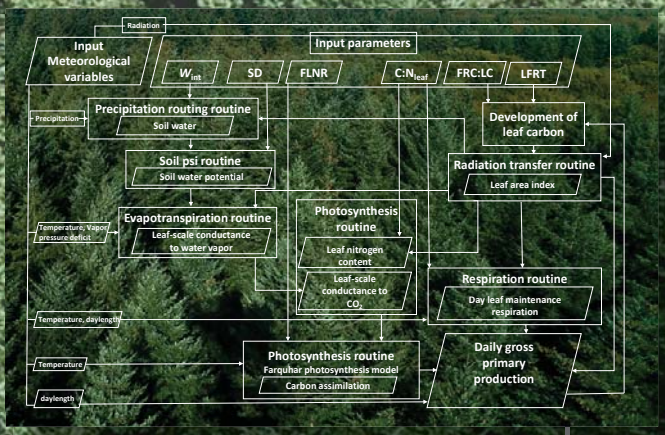

NEE = GPP - Reco

$p(\theta|z) \propto p(z|\theta)\, p(\theta)$

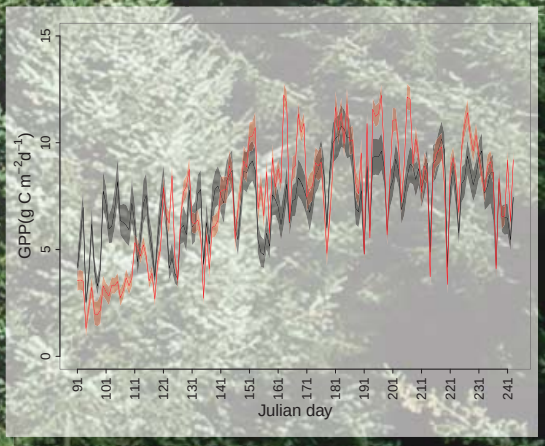

Rahul Raj

Quality assured estimates of forest gross primary production

—

Integration of flux tower data and a process-based simulator

Rahul Raj

PhD dissertation committee

Chair and Secretary	
Prof.dr.ir. A. Veldkamp	University of Twente
Promoter	
Prof.dr.ir. A. Stein	University of Twente
Co-promoters	
Dr. N.A.S. Hamm	University of Twente
Dr.ir. C. van der Tol	University of Twente
Members	
Prof.dr. P.S. Roy	University of Hyderabad
Prof.dr. W. Peters	Wageningen University
Dr. G.B.M. Heuvelink	Wageningen University
Prof.dr. A.A. Voinov	University of Twente
Prof.dr.ing. W. Verhoef	University of Twente

ITC dissertation number 293
ITC, P.O. Box 217, 7500 AA Enschede, The Netherlands

ISBN: 978–90–365–4235–7
DOI: "http://dx.doi.org/10.3990/1.9789036542357"
Printed by: ITC Printing Department, Enschede, The Netherlands

UNIVERSITY OF TWENTE.

FACULTY OF GEO-INFORMATION SCIENCE AND EARTH OBSERVATION

QUALITY ASSURED ESTIMATES OF FOREST GROSS PRIMARY PRODUCTION
—
INTEGRATION OF FLUX TOWER DATA AND A PROCESS-BASED SIMULATOR

DISSERTATION

to obtain
the degree of doctor at the University of Twente,
on the authority of the rector magnificus,
prof.dr. H. Brinksma,
on account of the decision of the graduation committee,
to be publicly defended
on Wednesday, November 9, 2016 at 16.45 hrs

by

Rahul Raj
born on April 15, 1981
in Patna, India

This dissertation is approved by:

Prof.dr.ir. A. Stein (promoter)
Dr. N.A.S. Hamm (co-promoter)
Dr.ir. C. van der Tol (co-promoter)

This dissertation is dedicated to my
father,
mother,
wife,
loving daughter, &
whole family.

Summary

Studies on terrestrial carbon sequestration are important for the exploration of opportunities to mitigate increasing atmospheric CO_2 concentration. Carbon sequestration is the process of fixing CO_2 through photosynthesis by plants and storing it as carbon in biomass. Forest ecosystems can capture and store large volumes of carbon over a long period of time. Gross primary production (GPP) is an important variable in the context of carbon sequestration as it represents the overall rate of carbon fixation. A well-established process-based simulator (PBS), BIOME-Biogeochemical cycle (BIOME-BGC), was used to simulate GPP of a forest ecosystem. Accurate simulation required reliable estimates of the input parameters. Moreover, a flux tower in a Douglas-fir stand within the Speulderbos area, the Netherlands, provided an opportunity to monitor carbon sequestration by measuring net ecosystem exchange (NEE) of CO_2 at very high temporal resolution. An estimate of GPP was obtained by partitioning it from NEE using flux partitioning model under the assumption that uncertainty in its input was well quantified. This partitioned GPP was used next in calibration (sometimes also referred to as inverse modelling), to obtain reliable estimates of the PBS parameters with reduced uncertainty. Three studies were carried out in this dissertation.

First, the uncertainties in BIOME-BGC parameters were identified based upon an extensive literature search and field inventory data. These uncertainties were defined in terms of probability distributions that included prior knowledge about the full range of parameters. This allowed us to implement a variance-based sensitivity analysis of BIOME-BGC for GPP and net primary production (NPP) output at the study site. This sensitivity analysis identified those parameters with the strongest influence on simulated GPP and NPP. Those parameters were fraction of leaf nitrogen in Rubisco, ratio of fine root carbon to leaf carbon, ratio of carbon to nitrogen in leaf and fine root, leaf and fine root turnover, water interception coefficient and soil depth. The study showed an efficient way of reducing complexity of calibrating BIOME-BGC by calibrating only the most influential input parameters. Calibration was further supported by prior knowledge of the input parameters in the form of probability distributions.

Second, GPP was separated from NEE using flux partitioning methods. I took half-hourly measurements of NEE from the flux tower and used a non-rectangular hyperbola (NRH) model to partition half-hourly GPP. The prior distribution of each NRH parameter was chosen based upon a literature

search, allowing use of a Bayesian statistical analysis to estimate partitioned GPP with the associated uncertainty from the posterior distribution. The transition from prior to posterior distributions of NRH parameters indicated a reduction in uncertainty. The obtained time series also allowed me to estimate GPP with the associated uncertainty at daily time steps. This provided relevant data for the calibration of BIOME-BGC. Furthermore, the obtained posterior distributions of NRH parameters were of interest for a range of applications such as in the study of photosynthetic nitrogen use efficiency.

Third, GPP data partitioned from flux tower measurements of NEE were used to calibrate BIOME-BGC in a Bayesian framework. The selected BIOME-BGC parameters and their prior distributions were taken from the first study. A Bayesian statistical method was used to estimate the uncertainty in the simulated GPP as well for the BIOME-BGC parameters. Uncertainty in estimated parameters was obtained as the posterior distributions. The estimated parameters, which were constant over the year, were further used to simulate daily GPP with the associated uncertainty. The results showed that the calibrated BIOME-BGC was able to simulate daily GPP that closely followed the flux tower GPP. Further, to obtain more precise GPP simulation, the possible impact of the variation in parameters was investigated by estimating the parameters at monthly time steps. Results indicated that the time varying parameters substantially improved the simulated GPP as compared to GPP obtained with constant parameters. Time varying estimation also revealed a seasonal effect in the parameters.

To summarize, this dissertation focused on obtaining forest GPP with its related accuracy using a Bayesian statistical modeling by integrating two sources: the BIOME-BGC simulator and flux tower measurements. The reduced uncertainties in the input parameters facilitated accurate simulation of GPP with their associated uncertainties. Similar integration can be applied across many forest sites around the world with different GPP characteristics, e.g., by obtaining prior information on the inputs for different tree species and by obtaining NEE data from the global databases, such as FLUXNET. In this sense, this dissertation contributed to present a complete method to obtain accurate and reliable simulations of forest GPP.

Samenvatting

Onderzoek naar de vastlegging van koolstof is een belangrijke stap richting het matigen van CO_2 toename in de atmosfeer. De vastlegging van atmosferische CO_2 gebeurt door middel van fotosynthese in planten, die de koolstof opslaan in de vorm van biomassa. Bossen kunnen grote hoeveelheden koolstof vastleggen gedurende lange periodes. De bruto primaire productie (GPP) is een belangrijke variabele in deze context: het geeft de algehele snelheid van opname van CO_2 aan. De GPP van bossen kan worden gesimuleerd met een bekend en veelgebruikt model, BIOME-Biochemical Cycle (BIOME-BGC): een model dat biochemische processen simuleert ('process-based simulator, PBS'). Voor een nauwkeurige simulatie zijn betrouwbare schattingen van de invoer variabelen en parameters nodig. Voor deze studie zijn gegevens van een fluxtoren in een douglasspar plantage in het Speulderbos op de Veluwe in Nederland gebruikt. Aan de hand van metingen van de netto opname van CO_2 (NEE) van het hele bos (inclusief bodem) met hoge temporele resolutie kon de primaire koolstofvastlegging door de bomen bepaald worden. GPP kon nauwkeurig geschat worden uit NEE met een verdeelmodel voor fluxen, onder de aanname dat de onzekerheid in de modelinvoer bekend was. De geschatte GPP is gebruikt voor kalibratie (ook wel modelinversie genoemd) van de PBS. Kalibratie van de PBS resulteert in betrouwbare schattingen van de parameters van de PBS met bijbehorende beperkte onzekerheid. Deze dissertatie bevat drie studies.

Als eerste zijn de onzekerheden in de parameters van BIOME-BGC gekwantificeerd aan de hand van een uitgebreide literatuurstudie en velddata. Deze onzekerheden zijn gedefinieerd in termen van waarschijnlijkheidsverdelingen waarin *a priori* kennis van het bereik van elke parameter is meegenomen. Hiermee kon een op varianties gebaseerde gevoeligheidsanalyse van BIOME-BGC voor GPP en de netto primaire productie (NPP) gemaakt worden. De gevoeligheidsanalyse bracht de parameters aan het licht die de grootste invloed uitoefenen op GPP en NPP, namelijk de coëfficiënten voor de fractie stikstof in Rubisco, de ratio koolstof in haarwortels: koolstof in naalden, de ratio koolstof: stikstof in naald en wortels, de snelheid van vernieuwing van naald en haarwortels, onderschepping van regenwater, en de diepte van de bodem. De studie heeft aangetoond hoe de complexiteit van BIOME-BGC verminderd kan worden door alleen de parameters te kalibreren die de meeste invloed uitoefenen. De kalibratie is verder ondersteund door *a priori* kennis in de vorm van waarschijnlijkheidsverdelingen.

Als tweede is GPP onderscheiden van NEE met behulp van flux partitiemodellen. Metingen van NEE elke 30 minuten zijn gebruikt om een niet-rechthoekige hyperbool (NRH) model te kalibreren, waarna de GPP per 30 minuten bepaald kon worden. De *a priori* verdeling van elke parameter van het NRH model is gekozen aan de hand van een literatuurstudie. Bayasiaanse statistiek is gebruikt om de GPP te schatten met bijbehorende onzekerheid uit de *posterior* verdeling van de parameters. De transitie van a priori naar posterior verdelingen van NRH ging gepaard met een afname van de onnauwkeurigheid. De verkregen tijdserie maakte het ook mogelijk om de dagelijkse som van GPP te schatten met bijbehorende onzekerheid. Deze dagelijkse som is nodig om BIOME-BGC te kalibreren (de derde studie). De gekalibreerde waardes van de parameters zijn ook van belang voor andere toepassingen, zoals het bestuderen van de efficiëntie van stikstofgebruik in fotosynthese.

Als derde zijn de GPP data uit de NEE metingen van de fluxtoren gebruikt om BIOME-BGC te kalibreren. Voor de gekozen BIOME-BGC parameters en hun *a priori* verdelingen is gebruik gemaakt van de eerste studie. Bayesiaanse statistiek is gebruikt om de onzekerheid in de gesimuleerde GPP en in de parameters van BIOME-BGC te schatten. De onzekerheid in de geschatte parameters volgde uit de *posterior* verdelingen. De geschatte parameters, die constant zijn voor de gesimuleerde periode, zijn verder gebruikt om dagelijkse GPP met bijbehorende onzekerheid te simuleren. Na kalibratie was BIOME-BGC in staat om de dagelijkse GPP van de fluxtoren te reproduceren. De mogelijke invloed van variatie van parameters in de tijd is ook gesimuleerd door de waardes van de parameters te kalibreren voor elke maand afzonderlijk. De resultaten met parameter waardes variërend in de tijd waren aanzienlijk beter dan die met constante waardes voor de parameters.

Dit proefschrift richt zich op het schatten van GPP van bos met bijbehorende onzekerheidsmarges door middel van Bayesiaanse statistiek. Twee benaderingen zijn gecombineerd: de BIOME-BGC simulator en metingen van een fluxtoren. De verminderde onzekerheid in de parameters maakte nauwkeurige simulatie van GPP mogelijk, en een kwantificering van de onzekerheid. De methode kan ook toegepast worden op bossen andere plaatsen op de wereld met een verschillende jaarlijks verloop van GPP, bijvoorbeeld door *a priori* informatie te verzamelen van de invoer voor verschillende boomsoorten en door NEE te gebruiken uit globale databestanden zoals FLUXNET. Dit proefschrift heeft bijgedragen met een complete methode voor nauwkeurige en betrouwbare simulaties van GPP van bossen.

Acknowledgements

Sometimes you don't have immediate answers to the questions that life brings for you. Sometimes you don't know the path of life you are following will lead to which direction. Sometimes the life throws you high to the sky that gives a feeling of charisma. Sometimes the life throws you back to the ground that shows the reality. Life always has some hidden agendas. For me, PhD and life are the two different names of the same thing. Besides my scientific development, a long journey of PhD made me observant, and gave me ability to recognise the patterns, I learnt somehow to see the hidden agendas of life. Pursuing PhD was both painful and enjoyable experience for me. When I found myself at the end of the journey, I realized that it would never be possible without the presence of those people, who made my journey easier during hard times with the words of encouragement, and sharpened my inner sense of expression by offering their constructive guidance. My words are, in fact, very small to express the gratitude to all those people.

First of all, I convey my sincere thanks and regards to my promoter Prof. Dr. Ir. Alfred Stein for showing trust and confidence in me when I started PhD. His thoughtful scientific ideas and words of appreciations always encouraged me to think beyond the horizons. Sometimes he pushed me a lot, but that is why I could bring my best in the stipulated time. I remember that whenever I got stuck in scientific thinking, he accelerated my thoughts in a way as if the problems were nothing. His level of dealing with problems always fascinated me. It was really an honour to work with him and I hope I worked up to his expectation.

I am deeply grateful to my first supervisor Dr. N.A.S. Hamm. I can't forget that he was that person who always encouraged me to do PhD. we had a fruitful discussion on the modelling issues and the flux tower data in India when I was working as a research fellow before joining PhD. He has been a complete pillar of support throughout my PhD journey. At every stage of my work, his countless guidance made me feel that I could achieve anything. His wide knowledge about the subject, logical way of thinking, and constructive comments on my work were of great value for me. He provided me a lot of space to think and debate even when we had a difference of opinion for specific problem. He trusted me to make an informed choice that provided a good basis to build my knowledge about the subject.

Similar, profound gratitude goes to my second supervisor Dr. Ir. Christiaan van der Tol. He is not just the kindest soul I know, but a person with

comprehensive and thorough knowledge about the subject. His input to my work was beyond the expectation. While discussing on the serious issues, I never felt that I was talking to my supervisor, it was an awesome friendly talk. Whenever he created a scientific wave in my work, it jumped to one step further. His encouraging words always brought me into the light when I was trapped by darkness.

I would like to thank the Erasmus Mundus mobility grant, and ITC, University of Twente for funding to carry out this research. My spacial thanks are given to Dr. J.-C. Domec (Department of Forestry and Environmental resources, North Carolina State University, USA) and Dr. Y.T. Mustafa (PhD alumni, University of Twente) to provide a part of data for this research. I highly appreciate all the assistant provided by the staff members of EOS department, ITC, especially Teresa Brefeld whose loving and caring attitude made my life very comfortable. I further appreciate the administrative support provided by Thereza van den Boogaard, Marie Chantal, Marion Pierik, Bettine Geerdink, John Horn, and Loes Colenbrander during my research and stay in Enschede. I also extend my gratitude to other PhD colleagues and friends who made made my life full of joy and provided me moral and scientific support throughout my PhD.

I am deeply indebted to my mother and father for their constant encouragement, love, and prayers without asking anything in return. They never asked me when I would finish my PhD, rather they always taught me "Do your best with honesty and your wish would be fulfilled". Their teaching and selfless love always motivated me to complete successfully the journey of PhD. I owe my loving thanks to my brothers, sisters, and in-laws for their immense moral support and love. Last but not least, I do not find suitable words to appreciate my wife for her understanding, care, and love during past few years. Her support and encouragement were the reason that made this thesis possible. We were blessed with little angel during my PhD. Her lovely smile was the great source of relaxation during the hard time. We dedicate our whole life to you my little angel.

Contents

List of Figures

List of Tables

Introduction 1

1.1 Carbon sequestration

The increase in atmospheric CO_2 concentration traps thermal radiation from the Earth surface and re-radiates a part back to the surface. In this way it causes the Earth surface to warm up, with the implications for global climate change. International concern about climate change has led to a series of negotiations aimed at producing a binding treaty to control worldwide emissions of CO_2. This issue has been debated widely to identify causes of warming trends in global temperature. It is uncertain whether the warming trends in temperature reflect natural variation in the Earth's climate, or whether the trend should be attributed to anthropogenic activities. The Intergovernmental Panel on Climate Change (IPCC), however, reported as a conclusion that "It is extremely likely that human influence has been the dominant cause of the observed warming since the mid-20th century" (IPCC, 2013, p. 15). Reduction in emission of CO_2 (produced excessively by anthropogenic activities) is a serious option for mitigating the risk of global climate change. Terrestrial carbon sinks play a significant role to partially offset the industrial CO_2 emission globally and they might serve as a low cost option for carbon sequestration. The effectiveness of terrestrial carbon sinks and the quantitative estimate of their strength have been reported elsewhere (Richards and Stokes, 2004; Stavins and Richards, 2005; Canadell et al., 2007; Thomson et al., 2008). If an ecosystem fixes more carbon than it emits, then this ecosystem will function as a sink of atmospheric CO_2, or carbon sink. In contrast, an ecosystem acts as carbon source when its emission exceeds its sequestration. Carbon sequestration in ecosystems involves a net uptake of CO_2 from the atmosphere for persistent storage (in the sinks) of terrestrial vegetation or soil pools. Land areas that consistently sequester carbon by growth in ecosystem production are potentially important as future sinks for industrial CO_2 emissions. Conversely, land areas that do not consistently sequester carbon over time may be adding to already increasing atmospheric CO_2 from fossil fuel burning sources.

Forests play a significant role in the global carbon cycle by controlling atmospheric CO_2 level. Functional characteristics such as carbon, nutrient, and energy fluxes are closely linked to the stand age and associated structural characteristics such as species composition, stand density, biomasses, and leaf area. As explained by Sedjo (2001), a carbon sink such as an old forest may not be capturing any new carbon but can continue to hold large volumes of carbon over long periods of time. The net rate of carbon uptake is greatest when forests are young, and slows down over time. A young forest, when growing rapidly, can sequester relatively large volumes of additional carbon that corresponds to the forests growth in biomasses. Stand age is expected to govern the magnitude and direction of the net exchange of CO_2 between forests and the atmosphere. Trees, as long-lived plants, develop large biomasses, thereby capturing large amounts of carbon over a growth cycle of several decades. Nearly 75% of the Earth's biomass is forests. Therefore, a forest ecosystems can capture and retain large volumes of carbon over long periods all over the world.

1.2 Gross primary production

Forest gross primary production (GPP) is an important variable in the context of carbon sequestration. GPP is defined as the overall rate of carbon (C) fixation or sequestration by plants via photosynthesis (Farquhar et al., 1980). The fixed available carbon is allocated to leaves, stems, roots, and reproduction and is the basic measure of biological productivity. GPP strongly controls tree growth, forage availability for grazing, food production, and fossil fuel production. In addition, GPP controls the exchange of CO_2 between land and atmosphere and thus provides the capacity of the terrestrial ecosystems, in particular forest ecosystem, to offset anthropogenic CO_2 emission (Beer et al., 2010). Accurate quantification of GPP is a central topic for carbon cycle researcher, forestry, and land and resource management. Continuous monitoring of spatial and temporal variation of GPP with high accuracy is important because: (a) their behaviour over time reflects key processes in plants and atmosphere interactions and thus improves our understanding of the feedbacks between them (Jung et al., 2008; He et al., 2014); and (b) it provides reliable data for carbon storage estimation, carbon-related climate change studies and ecosystem management (Wang et al., 2010).

1.3 Process-based simulators

Different models are available to simulate the GPP of forest ecosystems. First, regression models have been developed that are based on empirically derived statistical relationships between the biometric parameters such as height and volume of trees and production (Tatarinov and Cienciala, 2006). Second, light use efficiency (LUE) models simulate GPP as the product of the radiation flux absorbed by the plant canopy as the main driver of photosynthesis and a term accounting for the conversion efficiency of absorbed radiation into organic matter (Ruimy et al., 1994; Running et al., 2004). These regression and LUE models, however, do not incorporate changes due to forest growth, mortality, fires or other critical ecological processes. The third type of models, process-based simulators (PBS), simulate GPP development, keeping account of carbon, nutrient and water stocks. With a PBS, one could predict ecosystem activity by simulating different physiological plant responses to climatic conditions, atmospheric properties and plant structures, provided that they are well parameterized. A PBS can predict ecosystem activity at space and time scales beyond the limit of direct measurements by simulating our understanding of fundamental mechanistic ecological processes of energy and mass fluxes (Running, 1994). Several PBS have been established for the simulation of GPP, such as FOREST-BGC (Running and Gower, 1991), CASA (Potter et al., 1993), FORGFO (Mohren and van de Veen, 1995), 3-PG (Landsberg and Waring, 1997), BIOME-BGC (Thornton, 1998), TRIPLEX (Peng et al., 2002), CABALA (Mummery and Battaglia, 2004). In this dissertation, I used the BIOME-BGC (BIOME-Biogeochemical cycle) simulator. It is a widely employed PBS designed to simulate plant physiological processes and soil biogeochemistry with a very detailed scheme

and at a fine temporal scale (from daily to yearly). BIOME-BGC has been used widely by the forest research community and it has been applied to different types of forest ecosystems across the globe for the simulation of GPP (Ichii et al., 2005; Cienciala and Tatarinov, 2006; Chiesi et al., 2007; Ueyama et al., 2010; Chiesi et al., 2016).

BIOME-BGC requires site characteristics data, daily meteorological data, and ecophysiological parameters as the inputs. Site characteristics include soil texture (percentage of sand, silt, and clay), elevation, latitude, shortwave albedo, wet and dry atmospheric deposition of nitrogen, symbiotic and asymbiotic fixation of nitrogen, and effective soil rooting depth. BIOME-BGC is driven by meteorological variables to simulate the seasonal and inter-annual patterns of GPP. Meteorological variables include daily average, minimum, and maximum temperature (°C), daily total precipitation (cm), daylight average shortwave radiant flux density (W m^{-2}), daylight average vapour pressure deficit (Pa) and daylength from sunrise to sunset. BIOME-BGC generates output per square metre of a horizontally projected area on daily basis. The carbon budget simulated by BIOME-BGC includes all forest production output variables such as gross primary production (GPP), net primary production(NPP), net ecosystem production (NEP), and net ecosystem exchange (NEE). In addition, LAI, water, and nitrogen fluxes are simulated as output variables. The output of interest in this dissertation is mainly the simulated GPP, being a key variable in carbon sequestration.

1.4 Uncertainty in process-based simulators: a Bayesian approach

A PBS requires ecophysiological parameters representing a particular vegetation type. The accuracy of simulated GPP depends upon a correct parameterization of plant ecophysiology and site characteristics. The large number of input parameters explaining processes in trees, soils and the atmosphere makes the simulator complex, but the complexity provides strength to reproduce the complex dynamics of a forest ecosystem. A major challenge with the use of PBS is incomplete knowledge of input parameters, leading to uncertainty in the simulated outputs that needs to be quantified and reported in any inventory (van Oijen and Thomson, 2010; Odongo et al., 2014). Such complexity hampers parameterization and complicates the use of a PBS for assessment of GPP. Bayesian statistics provides a method for calibrating PBS (van Oijen et al., 2005; Reinds et al., 2008; Vrugt et al., 2008). The method involves quantification of uncertainties associated with input parameters used in the inventory calculation by expressing them as prior probability distributions. Observed output variables are then used to update the parameter distributions, providing updated posterior parameter distributions. In this way, the Bayesian statistical method combines probability distributions of input parameters and observed output variables to quantify uncertainty in parameters. It uses updated parameter uncertainty to perform an analysis of simulated output with the associated uncertainty.

In this dissertation, the Bayesian statistical method was used to calibrate BIOME-BGC. During calibration, output variables measured from different sources were used to update the probability distribution of input parameters. GPP could be estimated from flux tower data of the net ecosystem exchange (NEE). Therefore, estimated GPP were taken for the Bayesian calibration. The details of estimation of GPP from NEE data and Bayesian calibration are covered in the coming chapters. Below I provide a brief overview of GPP estimated from NEE data.

1.5 Estimation of GPP from flux tower data of NEE

The eddy covariance technique measures the net ecosystem exchange (NEE) of CO_2 at the flux tower installed within the forest ecosystem. NEE is the balance between CO_2 released by the ecosystem respiration (R_{eco}) and the gross CO_2 assimilated via photosynthesis. The fraction of carbon in assimilated CO_2 is the gross primary production (GPP). Therefore, GPP can be partitioned from NEE. Mathematically, NEE = GPP - R_{eco}, where the exchange of carbon into the ecosystem by means of photosynthesis is considered as a positive flux because it represents production and the loss of carbon through respiration is considered a negative flux. Flux partitioning methods are used to partition NEE into its component fluxes GPP and R_{eco} (Aubinet et al., 2012). A statistically efficient flux partitioning method relies on fitting the non-rectangular hyperbola (NRH) model to NEE data (Gilmanov et al., 2013). The NRH model includes variables that influence GPP, in particular radiation, vapor pressure deficit, and temperature. In addition, the NRH model provides a robust empirical relationship between radiation and GPP by including the degree of curvature of light response curve. The NRH model includes the separate equation for GPP and R_{eco}. The parameters of the NRH model are estimated using the NEE data, and the estimated parameters are used to obtain GPP estimates. In this dissertation, daily estimates of GPP were used in a Bayesian calibration of BIOME-BGC simulator.

1.6 Problem statement

The assessment of GPP using calibrated BIOME-BGC has been central in previous studies (Chiesi et al., 2007; Maselli et al., 2008; Imvitthaya et al., 2011; Kondo et al., 2013; Hlásny et al., 2014). In these studies, assessment of GPP was based upon the estimation of optimized input parameters for different vegetation types followed by running the BIOME-BGC for each of them. The uncertainty associated with parameters was not addressed in these studies, although it led to uncertainty in the simulated GPP. The quantification of uncertainty is important in the sense that it helps to determine how much confidence can be placed in the results of forest carbon related studies based on GPP. How to deal with parametric uncertainty using a Bayesian statistical method was addressed by van Oijen et al. (2005); Reinds et al. (2008); Vrugt et al. (2008) . This method represents the uncertainty in the parameters

(quantified by the prior belief) in terms of a probability distribution, which is updated conditional on the measured data of the simulated output. This dissertation considers the advantage of a Bayesian statistical method to estimate the BIOME-BGC input parameters with the associated uncertainty. Those were further propagated to quantify the uncertainty in the simulate GPP. In this dissertation, I have further investigated that the assumption of BIOME-BGC to treat parameters as a constant should be relaxed. This was done by estimating time varying BIOME-BGC parameters using a Bayesian statistical method over the simulation period. The effect of time varying parameters on the simulated GPP has not been investigated before, up to my best knowledge. It was expected that time varying parameters would improve the accuracy of simulated GPP as compared to GPP obtained with constant parameters.

1.7 Research objectives

The main objective of this dissertation was the accurate quantification of forest gross primary production (GPP) by integrating the output of BIOME-BGC with flux tower GPP. For the fulfilment of the main objective, the following sub objectives were achieved.

1. Quantify uncertainty in BIOME-BGC input parameters based upon literature search and field inventory data to construct prior distributions of parameters and identify the sensitivity of BIOME-BGC simulated GPP to the input parameters.
2. Partition GPP with the associated uncertainty from the flux tower measurements of net ecosystem exchange of CO_2.
3. Implement a Bayesian statistical method to integrate a flux tower GPP into BIOME-BGC to quantify the reliable estimate of parameters as a posterior distribution, and simulated GPP with the associated uncertainty, and investigate the effect of time varying BIOME-BGC parameters on the simulated GPP.

1.8 Outline of the dissertation

This dissertation is a compilation of five chapters. Besides the introduction and synthesis, three chapters are published in, or submitted to, ISI journals. Each of the three chapters is arranged as abstract, introduction, methods, results, discussion, and conclusions sections.

1. **Chapter 1** gives the general introduction of this dissertation. The importance of gross primary production (GPP) in carbon sequestration is highlighted. The role of process-based simulators, in particular BIOME-BGC, in simulating GPP and non-rectangular hyperbola model for partitioning of GPP from net ecosystem measurements are explained briefly. Research problems of the accurate quantification of simulated GPP using a Bayesian statistical method is presented. The objectives are mentioned to address the research problem.

2. **Chapter 2** provides the detailed method for quantifying the prior distribution of each BIOME-BGC parameter based on literature review and field inventory data. In this chapter, a sensitivity analysis of BIOME-BGC is presented to identify the key parameters on which simulated GPP was most sensitive. In addition, simulated net primary production (NPP) is included in the sensitivity analysis experiment. The role of key parameters on simulating GPP and NPP is also highlighted. Knowledge of prior distributions and results of sensitivity analysis is further used in chapter 4.
3. **Chapter 3** provides procedures for partitioning of GPP with the associated uncertainty from flux tower measurements of net ecosystem exchange. This chapter reviews different flux partitioning methods and a non-rectangular hyperbola model for partitioning is explained in detail. The parameters of the NRH model are estimated using a Bayesian statistical method. Therefore, the prior distribution of each NRH model parameter is obtained from a literature search. The partitioned GPP (flux tower GPP) is further used in in chapter 4.
4. **Chapter 4** provides the quantification of posterior uncertainty in BIOME-BGC input parameters and simulated GPP by integrating flux tower GPP (obtained from chapter 3) into BIOME-BGC using a Bayesian statistical method. Knowledge of prior distributions of BIOME-BGC parameters and which parameter to target in a calibration were obtained from chapter 2. Seasonality in the BIOME-BGC parameters is addressed by estimating the parameters at monthly time steps. The improvement in the accuracy of simulated GPP using time varying parameters is presented.
5. **Chapter 5** presents the synthesis of the results obtained in this dissertation. This chapter also provides the main conclusions of this dissertation and future recommendations.

2 Sensitivity analysis of process-based simulator BIOME-BGC

This chapter has been published as: Raj, R., Hamm, N. A. S., van der Tol, C., Stein, A., 2014. Variance-based sensitivity analysis of BIOME-BGC for gross and net primary production. Ecological Modelling 292, 26–36.

Abstract

Parameterization and calibration of a process-based simulator (PBS) is a major challenge when simulating gross and net primary production (GPP and NPP). The large number of parameters makes the calibration computationally expensive and is complicated by the dependence of several parameters on other parameters. Calibration can be simplified by first identifying those parameters for which GPP and NPP are most sensitive. For an appropriate application of a PBS a sensitivity analysis is an essential step. Sensitivity analysis based on local derivatives (i.e., one-at-a-time analysis) does not examine the PBS behaviour over the whole parameter space. This study therefore implements a variance-based sensitivity analysis (VBSA) addressing the full range of PBS input. A VBSA is also independent of non-linearity in a PBS. This study performs a VBSA of the process-based simulator BIOME-BGC for GPP and NPP output in a Douglas-fir stand at the Speulderbos forest site, The Netherlands. The results show that GPP and NPP are highly sensitive to the following parameters: fraction of leaf nitrogen in Rubisco, the ratio of fine root carbon to leaf carbon, the ratio of carbon to nitrogen in leaf and fine root, the leaf and fine root turnover, the water interception coefficient and soil depth. GPP and NPP are particularly sensitive to the ratio of fine root carbon to leaf carbon that is responsible for leaf area index development. The study concludes that a VBSA analysis provides a reliable and useful approach for a sensitivity analysis of process-based simulators with a complicated structure in the parameters.

Keywords: Process-based simulator, BIOME-BGC, gross and net primary production, sensitivity analysis

2.1 Introduction

Forest gross and net primary production (GPP and NPP) are crucial measures of vegetation dynamics, as they determine carbon storage and biomass. Knowledge of these carbon fluxes is indispensable for understanding the ecology of forests. GPP refers to the total photosynthesis of a stand (Farquhar et al., 1980), expressed either as moles or as mass of gross CO_2 uptake per unit of soil surface and per unit of time. A part of the energy stored through photosynthesis is lost by plant respiration, leading to the emission of CO_2. The difference between GPP and plant respiration is referred to as NPP. Their behaviour over time thus reflects key processes in soil, plants and atmosphere interactions (Jung et al., 2008). Forest play an important role in global carbon cycle by controlling atmospheric CO_2 level via the process of photosynthesis. The global database of forest carbon budget developed by Luyssaert et al. (2007) summarized the GPP and NPP across forest biomes, which shows GPP ranges from 900 to 4000 gC m^{-2} yr^{-1} and NPP from 270 to 900 gC m^{-2} yr^{-1} with the highest value and uncertainty by tropical humid evergreen forest. Verma et al. (2013) showed the variation of GPP from 1023 to 2240 gC m^{-2} yr^{-1}across biomes with the highest uncertainty of 913 and 592 gC m^{-2} yr^{-1} by evergreen broadleaf and needleleaf forest respectively. Accurate quantification of GPP and NPP is always necessary for studying the carbon cycle.

Different models are available to estimate the GPP and NPP of forest ecosystems. First, regression models are based on empirically derived statistical relationships between the biometric parameters such as height and volume of trees and production (Tatarinov and Cienciala, 2006). Second, light use efficiency (LUE) models estimate GPP as the product of the radiation flux absorbed by the plant canopy as the main driver of photosynthesis and a term accounting for the conversion efficiency of absorbed radiation into organic matter (Ruimy et al., 1994; Running et al., 2004) that is usually calibrated against flux tower measurements. Because of this calibration against actual conditions, regression and LUE models do not incorporate changes due to forest growth, mortality, fires or other critical ecological processes. The third type of models, process-based simulators (PBS), simulate these processes, keeping account of carbon, nutrient and water stocks, and simulate state variables such as LAI that would otherwise be parameters. With a PBS, one could anticipate ecosystem activity including GPP and NPP by simulating different physiological plant responses to climatic conditions, atmospheric properties and plant structures, provided that they are well parameterized.

PBS's require input parameters that describe vegetation physiological and morphological characteristics. Implementation of PBS for specific sites is difficult due to the large number of parameters for plants and soil. This difficulty arises due to the incomplete knowledge of site specific input parameters for the occurring species. Therefore, values for those parameters are often taken from the literature. Uncertainty in these inputs leads to uncertainty in the simulated production, making calibration to measured GPP and NPP necessary. Calibration of a PBS is often computationally demanding, because it includes the optimization of several input parameters.

It may not be necessary to calibrate all parameters, as some output variables may be independent of some specific parameters. Calibration can thus be simplified by first identifying the most influential parameters by means of a sensitivity analysis.

BIOME-BGC is a widely employed PBS to simulate carbon, water and nitrogen fluxes (Thornton, 1998; Thornton et al., 2002). BIOME-BGC requires 39 ecophysiological parameters, each having a different degree of influence on the simulated productivity. White et al. (2000) conducted a one-at-a-time (OAT) sensitivity analysis on BIOME-BGC for major natural temperate biomes in the USA. They tested sensitivity of simulated annual NPP to variation in parameter level of $\pm 20\%$ from the mean value. Variation in leaf and fine root C:N ratio and fraction of leaf nitrogen in Rubisco affected strongly the simulated NPP. Tatarinov and Cienciala (2006) reassessed the sensitivity as an OAT analysis of BIOME-BGC ecophysiological parameters (with $\pm 10\%$ variation from mean) to simulated NPP of major tree species in central Europe. They found that the effect of leaf C:N ratio was different for different species, whereas White et al. (2000) found that NPP decreased with increasing leaf C:N ratio for all woody biomes. The effect of the new stem carbon to new leaf carbon allocation ratio on NPP was also reported by Tatarinov and Cienciala (2006), but it was not observed by White et al. (2000). These studies suggest that results of a sensitivity analysis may vary according to specific species and region. This may also affect the choice of influencing parameters to be optimized in the calibration procedure of BIOME-BGC for specific species in different environmental and site conditions. OAT has two key limitations. First, it is a local sensitivity analysis (LSA) and it is thus only informative at the base point where it is computed and does not provide information over the rest of the input parameter space. This is contrast to a global sensitivity analysis (GSA) that quantifies the sensitivity over the whole input space and allows evaluation of interactions among the inputs (Saltelli et al., 2000). Second, it is not valid if the PBS output is non-linear or non-monotonic (Saltelli et al., 2008). BIOME-BGC, for example, shows a non-linear dependence between simulated fluxes (such as GPP) and the input parameters (Wang et al., 2001). Variance based sensitivity analysis (VBSA) is a form of GSA that quantifies the sensitivity of a model output for a given set of probability distributions over the model inputs (Saltelli et al., 2000, 2008). Such an analysis allows identification of the most influential input parameters and provides insight into the model function (Hamm et al., 2006; Saltelli et al., 2008; Odongo et al., 2013).

In this study, we applied VBSA to the simulation of GPP and NPP using BIOME-BGC for Douglas fir (*Pseudotsuga menziesii*) at the Speulderbos forest site, The Netherlands. Our objectives were to identify the sensitivity of BIOME-BGC to the input parameters and to use this knowledge to gain insight into the simulator function. This information is of value for subsequent studies concerned with the calibration of BIOME-BGC and for making decisions about which parameters to target in a field campaign.

2.2 Study area

The Speulderbos forest is located at $52^o15'08''$ N, $05^o41'25''$ E within a large forested area in the Netherlands. A flux tower is placed within a dense 2.5 ha Douglas fir stand planted in 1962. The tree density at Speulderbos varies between 765 trees ha^{-1} in the eastern part of the stand to 812 in the west, with a mean tree height of 18 m in 1989, 22 m in 1993 and approximately 30-32 m in 2006 (Steingrover and Jans, 1994; Su et al., 2009). The single-sided leaf area index (LAI) varies between 8 and 11 throughout the year. These LAI values were estimated from allometric relationships, established for different crown levels from destructive sampling in the period 1989-1994 (Steingrover and Jans, 1994). The values agreed with optical (LAI2000) estimates in 1992 after accounting for a needle-shoot ratio of 1.7 (Steingrover and Jans, 1994). The topography is slightly undulating with height variations of 10 to 20 m within distances of 1000 m. Dominant species in the neighbourhood of the Douglas fir stand are Japanese Lark (*Larix kaempferi*), Beech (*Fagus sylvatica*), Scots Pine (*Pinus sylvestris*) and Hemlock (*Tsuga spp*). At a distance of 1500 m east from the tower the forest is bordered by a large heather area. In all other directions the vegetation consists of forest for distances of several kilometres. The soil at Speulderbos is a Haplic Podzol which is well drained with textures ranging from fine sand to sandy loam consisting of ice-pushed fluviatile deposits (van Wijk et al., 2001).

2.3 Methodology

Fig. 2.1 represents the adopted methodology for the sensitivity analysis of BIOME-BGC for GPP and NPP. Details are given in the subsequent sections.

2.3.1 BIOME-BGC

BIOME-BGC simulates carbon, water and nitrogen fluxes within the vegetation, litter and soil compartment of terrestrial ecosystem with a daily time steps (Running and Hunt, 1993; Thornton et al., 2002). It was developed originally for biomes. Species are not defined explicitly, although species-specific physiological characterization are reported extensively (White et al., 2000; Hessl et al., 2004). BIOME-BGC has been used to simulate fluxes of particular species: e.g. boreal black spruce (Bond-Lamberty et al., 2005), Norway spruce, Scots pine, common beech and oak (Tatarinov and Cienciala, 2006). BIOME-BGC generates output per square metre of a horizontally projected area and can be extended to the regional scale. Maximum physical boundaries of the simulation are defined by this horizontally projected area as well as the vertical extent of the canopy and its rooting system (Trusilova et al., 2009). The carbon budget simulated by BIOME-BGC includes all forest production output variables such as gross primary production (GPP), net primary production(NPP), net ecosystem production (NEP), and net ecosystem exchange (NEE). NEP is the difference between NPP and the carbon loss by heterotrophic respiration, which is estimated as a proportion

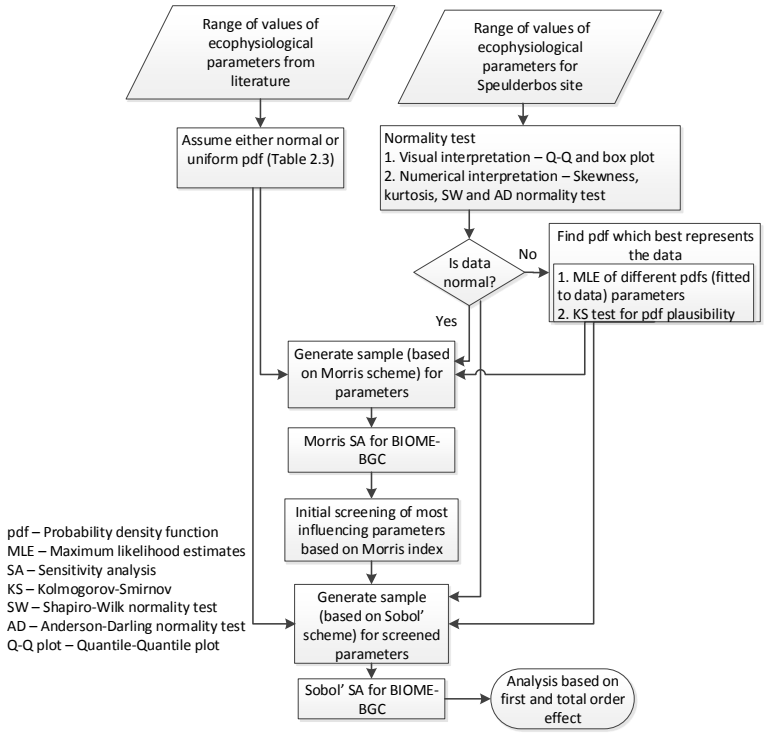

Figure 2.1 Variance based sensitivity analysis of BIOME-BGC simulated GPP and NPP to its input parameters.

of prescribed soil and litter carbon pool. NEE is the difference between NEP and the carbon loss by fire. BIOME-BGC uses the Farquhar biochemical model to estimate GPP (Farquhar et al., 1980; Thornton et al., 2002). This is estimated independently for the sunlit and shaded canopy fractions. Final GPP is the sum of these two fractions. GPP is a function of temperature, vapour pressure deficit, soil water content, solar radiation, atmospheric CO_2 concentration, LAI and leaf nitrogen concentration (Churkina and Running, 1998). Maintenance respiration is calculated as a function of leaf and root nitrogen concentration and tissue temperature. Growth respiration is the proportion of total new carbon allocated to growth. NPP is the difference between GPP and the sum of growth and maintenance respiration. There are two options for running BIOME-BGC: (1) spin-up simulation to achieve steady state condition of soil carbon and nitrogen pools under given climatic and site condition; (2) normal simulation to run BIOME-BGC using specific periods of meteorological data, CO_2 concentration and nitrogen deposition.

In this study, the spin-up simulation of BIOME-BGC version 4.2 was performed. For Speulderbos, BIOME-BGC reached the steady state condition in the maximum spin-up period of 3000 years. Normal simulation was then started with the steady state soil carbon and nitrogen pools. BIOME-BGC was run for four years (2007-2010) for Douglas fir using daily meteorological

Table 2.1 Speulderbos site characteristics. The last column indicates the values of the input data.

Parameter	Unit	Value
Effective soil depth	m	0.4 - 2
Soil sand percentage	%	94
Soil silt percentage	%	4
Soil clay percentage	%	2
Elevation	m	52
Latitude	degree	52.25225
Shortwave albedo	DIM	0.13
Wet+dry atmospheric deposition of N	kg N m^{-2} yr^{-1}	0.005
Symbiotic+asymbiotic fixation of N	kg N m^{-2} yr^{-1}	0.0001

data at Speulderbos. Douglas fir is categorized as evergreen needleleaf forest within BIOME-BGC.

2.3.2 BIOME-BGC inputs

Three groups of input data are required by BIOME-BGC, as follows:

1. *Site characteristics.* Table 2.1 gives the site characteristics used to run BIOME-BGC. Soil texture (percentage of sand, silt and clay), elevation, latitude and albedo were taken from the database of the Eagle 2006 field campaign (Su et al., 2009). Measurements of the wet and dry atmospheric deposition of nitrogen were carried out in 1995 (Simpson et al., 2006). The nitrogen input to the soil by fixation was found to be small (0.0001 kg N m^{-2} yr^{-1}) and almost constant at European forest sites (Sutton and Reis, 2011). We have fixed N-fixation at this value. The effective soil depth, hereafter referred as soil depth, defines the vegetation rooting depth and determines the maximum amount of soil water available for evapotranspiration. It affects the leaf scale conductance of CO_2 and thus GPP and NPP, by controlling the soil leaf water potential. As a result, uncertainty associated with the soil depth may produce uncertainty in the simulated GPP and NPP. Table 2.1 shows the range of soil depth at Speulderbos, which was taken from the literature (see Sect. 2.3.4). We therefore treat soil depth as an input parameter.

2. *Meteorological variables.* Daily meteorological data were collected during 2007 to 2010 from the flux tower situated in the Douglas fir plantation at Speulderbos. This includes daily observations of minimum and maximum temperature, precipitation, shortwave radiant flux density, vapour pressure deficit and daylength from sunrise to sunset. The daily observations were calculated from half hourly measurements. Meteorological variables impose the atmospheric constraint on the simulated forest productivity. Annual values (2007-2010) of ambient CO_2 concentration were also provided as an input. This was calculated as

the mean of daily ambient CO_2 concentration measured at the flux tower.

3. *Ecophysiological parameters.* The ecophysiologyof vegetation type is described by constant input parameters. Some parameters control the allocation of photosynthetically accumulated carbon to leaf, stems and root pools (White et al., 2000). Carbon to nitrogen ratio (C:N) defines the nutrient requirements for new growth, plant respiration rates and photosynthetic capacity. Water interception, canopy radiation absorption, rates and limitations of leaf conductance and the rate of carbon assimilation are controlled by several parameters. The distribution of LAI at the leaf and canopy level is controlled by three morphological parameters. Table 2.2 lists the 35 ecophysiological parameters needed to run BIOME-BGC for evergreen needleleaf forest/species.

Table 2.2 Ecophysiological parameters needed to run BIOME-BGC for evergreen needleleaf forests.

No.	Parameters	Symbol	Unit
1	Leaf and fine root turnover	LFRT	1 yr^{-1}
2	Annual live wood turnover fraction	LWT	1 yr^{-1}
3	Annual whole-plant mortality fraction	WPM	1 yr^{-1}
4	Annual fire mortality fraction	FM	1 yr^{-1}
5	new fine root C : new leaf C	FRC:LC	kg C (kg C)$^{-1}$
6	new stem C : new leaf C	SC:LC	kg C (kg C)$^{-1}$
7	new live wood C : new total wood C	LWC:TWC	kg C (kg C)$^{-1}$
8	new croot C : new stem C	CRC:SC	kg C (kg C)$^{-1}$
9	Current growth proportion	CGP	Prop.
10	C:N of leaves	$C:N_{leaf}$	kg C (kg N)$^{-1}$
11	C:N of leaf litter, after retranslocation	$C:N_{lit}$	kg C (kg N)$^{-1}$
12	C:N of fine roots	$C:N_{fr}$	kg C (kg N)$^{-1}$
13	C:N of live wood	$C:N_{lw}$	kg C (kg N)$^{-1}$
14	C:N of dead wood	$C:N_{dw}$	kg C (kg N)$^{-1}$
15	Leaf litter labile proportion	L_{lab}	%
16	Leaf litter cellulose proportion	L_{cel}	%
17	Leaf litter lignin proportion	L_{lig}	%
18	Fine root labile proportion	FR_{lab}	%
19	Fine root cellulose proportion	FR_{cel}	%
20	Fine root lignin proportion	FR_{lig}	%
21	Dead wood cellulose proportion	DW_{cel}	%
22	Dead wood lignin proportion	DW_{lig}	%
23	Canopy water interception coefficient	W_{int}	1 LAI^{-1} day^{-1}
24	Canopy light extinction coefficient	k	Unitless
25	All-sided to projected leaf area ratio	$LAI_{all:proj}$	LAI LAI^{-1}
26	Canopy average specific leaf area	SLA	m^2 (kg C)$^{-1}$
27	Ratio of shaded SLA:sunlit SLA	$SLA_{shd:sun}$	SLA SLA^{-1}
28	Fraction of leaf N in Rubisco	FLNR	Unitless
29	Maximum stomatal conductance	g_{smax}	m s^{-1}
30	Cuticular conductance	g_{cut}	m s^{-1}
31	Boundary layer conductance	g_{bl}	m s^{-1}
32	Leaf water potential: start of conductance reduction	LWP_i	Mpa
33	Leaf water potential: complete conductance reduction	LWP_f	Mpa
34	Vapor pressure deficit: start of conductance reduction	VPD_i	Pa
35	Vapor pressure deficit: complete conductance reduction	VPD_f	Pa

2.3.3 Theory of variance-based sensitivity analysis (VBSA)

An output Y of a simulator can be written as a function of its input parameters $\mathbf{X}$

$$Y = f(\mathbf{X}) = f(X_1, X_2, ..., X_n) \tag{2.1}$$

where each input parameter X_i (i=1,2,...,n) has a range of variation showing its uncertainty. The uncertainty in a given output can be expressed as the unconditional variance, V_Y. VBSA aims at decomposition of this uncertainty into components which can be attributed to each input X_i. V_Y is:

$$V_Y = \sum_i V_i + \sum_i \sum_{j>i} V_{ij} + \sum_i \sum_{j>i} \sum_{k>j} V_{ijk}..... + V_{1,2,.....,n} \tag{2.2}$$

where

$$V_i = V[E(\,Y|X_i = x_i^*)]. \tag{2.3}$$

$$V_{ij} = V[E(\,Y|X_i = x_i^*, X_j = x_j^*)] - V_i - V_j. \tag{2.4}$$

$$V_{ijk} = V[E(\,Y|X_i = x_i^*, X_j = x_j^*, X_k = x_k^*)] - V_i - V_j - V_k. \tag{2.5}$$

V_i is the variance of the conditional expectation (VCE) of Y given that the i^{th} input X_i has a fixed value x_i^*. V_{ij} is the VCE of Y given that i^{th} input X_i has a fixed value x_i^* and j^{th} input X_j has a fixed value x_j^*. V_{ijk} is the VCE of Y given that the inputs X_i, X_j, and X_k have fixed value x_i^*, x_j^*, and x_k^* respectively.

The first order sensitivity index, S_i, for X_i is given as,

$$S_i = \frac{V_i}{V_Y}. \tag{2.6}$$

where S_i is the main effect of X_i on V_Y. This quantifies the effect of varying X_i alone, but averaged over variation in other input parameters. The value of S_i is between 0 and 1. A high value signals an important input parameter. The second and third order sensitivity indices are obtained by dividing Eqs. 2.4 and 2.5 by V_Y respectively. The second order index quantifies the effect of interaction between pairs of input parameters on Y. The third order index quantifies the effect of interaction between the combinations of three input parameters on Y.

The total effect sensitivity index was introduced by Homma and Saltelli (1996):

$$S_{iT} = 1 - \frac{V[E(\,Y|X_{-i} = x_{-i}^*)]}{V_Y}. \tag{2.7}$$

where X_{-i} denotes all of the input parameters other than X_i. S_{iT} denotes the total effect of X_i, which includes the fraction of variance accounted for X_i alone and the fraction accounted by any combination of X_i with the remaining parameters. Input parameters with small first order indices but high total effect sensitivity indices affect the simulator output Y mainly through interactions. This study calculated only first and total order indices. The VBSA approach requires $N \times (2n + 2)$ executions of the simulator to compute the S_i and S_{iT} (Eqs. 2.6 and 2.7), where N is a base sample (see Sect. 2.4.2).

We used the method of Sobol' (1993) to calculate sensitivity indices. This provides a numerically efficient Monte Carlo sampling scheme for the calculation of first and total order indices. For example, $V[E(Y|X_i = x_i^*)]$ is calculated by using a set of Monte Carlo points to estimate the expectation for a fixed value of X_i and this procedure is repeated many times for different X_i values to estimate the variance. A brief description is provided by Hamm et al. (2006) with more detail provided by Saltelli et al. (2008).

2.3.4 Sensitivity analysis on BIOME-BGC

We considered initially 29 ecophysiological parameters (discussed further in this section) out of 35 (Table 2.2) as well as the soil depth for the sensitivity analysis. The large number of ecophysiological parameters makes VBSA computationally expensive. A common approach is to screen first the most influential parameters using the Morris method (Saltelli et al., 2008) and then considering only screened parameters in VBSA by fixing other input parameters in advance. Morris method belongs to the class of one-at-a-time sensitivity analysis, which requires few hundred runs (Sect. 2.3.4.2) compared to several thousand for VBSA (Sect. 2.4.2). The detailed explanation of the Morris method is provided in Appendix C. We used the Morris method to identify a short list of ecophysiological parameters that were influential for GPP and NPP. These parameters were then included in VBSA. The input sample space, for both Morris and VBSA, came from the knowledge of uncertainty in the simulator inputs. These are characterized by probability distribution functions (pdf). Hence acquiring the pdf for each input parameter is the first step for both Morris and VBSA. In this study, we defined the pdf of each ecophysiological parameters and the soil depth. Note that two meanings of the word "parameter" are used in this study. Soil depth and the ecophysiological parameters are the BIOME-BGC *input parameters*. The term *pdf parameters* indicates the parameters of the pdf of each input parameter. For example, if an input parameter follows the normal distribution, the mean and standard deviation are the pdf parameters.

2.3.4.1 Uncertainty in BIOME-BGC input parameters

We compiled information on uncertainty in each input parameter (Table 2.3) for Douglas fir, which is a type of evergreen needleleaf forest. Variability of seven input parameters C:N_{leaf}, C:N_{lit}, W_{int}, k, FLNR, g_{smax} and g_{bl} were obtained from the Douglas fir data at the Speulderbos site (Appendix A).

Variability of SLA was obtained from data provided by Dr. J.-C. Domec from the Department of Forestry and Environmental resources, North Carolina State University, USA, which were collected for 36-year old Douglas firs at the H.J. Andrews Experimental Forest within the Willamette national forest (Domec et al., 2012). We further used the variability of SLA to obtain the variability of fraction of leaf N in Rubisco (FLNR) at the Speulderbos site using Eq. A2.3. Variability of other input parameters was taken from White et al. (2000) and the United States department of Agriculture database (Hessl et al., 2004). The references cited in White et al. (2000) and Hessl et al. (2004) were also used. Other literature was also used to identify the variability of the input parameters (Table 2.3), which was obtained using a Web of Science search with keywords: Speulderbos, Douglas fir, *Pseudotsuga menziesii*, and individual input parameter names. The results obtained from via the literature search are provided in Appendix B. If variability of a particular input parameter was not available, we used either the variability for evergreen needleleaf forest or that for the relevant biome reported by White et al. (2000). The following procedures were followed to define the pdf of each input parameter.

(A) A normality test was conducted for seven input parameters calculated for the Douglas fir at Speulderbos (Appendix A) and for SLA. This test was supported by visual examination of the quantile-quantile (Q-Q) and box plot and quantitative interpretation using the calculation of skewness and kurtosis. Those input parameters were assumed to follow a normal distribution if both visual and quantitative evaluation supported it. If this was not the case, an assessment was made to define the family of pdf which best represented the data. Maximum likelihood estimates (MLE) were used to estimate the pdf parameters. The plausibility of the normal pdf was tested by the Shapiro-Wilk (SW) and Anderson-Darling (AD) normality tests. Whereas the plausibility of other pdfs were tested by the Kolmogornov-Smirnov (KS) goodness-of-fit test.

(B) Tiktak and Bouten (1990) suggested the extrapolation of Douglas fir root length to a depth of 2 m at Speulderbos. Tiktak and Bouten (1994) reported that almost 90% of the Douglas fir root length is situated in the top soil to a depth of 0.4 m. The root biomass distribution was also found to a depth of 1.3 m (Reyer et al., 2010). Hence, we had only three values for soil depth variability, which were not sufficient to fit the pdf. Therefore, we used uniform distribution with a minimum value at 0.4 m and a maximum value at 2 m.

(C) For some input parameters, we obtained information on the mean (μ) and standard deviation (σ) from the literature. However, the family of the pdf was not defined. A normal pdf was assumed for these input parameters. Where more than one citation of μ and σ was available for a input parameter, we chose the one with largest σ.

(D) For some input parameters only single values were reported. Therefore, a uniform pdf was assumed between the minimum and maximum values reported in the literature.

(E) A uniform pdf was assumed for those input parameters, which were taken from White et al. (2000) and for which only a single biome specific value was reported. The maximum and minimum limit of the uniform pdf was obtained by varying reported single value by ±50%. These limits were selected because values larger than ±50% made the minimum limit of the biome specific input parameters close to zero or negative, which is unacceptable. The value of 0.7 was reported for the biome specific annual live wood turnover fraction (LWT) parameter. The variation of ±50% makes the maximum limit of LWT greater than 1, which should not be the case because the maximum value of LWT can only be 1 (that means all woods are replaced annually). Therefore, the variation of ±25% was chosen for LWT.

The column "Procedure" in Table 2.3 indicates which of A to E was adopted for each input parameter. The details of pdf selection of each input parameter is provided in Appendix B.

Five input parameters (C:N_{lw}, L_{lab}, FR_{lab}, D_{cel}, and g_{cut}) were calculated from other input parameters (Table 2.3) as suggested by White et al. (2000). Therefore these were not included in the sensitivity analysis. In recent years there is no evidence of fire at Speulderbos. The fire mortality parameter was therefore set to zero (FM=0). However, fire would be expected during the spin-up period of 3000 years (Thornton and Rosenbloom, 2005). Since there is no possibility to separate the spin-up and normal (4-year) simulation, a check was performed to evaluate whether changing the FM parameter would affect the experimental results. The simulations were therefore re-run with FM=0.005 (the default value for evergreen needleleaf forest). This led to a change of less than 1% in the simulated GPP and NPP values and did not lead to any change in the interpretation of the experimental results. FM is therefore not included in the sensitivity analysis. Therefore, 30 input parameters (29 ecophysiological parameters and the soil depth) were considered in the Morris method.

2.3.4.2 Implementation of sensitivity analysis on BIOME-BGC

The Morris method operates on p level of quantile of distribution and r number of calculation of elementary effects (Appendix C). The number of simulator executions is $r \times (n+1)$ for n input parameters. The choice of $p = 4$ and $r = 10$ followed Saltelli et al. (2008). This resulted in 310 ($r \times (n+1)$) BIOME-BGC executions to calculate the Morris index, $\mu_i, i = 1, 2.., n$ (Eq. C2.2) for 30 input parameters, a number that is substantially less than that ($N \times (2n+2)$) required by the Sobol' approach. The number of BIOME-BGC executions for VBSA is given in the result Sect. 2.4.2.

The sample space of the input parameters, for both Morris and VBSA, was generated in SIMLAB version 2.2 (Saltelli et al., 2008) using defined pdfs (Table 2.3). The result was then exported from SIMLAB and reformatted to allow sequential simulator executions of BIOME-BGC version 4.2 on a Windows 7 system. For each input parameter vector, the BIOME-BGC was run for four years (2007-2010) to simulate daily value of GPP and NPP. The annual mean GPP and NPP for each year was then calculated by the

Table 2.3 Distribution of BIOME-BGC input parameters for Douglas-fir. The first column shows the symbol of input parameters as given in Table 2.2. The input parameters highlighted in bold were included in the variance-based sensitivity analysis experiment. Procedure indicates the procedure A to E used to obtain probability density function (pdf). See Sect. 2.3.4.1 for details. ENF - Evergreen needleleaf forest.

Douglas-fir				
Parameter	Source	Procedure	pdf	Distribution
LFRT	White et al. (2000); Hessl et al. (2004)	D	Uniform	α = 0.196 , β = 0.5
FM	Set to zero for Speulderbos site			
FRC:LC	White et al. (2000); Hessl et al. (2004)	D	Uniform	α = 0.78 , β = 3.5
SC:LC	White et al. (2000); Hessl et al. (2004)	D	Uniform	α = 0.96 , β = 5.32
CRC:SC	White et al. (2000); Hessl et al. (2004)	D	Uniform	α = 0.151 , β = 0.472
$C{:}N_{leaf}$	Speulderbos site data	A	Normal	μ = 26.7 , σ = 3.731
$C{:}N_{lit}$	Speulderbos site data (Portillo-Estrada et al., 2013)	A	Normal	μ = 31.625 , σ = 3.27
$C{:}N_{fr}$	Hobbie et al. (2010)	C	Normal	μ = 54.8 , σ = 11.628
$C{:}N_{lw}$	assigned equal to $C{:}N_{fr}$			
$C{:}N_{dw}$	White et al. (2000); Hessl et al. (2004)	D	Uniform	α = 667 , β = 1314
L_{lab}	1-(L_{cel} + L_{lig})			
L_{cel}	Harmon et al. (1990)	C	Noraml	μ = 0.201 , σ = 0.01
L_{lig}	Harmon et al. (1990)	C	Noraml	μ = 0.155 , σ = 0.012
DW_{cel}	1-DW_{lig}			
DW_{lig}	Edmonds (1987)	C	Normal	μ = 0.228 , σ = 0.004
W_{int}	Speulderbos site data(Klaassen et al., 1998)	A	Normal	μ = 0.04 , σ = 0.02
k	Speulderbos site data (Mustafa, 2012)	A	Normal	μ = 0.453 , σ = 0.071
SLA	Domec et al. (2012)	A	Normal	μ = 14.65 , σ = 1.94
FLNR	Speulderbos site data (Dekker, 2000; Domec et al., 2012; White et al., 2000)	A	Beta	α= 25.64 , β= 756.28
g_{smax}	Speulderbos site data (van Wijk et al., 2000)	A	Normal	μ = 0.0051 , σ = 0.0009
g_{cut}	assigned 1/100th of g_{smax}			
g_{bl}	Speulderbos site data (Duyzer et al., 2004; Nobel, 2009)	A	Log-normal	μ = -2.604 , σ = 0.164
ENF				
LWC:TWC	White et al. (2000)	D	Uniform	α= 0.056 , β= 0.1
CGP	White et al. (2000)	E	Uniform	α= 0.25 , β= 0.75
FR_{lab}	1-(FR_{cel} + FR_{lig})			
FR_{cel}	White et al. (2000)	D	Uniform	α= 0.378 , β= 0.495
FR_{lig}	White et al. (2000)	D	Uniform	α= 0.095 , β= 0.361
$LAI_{all:proj}$	White et al. (2000)	D	Uniform	α= 2.3 , β= 3.14
LWP_i	White et al. (2000)	D	Uniform	α= -1.0 , β= -0.2
LWP_f	White et al. (2000)	D	Uniform	α= -5.0 , β= -1.4
VPD_i	White et al. (2000)	D	Uniform	α= 500 , β= 1000
VPD_f	White et al. (2000)	D	Uniform	α= 2000 , β= 6000
BIOME				
LWT	White et al. (2000)	E	Uniform	α= 0.525 , β= 0.875
WPM	White et al. (2000)	E	Uniform	α=0.0025 , β=0.0075
$SLA_{shd:sun}$	White et al. (2000)	E	Uniform	α=1 , β=3
Site characteristic				
Soil Depth		B	Unifrom	α=0.4 , β=4

mean of daily simulated GPP and NPP respectively. These outputs were then arranged in a suitable format to read back into SIMLAB to calculate the sensitivity indices (Eqs. C2.2, 2.6, and 2.7). Each simulated output resulted in four values of each sensitivity index for each input parameter. Input parameters were initially short listed for GPP and NPP based on the Morrix index μ_i. A very low threshold value of $\mu_i = 0.05$ was chosen for both GPP and NPP. Input parameters with $\mu_i \leq 0.05$ were considered to have negligible influence on GPP and NPP. This threshold was low enough in comparison to the most influential input parameters to justify exclusion from VBSA (Figs. C2.1 and C2.2). The choice of value 0.05 is in line with the choice of those suggested by Saltelli et al. (2008). Eight input parameters for GPP and ten for NPP had a Morris index μ_i below 0.05 for any simulated year (Figs. C2.1 and C2.2). The eight parameters that did not meet the low threshold for both GPP and NPP were excluded from the VBSA analysis, and fixed at their mean values. The remaining 22 parameters, highlighted in bold in Table 2.3, were included in the VBSA analysis.

BIOME-BGC imposes the condition that the $C:N_{lit}$ should always be greater than $C:N_{leaf}$. Morris and VBSA sampling may violate this condition. Therefore, if the $C:N_{lit}$ was found smaller than $C:N_{leaf}$ in any input parameter vector, the $C:N_{leaf}$ was assigned to $C:N_{lit}$.

2.3.4.3 Fine root carbon to leaf carbon (FRC:LC)

White et al. (2000) reported that the leaf area index (LAI) development in BIOME-BGC is photosynthetically limited by the fine root carbon consumption. This consumption is controlled by the FRC:LC parameter. Higher value of FRC:LC may produce plants with no LAI development and in turn no production. For sensitivity analysis, we assumed the uniform distribution on FRC:LC (point D of Sect. 2.3.4) for Douglas fir with lower and upper bound both taken from White et al. (2000) and Hessl et al. (2004). The lower bound was fixed at 0.78; however, a reasonable selection of upper bound for the Douglas fir at the Speulderbos site is required in view of LAI development with FRC:LC. This choice was made by the following steps.

1. Three values of FRC:LC (i.e., 6.85, 3.5 and 2.16) were selected as possible upper bound values from White et al. (2000) and Hessl et al. (2004).

2. BIOME-BGC was simulated for four years (2007-2010) for each FRC:LC value with other parameters fixed at their mean value. LAI did not develop for any year of simulation with FRC:LC = 6.85. This simulated Speulderbos with no production. Development of LAI was observed with FRC:LC value at 2.16 and 3.5. The value of 3.5 comes from a study site with loamy sand soil derived from a glacial outwash (Keyes and Grier, 1981; Hessl et al., 2004). This soil type is similar to that of Speulderbos (i.e., sandy loam consisting of ice-pushed fluviatile deposits) (van Wijk et al., 2001). In the view of LAI development and the soil type, the upper bound of FRC:LC at 3.5 was selected.

Seven values (excluding 6.85) of FRC:LC for Douglas fir were reported by White et al. (2000) and Hessl et al. (2004) with 50 % taking values less than 1 and 50 % taking values higher than 1. The distribution of FRC:LC should reflect this ratio as we are relying on the literature for FRC:LC. We therefore sampled from the uniform distribution between $\log_{10}0.78$ and $\log_{10}3.5$ and back transformed the values before running BIOME-BGC. This ensured a reasonable spread of values less than and greater than 1. Our results showed that LAI development was very sensitive to the FRC:LC value. Therefore, we also investigated the influence of changing the upper bound $\log_{10}3.5$ to $\log_{10}2.16$ on GPP and NPP in the VBSA experiment.The Morris experiment was conducted only with the uniform distribution of FRC:LC with upper bound at $\log_{10}3.5$.

2.4 Results

2.4.1 Uncertainty in simulated GPP and NPP

We first examined the uncertainty in the simulator output that arises due to the uncertainty in the input, as obtained from VBSA. The uncertainty in the output is summarized by histograms and summary statistics. Because the uncertainty appeared similar for all years, we present histograms (Figs. 2.2a and 2.2b)) and summary statistics for 2007 only (Table 2.4). The ranges of GPP and NPP were approximately 0-9 (Fig. 2.2a) and 0-4 (not shown) g C m^{-2} d^{-1} respectively. In a small proportion (2342 out of 47104 simulations), both GPP (Fig. 2.2a) and NPP (not shown) were zero, indicating that the forest had diminished during the spin-up of the simulator. The combination of parameter values that cause this, represent an unsustainable forest. A closer inspection revealed that this simulator behaviour can be attributed to the allocation parameter FRC:LC. The number of these cases dropped to 761 when the upper bound of of FRC:LC from $\log_{10}3.5$ to $\log_{10}2.16$, but this did not affect the range of GPP (Fig. 2.2b) and NPP (not shown) for all simulations.

The range of GPP (0-9 g C m^{-2} d^{-1}) obtained in this research are comparable to previous research undertaken at Speulderbos from 2002 to 2006 (Marcelis, 2011). The results of sensitivity analysis experiments presented here can, therefore, be considered realistic.

Table 2.4 Summary statistics of BIOME-BGC simulated annual mean GPP and NPP (g C m^{-2} d^{-1}) for 2007.

	FRC:LC $\sim$ U($\log_{10}0.78$,$\log_{10}3.5$)		FRC:LC $\sim$ U($\log_{10}0.78$,$\log_{10}2.16$)	
	GPP 2007	NPP 2007	GPP 2007	NPP 2007
5^{th} percentile	0.00	0.00	2.30	0.95
25^{th} percentile	3.57	1.36	3.98	1.55
Mean	4.31	1.73	4.71	1.93
Median	4.53	1.78	4.78	1.93
75^{th} percentile	5.39	2.20	5.59	2.34
95^{th} percentile	6.68	2.84	6.86	2.94
Standard deviation	1.70	0.73	1.43	0.63

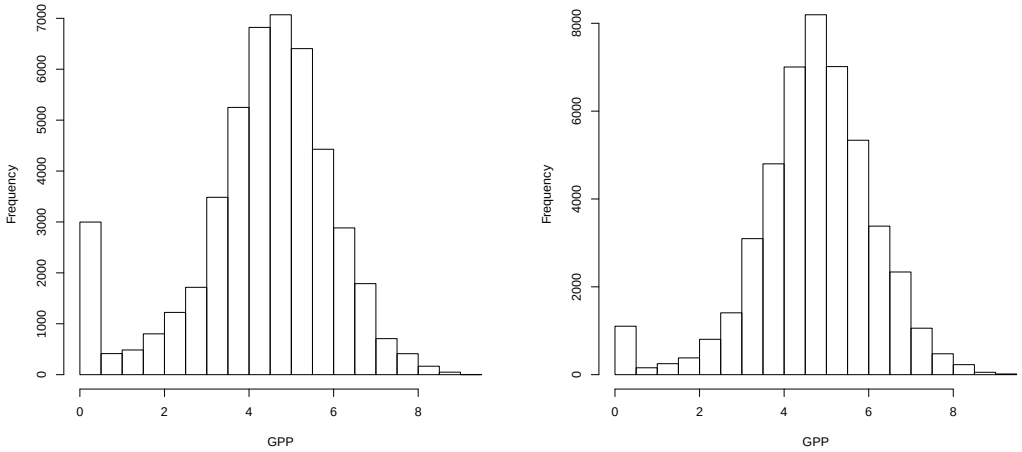

a FRC:LC $\sim$ U($\log_{10}0.78$, $\log_{10}3.5$) **b** FRC:LC $\sim$ U($\log_{10}0.78$, $\log_{10}2.16$)

Figure 2.2 Histograms of annual mean simulated GPP (g C m^{-2} d^{-1}) for year 2007 for two different distributions of FRC:LC.

2.4.2 Variance-based sensitivity analysis (VBSA)

We selected the number of BIOME-BGC iterations for VBSA based on the convergence of the first and total order sensitivity indices (Saltelli et al., 2008). We conducted preliminary VBSA experiments to test for convergence for the base sample N = 256, 512, 1024, and 2048. Because similar results were obtained for N=1024 and N=2048, N was fixed 1024, resulting in 47104 ($N \times (2n + 2)$) BIOME-BGC iterations for $n = 22$ (number of screened input parameters based on Morris method) for all subsequent experiments. The first and total order indices (S_i and S_{iT}) for an upper bound of FRC:LC = $\log_{10}3.5$ and $\log_{10}2.16$ are shown in Figs. 2.3 and 2.4. Those input parameters are not shown, whose both S_i and S_{iT} were approximately equal to zero.

GPP and NPP are consistently most sensitive to FLNR. This is apparent from the first order index. The total order indices show that GPP and NPP are highly sensitive to FLNR through interaction with other input parameters within BIOME-BGC. The second most influential parameter is FRC:LC, controlling GPP and NPP either directly or through interaction. LFRT influences GPP much more than NPP ($S_i < 0.05$) through interactions. The carbon to nitrogen ratios C:N_{leaf} and C:N_{fr} affected GPP and NPP through interaction rather than directly. SC:LC strongly influences GPP and NPP only through interactions. A considerable influence of W_{int} was observed on GPP and NPP. The first order and interaction effects of soil depth are similar for GPP and NPP. All other input parameters exhibited small (S_i and $S_{iT} < 0.05$) or negligible (S_i and $S_{iT} \approx 0$) main and interaction effect on GPP and NPP for any year of simulation.

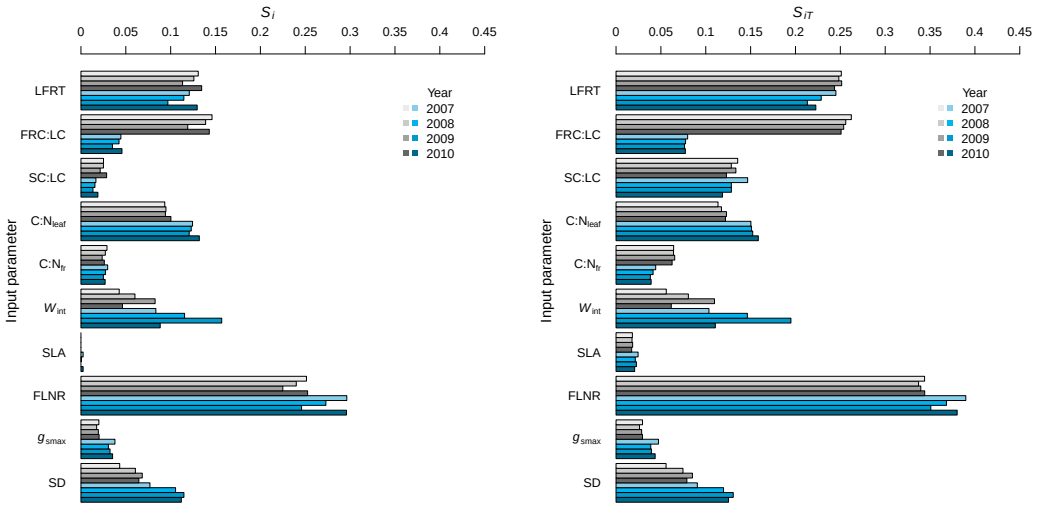

a Sobol' first order index S_i **b** Sobol' total order index S_{iT}

Figure 2.3 Sobol' indices for annual mean GPP for FRC:LC $\sim$ U($\log_{10}0.78$, $\log_{10}3.5$) (grey) and FRC:LC $\sim$ U($\log_{10}0.78$, $\log_{10}2.16$) (blue). Symbols in y-axis indicate the ecophysiological parameters given in Table 2.2. SD is soil depth.

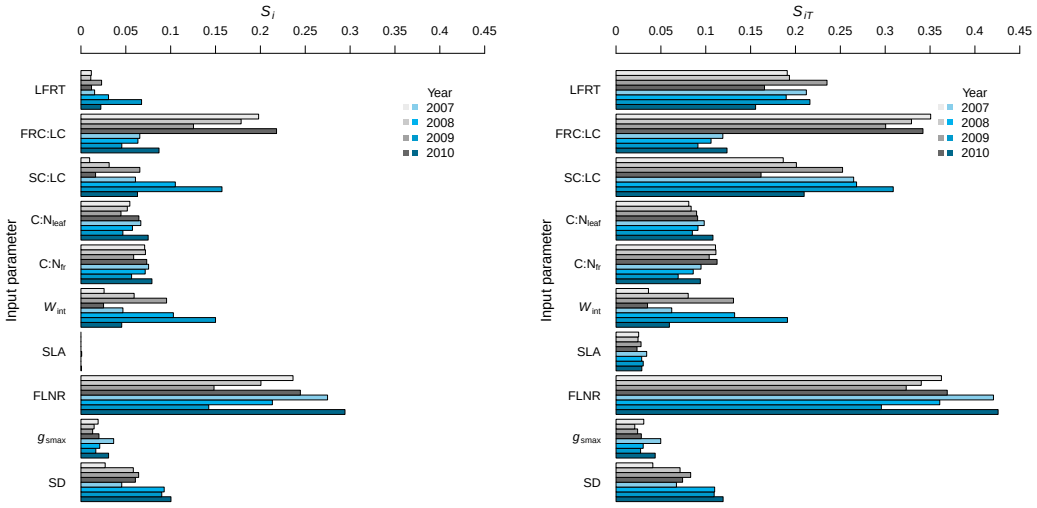

a Sobol' first order index S_i **b** Sobol' total order index S_{iT}

Figure 2.4 Sobol' indices for annual mean NPP for FRC:LC $\sim$ U($\log_{10}0.78$, $\log_{10}3.5$) (grey) and FRC:LC $\sim$ U($\log_{10}0.78$, $\log_{10}2.16$) (blue). Other details as for Fig. 2.3.

Decreasing the upper limit of FRC:LC from 3.5 to 2.16 reduces the sensitivity of GPP and NPP to FRC:LC both directly and through interactions, and increases the sensitivity indices of all other input parameters. This increase in sensitivity to the other input parameters is nearly proportional, such that the ranking of these input parameters in terms of sensitivity remains unchanged. For example, the dominance of FLNR remains after decreasing the upper limit of FRC:LC.

2.5 Discussion

2.5.1 Identification of uncertainty in input parameters

Although the use of site specific input parameter values is recommended (Thornton, 1998; Thornton et al., 2002), it is tedious and difficult to obtain site specific probability density functions of parameter values for two reasons: (1) the large number of input parameters, and (2) the fact that input parameters, in particular those related to allocation, are not directly observable. We obtained the distribution of site-specific values of seven ecophysiological parameters and the soil depth from data of earlier studies at the Speulderbos site. Reported measurements of leaf area index (LAI), although not an input parameter of BIOME-BGC, supported the estimation of several ecophysiological parameters (Appendix A).

2.5.2 Variance-based sensitivity analysis (VBSA)

The results of VBSA showed the highest direct influence, as indicated by the S_i, of FLNR on GPP and NPP. The FLNR parameter controls the carboxylation capacity V_{cmax}), which is the first step to fixation of atmospheric CO_2 by the ribulose-1,5-biphosphate protein. In BIOME-BGC, V_{cmax} is a state variable rather than a parameter. The significance of V_{cmax} has been recognized since its introduction (Farquhar et al., 1980), since it is an influential parameter with high spatial variability that is difficult to obtain (Houborg et al., 2012). It is therefore not surprising that FLNR exerts the strongest influence on GPP and NPP. The carbon to nitrogen ratio of leaves ($C:N_{leaf}$) also influences the GPP and NPP directly for the same reason: the fact that $C:N_{leaf}$ controls the nitrogen content of the sunlit and shaded leaf, which is further used in BIOME-BGC to estimate V_{cmax}. Our results indicate that only NPP is sensitive to carbon to nitrogen ratio of fine roots ($C:N_{fr}$). The relatively high sensitivity of NPP to this ratio is explained by the fact that it affects the allocation of nitrogen to roots and shoot, and hence the respiration flux (White et al., 2000). One would also expect a sensitivity of GPP, because GPP depends on the allocation of nitrogen to shoots. Our results do not show this sensitivity. Our results suggest that $C:N_{leaf}$ is the only parameter used to calculate leaf nitrogen content.

Direct influence of LFRT is observed on GPP, and an effect through interaction on NPP. The LFRT is calculated as the inverse of the leaf longevity (White et al., 2000). In their study of various tree species, Reich

et al. (1999) found that the leaf longevity is (weakly) inversely related to the net photosynthetic capacity. For BIOME-BGC this would imply a positive correlation between FLNR and LFRT. Quantification of this (and possibly other) correlation(s) between parameters could potentially constrain the simulator output to more realistic ranges for vegetation traits.

The input parameter W_{int} determines the amount of precipitation intercepted by the canopy, which in turns controls the amount of precipitation infiltrating. The soil depth (SD) determines the volumetric water content in the soil as implemented in the BIOME-BGC code. Our results indicate that GPP and NPP are highly affected by these two parameters through the soil water content.

The allocation parameters in BIOME-BGC are used to allocate total assimilated carbon to different parts of the plant. The allocation parameters therefore have an indirect effect on GPP, mainly through the evolution of LAI. Our results revealed the influence of fine root carbon to leaf carbon (FRC:LC) is strong (second after FLNR when the upper limit was set to 3.5), probably due to the unrealistic values of zero GPP and NPP after the forest had disappeared. The first order sensitivity reduced substantially when the upper limit was reduced to 2.16 ($<$0.05), although the total order index (S_{iT}) remained high for GPP. The histograms of GPP and NPP also indicate the importance of FRC:LC, where a decrease in the upper bound of FRC:LC decreases the number of simulations of BIOME-BGC with zero GPP and NPP. A careful selection of the value for FRC:LC is therefore required to avoid unrealistic simulations. Unfortunately, the exact role of FRC:LC in BIOME-BGC for carbon assimilation is not clearly documented and it is necessary to infer its role through sensitivity analysis or by scrutinizing the simulator code.

Previous one-at-a-time (OAT) sensitivity analyses of BIOME-BGC for NPP (White et al., 2000; Tatarinov and Cienciala, 2006) of evergreen needleleaf forest/species also highlighted the influence of FLNR, C:N_{leaf}, C:N_{fr}, LFRT and FRC:LC. This indicates that these parameters are consistently influential, independent of site or the type of sensitivity analysis.

A high interaction effect of the FLNR, LFRT, C:N_{leaf}, C:N_{fr}, W_{int}, and SD was observed in addition to their main or direct effect. The stem carbon to leaf carbon (SC:LC), showed a high interaction, but no first order effect. Further insight might be obtained by computing second and third order sensitivity indices, although this lay outside of the scope of our study.

In order to implement a sensitivity analysis it is necessary to specify the uncertainty on the input parameters. As discussed in Sect. 2.3.4.1, information on the uncertainty was obtained from site specific data and an extensive literature review. This is described in detail in Appendix B. Despite this, we were unable to obtain detailed information on the distribution of several parameters and in some cases only single values were available (Point D & E in Sect. 2.3.4.1 and Table 2.3). In such cases a wide uncertainty range was specified, in order to avoid underspecifying the uncertainty. The characterization of the uncertainty in the input parameters is the most extensive that has been published to date; however, this matter should be explored further in future research. In particular the impact of different

uncertainty specifications on the output of the sensitivity analysis should be evaluated. The possibility of obtaining uncertainty specifications through expert elicitation (Oakley, 2002; Bastin et al., 2013) should also be explored.

Quantifying correlations between simulator inputs is recommended (Saltelli et al., 2008) in order to avoid the unrealistic combination of inputs in the VBSA sampling. This is neatly illustrated by Hamm et al. (2006). The correlation between input parameters was not included in this study due to a lack of site specific information on correlations, although site specific parameter values and distributions were selected as much as possible. Reported correlations between parameters refer mainly to biomes, leaf traits and species (Reich et al., 1999; Houborg et al., 2013), rather than for one species or site. There are two cases where information about correlations may be useful. First, some input parameter combinations caused the forest to disappear in the spin-up (Figs. 2.2a and 2.2b). Accounting for correlations typically restrict the input parameter space and may eliminate this problem. Second, we obtained realizations where $\mathrm{C{:}N_{leaf}} > \mathrm{C{:}N_{lit}}$, which is physically unrealistic and which conflicts with a condition of BIOME-BGC. There is no straightforward solution to this problem, because information about correlations is simply not provided in the literature. One possibility might be to obtain these through expert elicitation (Oakley, 2002; Bastin et al., 2013).

2.6 Conclusions

This study identified the uncertainty in the ecophysiological parameters of the process-based BIOME-BGC simulator in the form of probability density functions (pdf). The sensitivity analysis experiment carried out in the study identified the ecophysiological parameters that most influence simulated GPP and NPP. Earlier studies based on one-at-a-time (OAT) sensitivity analysis did not find a significant influence of water interception coefficient (W_{int}), but identified specific leaf area (SLA) and maximum stomatal conductance (g_{smax}) as being influential. Sensitivity to these parameters was not found in our experiment. This emphasizes the importance of undertaking a global variance-based sensitivity analysis given the known limitations of OAT analyses. The Speulderbos forest was covered by a single species. The procedures applied in this study could serve to expand research towards other forests containing multiple species. For example, the study could be carried out for several species independently, followed by integration of the several results. Such research, however, is outside the scope of the current study. There is apparently also not a problem to repeat the study in a different area under similar conditions. Collection of necessary input information, however, may be more complicated than for the current site where the data have been systematically collected during the past decades. The study further assumed no changes in nitrogen over time, whereas it used yearly changing CO_2 values. The model would have allowed to also vary the nitrogen deposition level according to the reported CO_2 level. As we observed only a small variation ($< 2\,\%$) in yearly CO_2 values during the years under investigation (2007-2010) we decided not to do so. It would have increased the complexity and the

effects would most likely be negligible, also because of the short (4 years) time period. In summary, the study showed that our approach presented an efficient way of reducing the complexity of calibrating the BIOME-BGC simulator by considering only the key influential input parameters that were reported above. Calibration can be further supported by prior knowledge of the input parameters in the form of probability density functions.

2.7 Appendices

Appendix A: Calculation of Speulderbos site specific input parameters

(I) Carbon to nitrogen ratio of leaf ($C:N_{leaf}$): We calculated 252 values for $C:N_{leaf}$ of as a ratio of C and N concentration of Douglas fir leaves, which were collected for three years (2008-2010) at Speulderbos.

(II) Carbon to nitrogen ratio of litter ($C:N_{lit}$): We extracted 38 values for Douglas fir $C:N_{lit}$ from the Fig. 5 of Portillo-Estrada et al. (2013). This is based on the chemical analysis of Douglas fir litter collected for 43 months (June 2007 to December 2010) at Spelderbos.

(III) Canopy water interception coefficient (W_{int}): We extracted 30 values for interception (I) and precipitation (P) for all rain events (between May and Dec 1989) at Speulderbos from the Fig. 4 of Klaassen et al. (1998). The mean of minimum and maximum value of leaf area index (LAI) reported in Klaassen et al. (1998) was taken as mean LAI. The W_{int} for each rain event was calculated as

$$W_{int} = \frac{I}{P \times \text{mean LAI}} \tag{A2.1}$$

(IV) Canopy light extinction coefficient (k): We calculated 104 values for k using the data of leaf area index (LAI) and transmittance (T), which were measured around solar noon from April, 2011 to June, 2011 at Speulderbos for Douglas fir species (Mustafa, 2012). The fish-eye photographs of Douglas fir canopy were taken by plant canopy imager, which were further processed by gap light analyser software to measure leaf area index (LAI) and T. These data were used in the Beer-Lambert equation (see below) to calculate k.

$$\text{k} = \frac{\log T}{\text{LAI}} \tag{A2.2}$$

(V) Fraction of leaf N in Rubisco (FLNR): It was calculated by the following equation (White et al., 2000).

$$\text{FLNR} = \frac{V_{cmax} \times \text{SLA} \times C:N_{leaf}}{\Gamma \times \text{act}} \tag{A2.3}$$

V_{cmax} is the maximum rate of carboxylation (μmol CO_2 m^{-2} s^{-1}), SLA is the specific leaf area, $C:N_{leaf}$ is the leaf C:N ratio, Γ is the ratio of the mass of Rubisco to the mass of nitrogen in Rubisco [7.16], and act is the Rubisco activity at 25°C [60,000 μmol CO_2 kg $Rubisco^{-1}$ s^{-1}]. We calculated 2724 values for FLNR using: (a) mean value of V_{cmax} (= 36) for Douglas fir at Speulderbos (Dekker, 2000); (b) 12 values of SLA for Douglas fir (Domec et al., 2012); and (c) 252 values of $C:N_{leaf}$ as mentioned above.

(VI) Needle maximum stomatal conductance (g_{smax}): We extracted 25 values for canopy maximum stomatal conductance (G_{smax}) for Douglas fir at Speulderbos from the Fig. 1 of van Wijk et al. (2000). The mean of minimum and maximum value of LAI reported in van Wijk et al. (2000) was taken as mean LAI. Each G_{smax} was divided by mean LAI to get 25 values of g_{smax}.

(VII) Boundary layer conductance (g_{bl}): It was calculated as a ratio of diffusion constant of water vapor ($D = 2.27 \times 10^{-5}$ ms^{-1} at 10°C) and the thickness of boundary layer (δ_{bl}) (Nobel, 2009).

$$g_{\mathrm{bl}} = \frac{D}{\delta_{\mathrm{bl}}} \tag{A2.4}$$

δ_{bl} was calculated as

$$\delta_{\mathrm{bl}}(\mathrm{mm}) = 4 \times \sqrt{\frac{L}{V}} \tag{A2.5}$$

L (m) is the leaf length and V (ms^{-1}) is the ambient wind velocity. We calculated 1460 values for δ_{bl} and then g_{bl} using: (a) mean leaf length [0.02 m] of Douglas fir at Speulderbos (Duyzer et al., 2004); and (b) daily mean value of wind speed (2007 to 2010) measured at flux tower at Speulderbos.

Appendix B: Details of probability distribution function of each input parameter

We provide an excel file to give details of pdf (probability distribution function) selection of each input parameter. Each sheet of the excel file, excluding first and last sheet, includes the information on a BIOME-BGC ecophysiological parameter. The name of each sheet is chosen to reflect the symbol of a BIOME-BGC parameter. For example, the excel sheet C:N_leaf refers to $C:N_{leaf}$ (the carbon to nitrogen ratio of leaf). The following information is provided in each excel sheet.

1. The values of the BIOME-BGC ecophysiological parameter with the source references are reported. The information from some sources is also provided under the column Remarks from the source paper.
2. The remarks written on the top of a sheet explain the probability density function (pdf) for the BIOME-BGC ecophysiological parameter.
3. The pdf parameters are provided. For example, minimum and maximum for a uniform pdf, and mean and standard deviation for a normal pdf.

The last sheet provides the theoretical basics of the normality test conducted for the BIOME-BGC parameters: carbon to nitrogen ration of leaf and litter ($C:N_{leaf}$ and $C:N_{lit}$), specific leaf area (SLA), water interception coefficient (W_{int}), light extinction coefficient (k), fraction of leaf N in Rubisco (FLNR), maximum stomatal conductance (g_{smax}), and boundary layer conductance (g_{bl}). The excel sheets corresponding to these BIOME-BGC ecophysiological parameters include the normality test results as well as the results of other fitted pdfs, if considered.

The excel file can be downloaded from ***this link***. All references cited in the excel file can be found in the bibliography section of this thesis.

Appendix C: Morris sensitivity analysis

Theoretical background

The Morris method is a randomized OAT sensitivity analysis, which is based on the idea of elementary effects (Morris, 1991; Saltelli et al., 2008). It follows these steps:

1. A set of starting values (e.g., the medians) for all input parameters is selected within the defined ranges of possible values. The outcome is simulated.
2. The value of one parameter is changed by Δ and all other parameters are kept at their starting values. The outcome is simulated.
3. The value of another parameter is then changed and the previous parameter (step 2) is kept at its changed value. All other parameters are kept at their starting values. The outcome is simulated. This goes on until all input parameters are changed.
4. The steps 1,2, and 3 are repeated r times, each time with a different set of starting values.

The Morris method leads to r changes in the simulator outcome. This information is expressed as elementary effects. Consider a simulator with n input parameters X_i, $i = 1, 2, ..., n$ and output $Y = f(X_1, X_2, ..., X_n)$. Each parameter is varied at p selected levels, which correspond to the quantile of the input parameter distribution. The elementary effect EE_i of X_i is defined as

$$EE_i = \frac{[f(X_1, X_2, ..., X_i + \Delta, ..., X_n) - f(X_1, X_2, ..., X_i, ..., X_n)]}{\Delta} \quad \text{(C2.1)}$$

EE_i is thus calculated r times providing an outcome $EE_i^{(j)}$. The mean of r elementary effects are reported as the Morris index for X_i. Campolongo et al. (2007) proposed taking the mean (μ_i) of the absolute value of the elementary effects and it is given as

$$\mu_i = \frac{1}{r} \sum_{j=1}^{r} |EE_i^{(j)}| \quad \text{(C2.2)}$$

The Morris approach requires $r \times (n + 1)$ executions of the simulator to compute the index given by Eq. C2.2. The μ_i may take any positive value. When μ_i is high compared to other input parameters, the simulator outcome is highly sensitive to the input parameter X_i. The decrease in μ_i from the high value makes the simulator outcome less sensitive to X_i.

Results of Morris sensitivity analysis

The results of Morris sensitivity analysis are shown in Fig. C2.1 for GPP and Fig. C2.2 for NPP. Eight input parameters for GPP and ten for NPP had a Morris index (μ_i) below the selected minimum threshold value (0.05). The

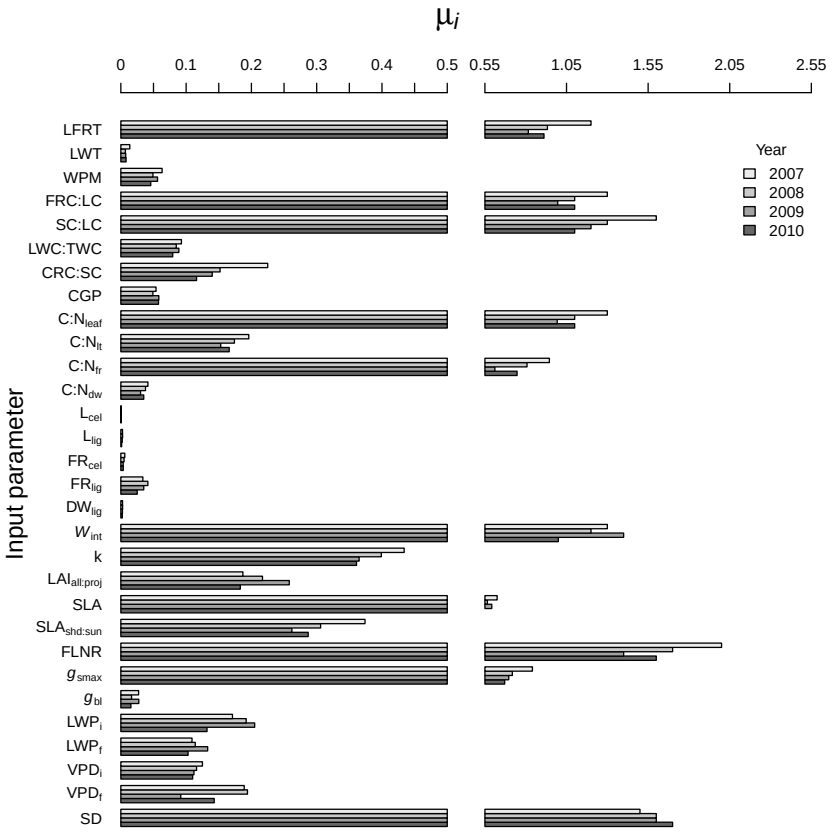

Figure C2.1 Morris sensitivity, μ_i, of annual mean GPP to the input parameters. The symbols in the y-axis correspond to the ecophysiological parameters given in Table 2.2. SD is soil depth.

eight parameters (LWT, C:N_{dw}, L_{cel}, L_{lig}, FR_{cel}, FR_{lig}, DW_{lig}, and g_{bl}) that did not meet the minimum threshold for both GPP and NPP were excluded from the variance-based sensitivity analysis, and fixed at their mean values.

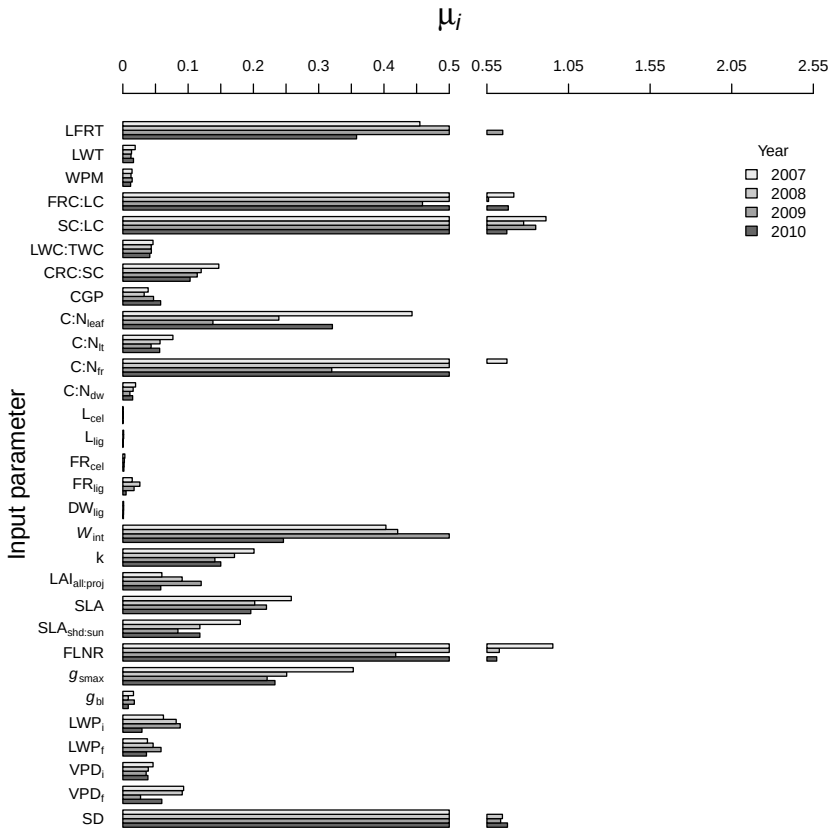

Figure C2.2 Morris sensitivity, μ_i, of annual mean NPP to the input parameters. Other details as for Fig. C2.1.

Partitioning of GPP from flux tower measurements of NEE

3

This chapter has been published as: Raj, R., Hamm, N. A. S., van der Tol, C., Stein, A., 2016. Uncertainty analysis of gross primary production partitioned from net ecosystem exchange measurements. Biogeosciences 13 (5), 1409-1422.

Abstract

Gross primary production (GPP) can be separated from flux tower measurements of net ecosystem exchange (NEE) of CO_2. This is used increasingly to validate process-based simulators and remote sensing-derived estimates of simulated GPP at various time steps. Proper validation includes the uncertainty associated with this separation. In this study, uncertainty assessment was done in a Bayesian framework. It was applied to data from the Speulderbos forest site, The Netherlands. We estimated the uncertainty in GPP at half-hourly time steps, using a non-rectangular hyperbola (NRH) model for its separation from the flux tower measurements. The NRH model provides a robust empirical relationship between radiation and GPP. It includes the degree of curvature of the light response curve, radiation and temperature. Parameters of the NRH model were fitted to the measured NEE data for every 10-day period during the growing season (April to October) in 2009. We defined the prior distribution of each NRH parameter and used Markov chain Monte Carlo (MCMC) simulation to estimate the uncertainty in the separated GPP from the posterior distribution at half-hourly time steps. This time series also allowed us to estimate the uncertainty at daily time steps. We compared the informative with the non-informative prior distributions of the NRH parameters and found that both choices produced similar posterior distributions of GPP. This will provide relevant and important information for the validation of process-based simulators in the future. Furthermore, the obtained posterior distributions of NEE and the NRH parameters are of interest for a range of applications.

Keywords: Net ecosystem exchange, gross primary production, non-rectangular hyperbola model, Bayesian framework.

3.1 Introduction

Net ecosystem exchange (NEE) is a terrestrial component of the global carbon cycle. It is the exchange of CO_2 between the terrestrial ecosystem and the atmosphere. The measurement of NEE by the eddy covariance technique is well-established (Baldocchi, 2003). Specifically, NEE is the balance between the CO_2 released by the ecosystem respiration (R_{eco}) and the gross CO_2 assimilated via photosynthesis. The fraction of carbon in the assimilated CO_2 is the gross primary production (GPP). Estimates of GPP provide information about the physiological processes that contribute to NEE (Aubinet et al., 2012). Measured NEE data are used to validate the NEE that is simulated by ecosystem process-based simulators such as BIOME-BGC (BioGeochemical Cycles) (Thornton, 1998). It is often desirable to validate the simulated component flux (R_{eco} and GPP) independently. This is particularly important for diagnosing the misrepresentation (overestimation or underestimation) of assimilation processes in the simulator (Reichstein et al., 2005), which can only be achieved by comparing the GPP partitioned from NEE data with the simulated one. Furthermore, remote sensing-derived light use efficiency (LUE) models address the spatial and temporal dynamics of GPP (Running et al., 2004). The reliability of such models at the regional scale relies on the validation using GPP partitioned from NEE data (Wang et al., 2010; Li et al., 2013).

Flux partitioning methods (FPM) are used to partition NEE into its component flux (GPP and R_{eco}). These methods are based on fitting a non-linear empirical model to the measured NEE data and other meteorological data in order to estimate the parameters. The estimated parameters of the non-linear model are then used to predict daytime R_{eco} and GPP. There are two types of FPM: (1) those that use only nighttime NEE data, and (2) those that use either daytime NEE data or both daytime and nighttime data (Stoy et al., 2006; Lasslop et al., 2010; Aubinet et al., 2012).

A nighttime-based FPM assumes that NEE is equal to R_{eco} ($\text{GPP} = 0$ during the night) and that it varies with air and soil temperature (Richardson et al., 2006a). A daytime-based FPM assumes that the variation of NEE occurs with photosynthetic photon flux density (PPFD) and the light response curve (plot of NEE against PPFD) can be represented by a rectangular hyperbola (RH) model (Ruimy et al., 1995). Lasslop et al. (2010) proposed a daytime-based FPM using the RH model by incorporating the variation of NEE as a function of global radiation, air temperature, and vapour pressure deficit (VPD) because these affect GPP via stomatal regulation. A daytime-based FPM was proposed that uses the non-rectangular hyperbola (NRH) model to incorporate the effect of the degree of curvature (θ) of the light response curve (Rabinowitch, 1951; Gilmanov et al., 2003). θ represents the convexity of the light response curve as the NEE and radiation relationship approaches saturation. Further, the light response curve represented by the NRH model has been found to fit NEE data better than the RH model (Gilmanov et al., 2003; Aubinet et al., 2012). Gilmanov et al. (2013) further improved the NRH model by incorporating the effect of VPD and temperature as proposed by Lasslop et al. (2010). They used PPFD and

soil temperature instead of global radiation and air temperature respectively. This improvement incorporates the influence of PPFD, air or soil temperature, VPD, and θ by taking advantage of better representation of the light response curve by comparison to the RH model.

A quantification of uncertainty in partitioned GPP provides an associated credible interval that can be used for proper implementation of calibration and validation of a process-based simulator against partitioned GPP (Hagen et al., 2006). The temporal resolution of process-based simulators may vary from half-hourly to monthly. It is therefore necessary to quantify uncertainty associated with the partitioned GPP at half-hourly to monthly time scales. For example, the partitioned GPP and associated uncertainty at a daily time scale can provide data for the calibration of process-based simulators such as BIOME-BGC.

In this study, we adopted the NRH model to partition half-hourly GPP from NEE data. In the past, numerical optimization has been used to estimate a single optimized value of each model parameters (Gilmanov et al., 2003, 2013). This did not quantify the uncertainty in half-hourly partitioned GPP. The measurements of half-hourly NEE are uncertain. Therefore, the optimized parameters are also uncertain (Richardson and Hollinger, 2005). Obtaining the underlying probability distribution of the NRH parameters gives a measure of uncertainty in parameters, which can be further propagated towards the NRH model to estimate uncertainty in partitioned GPP. A Bayesian implementation provides a solution to quantify the uncertainty in model parameters in the form of probability distributions (Gelman et al., 2013). The Bayesian approach was used in other studies to constrain the parameters of process-based simulators by using either eddy covariance data, biometric data, or both (Ricciuto et al., 2008; Du et al., 2015; Minet et al., 2015). We applied the Bayesian approach to a different type of model. We fitted the non-linear empirical NRH model to NEE data and quantified the uncertainty in NRH parameters to partition GPP with uncertainty.

The objective of this study was to implement a Bayesian approach for quantification of the uncertainty in half-hourly partitioned GPP using the NRH model given the availability of half-hourly NEE and other meteorological data. The time series of empirical distributions of half-hourly GPP values also allowed us to estimate the uncertainty in GPP at daily time steps. Data were available from a flux tower in the central Netherlands at the Speulderbos forest. This will provide relevant and important information for the validation of process-based simulators.

3.2 Methods

3.2.1 Study area and data

The Speulderbos forest is located at $52^o15'08''$ N, $05^o41'25''$ E within a large forested area in the Netherlands. There is a flux tower within a dense 2.5 ha Douglas fir stand. The stand was planted in 1962. The vegetation, soil, and

climate of this site have been thoroughly described elsewhere (Steingrover and Jans, 1994; van Wijk et al., 2001; Su et al., 2009).

The CSAT3, Campbell Sci, LI7500 LiCor Inc, and CR5000 instruments were installed in June 2006 and have been maintained, and the data processed (software AltEddy, Alterra) by C. van der Tol (University of Twente, co-author) and A. Frumau (Energy Centre Netherlands). We examined half-hourly NEE data (measured at the flux tower) for the growing season (April to October) of 2009. The quality of the NEE data were assessed using the Foken classification system, which provides a flag to each half-hourly NEE datum from 1 through 9 (Foken et al., 2005). Each flag is associated with: (a) the range of the steady state condition of the covariance of vertical wind speed and CO_2 concentration of half-hour duration, (b) the range of the integral turbulence characteristic parameter indicating the developed turbulence; and (c) the range of the orientation of the sonic anemometer to make sure that the probe is omnidirectional at the time of measurements. We followed the suggestion of Foken et al. (2005) and accepted only those NEE data that were labelled from 1 to 3. For the growing season, we acquired half-hourly PPFD from the sensor PARlite (Kipp & Zonen. Delft, the Netherlands) and half-hourly T_a from the weather sensor WXT510 (Vaisala, Finland) installed at the flux tower.

3.2.2 The non-rectangular hyperbola (NRH) model

NEE is given as:

$$\mathrm{NEE} = P_a - R_{eco} \tag{3.1}$$

where NEE is measured by the eddy covariance technique and P_a is gross CO_2 assimilation. The exchange of carbon into the system through photosynthesis is considered a positive flux because it represents production and the loss of carbon through respiration is considered a negative flux.

The light response curve is represented using the NRH model (Gilmanov et al., 2003; Rabinowitch, 1951):

$$P_a = \frac{1}{2\theta} \times \left(\alpha \cdot \mathrm{PPFD} + A_{max} - \sqrt{(\alpha \cdot \mathrm{PPFD} + A_{max})^2 - 4\alpha \cdot A_{max} \cdot \theta \cdot \mathrm{PPFD}}\right), \tag{3.2}$$

where α is the apparent quantum yield, A_{max} is the photosynthetic capacity at light saturation, and θ is the degree of curvature of the light response curve.

Gilmanov et al. (2013) modelled ecosystem respiration R_{eco} using the temperature-dependent term according to Van't-Hoff's equation in its exponential form (Thornley and Johnson, 2000):

$$R_{eco} = r_0 \times \exp\left(k_T T_a\right), \tag{3.3}$$

where T_a is the air temperature and r_0 and k_T are the temperature sensitivity coefficients. Eqs. 3.2 and 3.3 are substituted in Eq. 3.1 to obtain the model for net ecosystem exchange NEE:

$$\begin{aligned}\mathrm{NEE} = \frac{1}{2\theta}\times \\ \left(\alpha\cdot\mathrm{PPFD} + A_{\max} - \sqrt{(\alpha\cdot\mathrm{PPFD}+A_{\max})^2 - 4\alpha\cdot A_{\max}\cdot\theta\cdot\mathrm{PPFD}}\right) \\ - r_0 \times \exp\left(k_T T_a\right).\end{aligned} \tag{3.4}$$

Both daytime and nighttime half-hourly NEE, PPFD, and T_a data were used to estimate the NRH model parameters $\boldsymbol{\beta} = (\theta,\ \alpha,\ A_{\max},\ r_0,\ k_T)$ (Eq. 3.4). For nighttime data, Eq. 3.4 includes only the respiration term because PPFD is equal to zero during the night. These estimated parameters, together with half-hourly PPFD, were used in Eq. 3.2 to calculate half-hourly P_a. Values of half-hourly GPP were calculated by multiplying P_a by 12/44 (12 is the atomic mass of carbon, and 44 is the atomic mass of CO_2) in order to convert the mass of CO_2 into the mass of carbon (C). This gives GPP in mg C $m^{-2}\,s^{-1}$. This unit is the same as the unit of GPP simulated by process-based simulators such as BIOME-BGC. Therefore, the simulated GPP could be directly compared to the partitioned GPP in the future at the study area. The unit of P_a is the same as the unit of measured NEE in mg $CO_2\,m^{-2}\,s^{-1}$. The unit of each parameter and other variables used in the above equations are shown in Table 3.1. Gilmanov et al. (2013) proposed to incorporate the effect of VPD by multiplying Eq. 3.2 by the VPD-response function, ϕ, that accounts for the VPD limitation on P_a. The function ϕ is set equal to 1 if VPD is below some critical value ($\mathrm{VPD_{cr}}$) that indicates that water stress does not affect photosynthesis. Above the critical value ($\mathrm{VPD} > \mathrm{VPD_{cr}}$), ϕ decreases exponentially with the curvature parameter σ_{VPD}, which may vary between 1 and 30 kPa. Low values of σ_{VPD} indicate a strong water stress effect, whereas higher values indicate a weak water stress effect. We calculated half-hourly VPD from relative humidity (RH) using the procedure provided in Monteith and Unsworth (1990). We found that 90 % of the total half-hourly VPD values in the growing season of 2009 were less than 1 kPa and 9 % were between 1 kPa and 1.5 kPa. We therefore neglected the influence of VPD as a limiting factor for the water stress at Speulderbos. This follows Körner (1995) and Lasslop et al. (2010) who specified $\mathrm{VPD_{cr}} = 1$. We, therefore, assumed ϕ equal to 1.

3.2.3 Theory of Bayesian inference for the model parameters

Bayesian inference treats all parameters as random variables (Gelman et al., 2013). Bayes rule is given as

$$p(\boldsymbol{\beta}|\mathbf{y}) = \frac{p(\mathbf{y}|\boldsymbol{\beta})p(\boldsymbol{\beta})}{p(\mathbf{y})} \propto \text{likelihood} \times \text{prior}, \tag{3.5}$$

Table 3.1 List of symbols with unit.

NEE, $\mathbf{y}$	net ecosystem exchange	mg $CO_2\,m^{-2}\,s^{-1}$
P_a	gross CO_2 assimilation	mg $CO_2\,m^{-2}\,s^{-1}$
GPP	gross primary production	mg C $m^{-2}\,s^{-1}$; g C $m^{-2}\,d^{-1}$
R_{eco}	ecosystem respiration	mg $CO_2\,m^{-2}\,s^{-1}$
PPFD	photosynthetic photon flux density	µmol quanta $m^{-2}\,s^{-1}$
T_a	air temperature	°C
α	quantum yield	mg CO_2 (µmol quanta)$^{-1}$
θ	degree of curvature of light response curve	unitless
A_{max}	photosynthetic capacity at light saturation	mg $CO_2\,m^{-2}\,s^{-1}$
k_T	temperature sensitive parameter	(°C)$^{-1}$
r_0	ecosystem respiration at reference temperature $T_a = 0\,°C$	mg $CO_2\,m^{-2}\,s^{-1}$
τ_e	precision of the normal distribution of the likelihood	
$\boldsymbol{\beta}$	(θ, α, A_{max}, r_0, k_T)	
R_b	ecosystem respiration at reference temperature $T_a = 15\,°C$	g $CO_2\,m^{-2}\,d^{-1}$
Q_{10}	multiplication factor to respiration with 10 °C increase in T_a	
RH	relative humidity	%
VPD	vapour pressure deficit	kPa
VPD_{cr}	critical value of vapour pressure deficit	kPa
ϕ	vapour pressure deficit response function	
σ_{VPD}	curvature parameter for ϕ	kPa

where $p(\boldsymbol{\beta})$ is the prior distribution, representing the prior understanding of uncertainty in the model parameters values before the observations are taken into account. This understanding may come from expert judgement or previously published research on the parameters (Oakley and O'Hagan, 2007; Raj et al., 2014). If no prior knowledge is available, non-informative priors may be used (i.e., a wide prior distribution that conveys no prior information). The term $p(\boldsymbol{\beta}|\mathbf{y})$ is the posterior distribution of $\boldsymbol{\beta}$ after combining prior knowledge and data $\mathbf{y}$ and represents the uncertainty in $\boldsymbol{\beta}$ given the data and the prior. The marginal effect of each parameter $p(\beta_i|\mathbf{y}), i = 1, 2, \ldots, n$, is the main quantity of interest, expressing the uncertainty in each parameter separately. The term $p(\mathbf{y}|\boldsymbol{\beta})$ is the conditional probability of observing data $\mathbf{y}$ given $\boldsymbol{\beta}$ and is also called the likelihood. The term $p(\mathbf{y})$ is the probability of observing the data $\mathbf{y}$ before observations were taken. This acts as the normalising constant that ensures that $p(\boldsymbol{\beta}|\mathbf{y})$ is a valid probability distribution that integrates to 1. For most real-world problems it is not possible to write down analytical solutions for Eq. 3.5 and it is usual to perform inference using Markov Chain Monte Carlo (MCMC) simulation (Gelman et al., 2013).

MCMC is a method for conducting inference on $p(\boldsymbol{\beta}|\mathbf{y})$. It requires evaluation of the joint distribution $p(\mathbf{y}|\boldsymbol{\beta})p(\boldsymbol{\beta})$, which represents the dependence structure in the data. MCMC constructs Markov chains of the parameters

space and generates samples $\boldsymbol{\beta}^{(1)}, \boldsymbol{\beta}^{(2)}, \ldots, \boldsymbol{\beta}^{(m)}$ of $\boldsymbol{\beta}$ whose unique stationary distribution is the posterior distribution of interest $p(\boldsymbol{\beta}|\mathbf{y})$. The m samples are then used to conduct inference on each β_i. For example the mean, median and 95 % credible interval can all be calculated over these m samples. It is usual to construct multiple Markov chains and to assess whether they converge to the same stationary distribution. We refer the reader to chapter 4 in Lunn et al. (2013) and chapter 11 in Gelman et al. (2013) for further explanation.

3.2.4 Implementation of Bayesian inference for the NRH model parameters

We treated Eq. 3.4 as a non-linear regression problem:

$$\begin{aligned} y_i = & \frac{1}{2\theta} \times \\ & \left(\alpha \cdot \mathrm{PPFD}_i + A_{\max} - \sqrt{(\alpha \cdot \mathrm{PPFD}_i + A_{\max})^2 - 4\alpha \cdot A_{\max} \cdot \theta \cdot \mathrm{PPFD}_i}\right) \\ & - r_0 \times \exp\left(k_{\mathrm{T}} T_{\mathrm{a}_i}\right) + \varepsilon_i = \mu_i - \nu_i + \varepsilon_i \end{aligned} \tag{3.6}$$

where y is the response variable (NEE), PPFD and T_{a} are the predictor variables and ε is the residual error. The residual error arose because the model did not perfectly fit the data. The subscript i indicates a single observation. For brevity we use μ_i to refer to the first term on the RHS and ν_i to refer to the second term on the right hand side of Eq. 3.6.

As is usual in regression modelling, we assumed normally distributed errors, hence $\varepsilon_i \sim N(0, \sigma^2)$ and the likelihood also followed a normal distribution, such that $y_i \sim N(\mu_i - \nu_i, \sigma^2)$. In the above notation, $\boldsymbol{\beta} = (\alpha, A_{\max}, \theta, r_0, k_{\mathrm{T}})^T$ and the likelihood is $p(\mathbf{y}|\boldsymbol{\beta}, \sigma^2)$, where $\mathbf{y} = (y_1, y_2, \ldots, y_n)^T$ for n observations. The superscript T represents the transpose.

In Bayesian analysis it is usual to refer to precision, which is the inverse of the variance, hence $\tau_e = 1/\sigma^2$. Further, the assumption of prior distributions for each β_i together with τ_e is required. No prior information was available for τ_e so a non-informative prior was selected. We assumed a Gamma distribution for τ_e with shape and rate parameters equal to 0.001. This ensures a non-negative non-informative prior for τ_e (Lunn et al., 2013).

We made two choices for the prior distribution for each β_i. First, a non-informative prior was used (Sect. 3.2.4.1). Second, prior information for each β_i was obtained from the literature, being called an informative prior distribution (Sect. 3.2.4.2). Note that the same non-informative prior for τ_e was used in both choices. The results for informative an non-informative priors were compared.

3.2.4.1 Non-informative prior distributions

We assumed a normal distribution for each β_i with mean equal to 0 and standard deviation equal to 32, which gives small value of the the precision

equal to 0.001 to make the distribution wide. NRH is a non-linear model and therefore appropriate constraints should be imposed to ensure the meaningful values of the prior parameter distribution (Lunn et al., 2013). Each β_i parameter must be positive (Sect. 3.2.4.2) so we truncated the normal distribution on each β_i except θ to ensure only positive values. For θ, we truncated the normal distribution to occur between 0 and 1 by setting the obvious limit to this parameter (see also item 2 in Sect. 3.2.4.2). The above choices ensure wide non-informative prior distributions whilst specifically excluding physically unrealistic values.

3.2.4.2 Informative prior distributions

Below we justify choices for the informative prior distributions on $\boldsymbol{\beta}$.

1. The quantum yield, α, represents the amount of absorbed CO_2 per quanta of absorbed light. Cannell and Thornley (1998) reported that α varies little among C_3 species and has a value from 0.09 to 0.11 and from 0.04 to 0.075 mol CO_2 (mol quanta)$^{-1}$ in saturated and ambient CO_2 conditions respectively. The typical value of α equals 0.05 mol CO_2 (mol quanta)$^{-1}$ for a C_3 species in an ambient atmosphere (Bonan et al., 2002; Long et al., 2006; Skillman, 2008). Douglas fir at Speulderbos is a C_3 species. We used this information to construct the prior distribution on α, as follows:
    - A value of α around 0.05 has the highest probability. The probability decreases as the value of α decreases or increases from 0.05 and cannot be negative. The maximum value that α can attain is 0.11.
    - We assumed a normal distribution of α with mean, $\mu_\alpha = 0.05$, and variance, $\sigma_\alpha^2 = (0.015)^2$ (i.e, standard deviation, $\sigma_\alpha = 0.015$). The choice of mean ensures that the highest probability is assigned to the values around 0.05. The choice of variance ensures that 99.7 % ($\mu \pm 3\sigma_\alpha$) of α is positive and lies in the interval between 0 and 0.11. We also truncated 0.3 % of negative α values from the assumed normal distribution. In the unit of mg CO_2 (µmol quanta)$^{-1}$, the assumed normal distribution ($N(\mu_\alpha = 0.05,\ \sigma_\alpha = 0.015)$) is expressed as $N(0.0022, 0.00066)$ (Fig. 3.1a).
2. The curvature parameter θ can take values from 0, which reduces Eq. 3.4 to the simpler rectangular hyperbola, to 1, which describes the Blackman response of two intersecting lines (Blackman, 1905). The physiological range for θ has been observed to be between 0.5 and 0.99 (Ogren, 1993; Cannell and Thornley, 1998). A value of $\theta = 0.9$ was recommended by Thornley (2002) and at $\theta = 0.8$ by Johnson et al. (2010) and Johnson (2013). The estimate of θ, as a result of fitting the NRH model to either measured photosynthesis or NEE data was found to be in the range of 0.7 to 0.99 (Gilmanov et al., 2003, 2010). These findings for θ indicated that a higher probability should be assigned to the values around 0.8 and the probability should approach to zero below 0.5. This means that the distribution of θ can be assumed to be

negatively skewed with $\Pr(\theta < 0.5)$ approaching zero and $\Pr(\theta \approx 0.8)$ at a maximum. These conditions were modelled using a beta distribution with shape parameters at 10 and 3 for θ (Fig. 3.1b).

3. The photosynthetic capacity at light saturation $A_{\max}$ is reached when the photosynthesis is Rubisco limited and varies among different tree species (Cannell and Thornley, 1998). At the canopy level, $A_{\max}$ also depends upon the structure of the canopy (i.e., arrangement of the canopy leaves) and the area of leaves available to absorb photons. Both are determined by the leaf area index (LAI) (Ruimy et al., 1995). We compiled the prior information on $A_{\max}$ for Douglas fir species from the literature. Values of $A_{\max}$ were mainly reported for needles, whereas the NRH model (Eq. 3.4) requires $A_{\max}$ values for the canopy. Scaling $A_{\max}$ from needle to the canopy equivalent is not a trivial task because this depends on the light distribution and the vertical profile of $A_{\max}$ in the canopy. Here we analysed plateau values of photosynthesis at needle and canopy level with simulations by a model that takes this into account: the model SCOPE (van der Tol et al., 2009). These simulations (not shown) indicated that the relation between the two plateaus (canopy : needle $A_{\max}$) increased with LAI but saturated at a value of 2.8. The mean value of LAI at the Speulderbos site is high (approximately 9 Steingrover and Jans, 1994; van Wijk et al., 2000) and therefore we could translate the reported range of $A_{\max}$ values for the Speulderbos (Mohren, 1987) of 0.26 to $0.52\,\mathrm{mg\,CO_2\,m^{-2}\,s^{-1}}$ into values of 0.73–$1.46\,\mathrm{mg\,CO_2\,m^{-2}\,s^{-1}}$ for canopy $A_{\max}$. van Wijk et al. (2002) reported slightly higher canopy $A_{\max}$ values of 1.86 and $1.06\,\mathrm{mg\,CO_2\,m^{-2}\,s^{-1}}$ at the Speulderbos site. The highest and lowest value for needle $A_{\max}$ for Douglas fir (irrespective of the site) we found in the literature were 0.097 (canopy $A_{\max} = 0.27$) and $1.01\,\mathrm{mg\,CO_2\,m^{-2}\,s^{-1}}$ (canopy $A_{\max} = 2.8$) respectively (Lewis et al., 2000; Ripullone et al., 2003; Warren et al., 2003). To cover this rather wide range of values, a Gamma distribution with shape and rate parameters equal to 4 and 2.5 respectively was selected to ensure higher probabilities are assigned to the values between 1 and 2.5 with decreasing probabilities down to 0 and up to 4.5 (Fig. 3.1c). The $A_{\max}$ values at Speulderbos are well placed in the overall distribution.

4. The parameters for temperature sensitivity k_{T} and Q_{10} are related as $Q_{10} = \exp(10k_{\mathrm{T}})$ (Davidson et al., 2006). Q_{10} is the factor by which respiration (Eq. 3.3) is multiplied when temperature increases by 10 °C. Mahecha et al. (2010) carried out experiments across 60 FLUXNET sites to check the sensitivity of ecosystem respiration to air temperature. They suggested that Q_{10} does not differ among biomes and is confined to values around 1.4 ± 0.1 (corresponding to k_{T} around 0.034 ± 0.008). Hence $k_{\mathrm{T}} \approx 0.034$ should have the highest probability of occurrence. Q_{10} data reported in the supporting material of Mahecha et al. (2010) showed that that Q_{10} becomes less frequent as it increases or decreases from 1.4 and attains a highest value of ~ 2.72 (corresponding to $k_{\mathrm{T}} = 0.1$). To model these conditions, a Gamma

prior distribution was chosen with shape and rate parameters equal to 4 and 120 respectively (Fig. 3.1d).

5. The r_0 parameter represents the ecosystem respiration at 0 °C. We adopted the following steps to define the prior distribution for r_0.
   - Mahecha et al. (2010) presented a graph of seasonal variation of ecosystem respiration at 15 °C (R_b) for 60 FLUXNET sites. We extracted the values of R_b (in g $CO_2\,m^{-2}\,d^{-1}$) from the graph for those sites that belong to evergreen needle leaf forest (ENF). We obtained the values of r_0 from R_b using the following equations:

     $$r_0 = \frac{R_b}{\exp(k_T \times 15)} \tag{3.7}$$

     where k_T was obtained from Q_{10} as reported in point 4 above. Site specific Q_{10} value is used here. The unit of r_0 is converted into mg $CO_2\,m^{-2}\,s^{-1}$.
   - We identified values of r_0 for ENF in the range 0.013 to 0.07 mg $CO_2\,m^{-2}\,s^{-1}$. We also identified values of r_0 in the range 0.019 to 0.043 at the Loobos FLUXNET site in the Netherlands (Mahecha et al., 2010), which is close to Speulderbos. Therefore, we assumed that the most frequent values of r_0 at Speulderbos are in this range. To model these conditions we chose a Beta distribution with shape parameters at 2 and 64 (Fig. 3.1e).

3.2.4.3 Bayesian inference of β

We used WinBUGS software version 1.4.3 (Lunn et al., 2000) to implement the Bayesian full probability models (Eq. 3.5) for the inference of $\boldsymbol{\beta}$. WinBUGS is a windows implementation of the original BUGS (Bayesian Inference Using Gibbs Sampling) software. This was a joint initiative between the MRC Biostatistics Unit, Cambridge and the Imperial College School of Medicine, London (Lunn et al., 2013). WinBUGS implements MCMC for Bayesian inference. The major inputs of WinBUGS are: (a) the model file specifying the definition of the prior distribution of each β_i and likelihood function, (b) the number of Markov chains to create, (c) the number of iterations for MCMC to carry out for each Markov chain, (d) the burn-in period for which the MCMC runs are discarded, (e) initial values of each β_i for each Markov chain. The burn-in period is the number of samples after which the Markov chains converge to a stationary distribution. The post burn-in samples are used to perform inference on the β_i s.

We obtained the posterior distribution of each β_i for every 10-day block (total 22 blocks) in the growing season of 2009. More precisely, we obtained varying parameters and did not assume values to be constant for the whole study period. This approach is recommended by Aubinet et al. (2012), since obtaining varying parameters incorporates indirectly the temporal changes in the factors such as canopy structure, soil moisture and ecosystem nutrient levels that affect GPP. NRH model does not include these factors directly. Hence, although these factors are not included in the NRH model

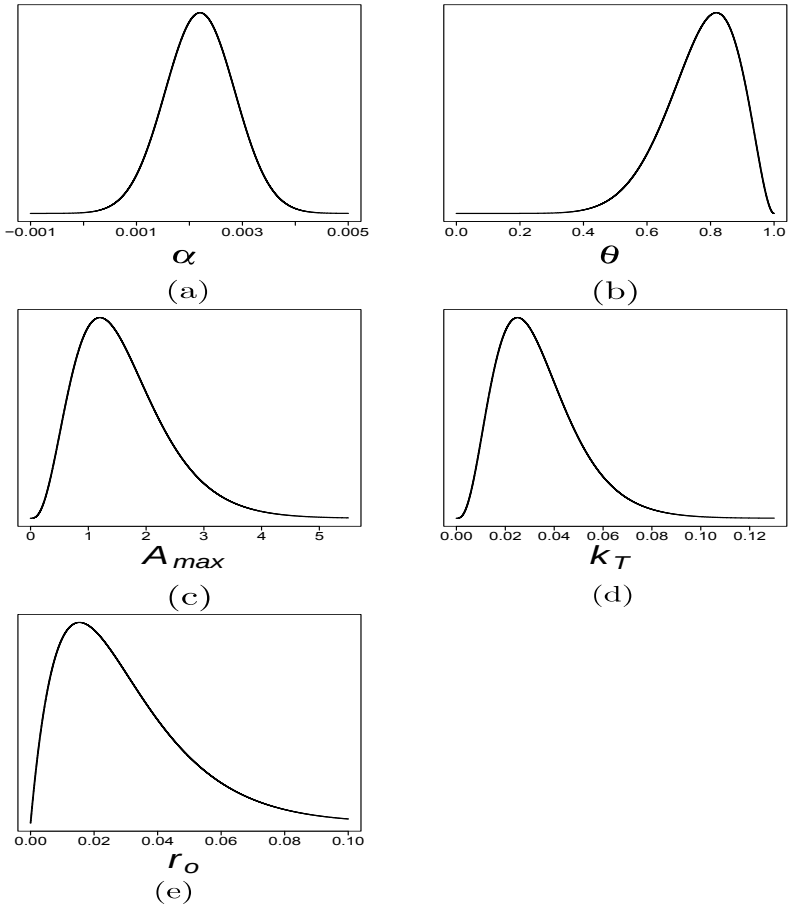

Figure 3.1 Informative prior distribution of the NRH model parameters: **(a)** $\alpha \sim N(\mu_\alpha = 0.0022,\ \sigma_\alpha = 0.00066)$, **(b)** $\theta \sim$ Beta(shape1 $= 10,$ shape2 $= 3)$, **(c)** $A_{\text{max}} \sim$ Gamma(shape $= 4,$ rate $= 2.5)$, **(d)** $k_{\text{T}} \sim$ Gamma(shape $= 4,$ rate $= 120)$, **(e)** $r_0 \sim$ Beta(shape1 $= 2,$ shape2 $= 64)$. Information about the NRH parameters is given in Table 3.1. The y axis represents the density of corresponding distribution.

our implementation does account for them. The 10-day block was chosen because it was sufficiently long to ensure a suitably large NEE dataset *within* the 10-day block but was short enough that we could account for temporal changes *between* the 10-day blocks. Thus the temporal change is observed between consecutive blocks, not within a block. The sample size within a 10-day block was limited because $\sim 30\,\%$ of the data were typically discarded as being of low quality (Foken flag 4 or higher, see Sect. 3.2.1).

We identified the appropriate length of the burn-in for both informative and non-informative prior distributions. We calculated the Gelman–Rubin potential scale reduction factor (PSRF) to evaluate the convergence of Markov chains for each β_i for the post burn-in period. Graphically, we assessed the convergence of Markov chains by plotting them together for each β_i. This plot is known as trace plot. A visual observation of a proper mixing of these chains indicates the convergence of Markov chains to the stationary distribution. An explanation of PSRF and the identification of the length of the burn-in are given in Appendix A. We refer the reader to pages 71–76 in Lunn et al. (2013) and pages 281–285 in Gelman et al. (2013) for further explanation. Based on that analysis we used three Markov chains with 16 000 and 25 000 iterations for each chain for informative and non-informative prior distributions respectively. We stored the posterior samples of each β_i and τ_e for the remaining 30 000 samples (i.e., 10 000 post burn-in samples for each of three Markov chains). The BUGS code (model file for WinBUGS) is given in Appendix B.

3.2.5 Posterior prediction

To perform prediction for a given PPFD_0 and T_{a_0}, m post burn-in samples of $\boldsymbol{\beta}$ and σ^2 were used as follows:

$$
\begin{aligned}
\mu_0^{(l)} &= \frac{1}{2\theta^{(l)}} \times \\
&\quad \left(\alpha^{(l)} \cdot \mathrm{PPFD}_0 + A_{\max}^{(l)} - \sqrt{(\alpha^{(l)} \cdot \mathrm{PPFD}_0 + A_{\max}^{(l)})^2 - 4\alpha^{(l)} \cdot A_{\max}^{(l)} \cdot \theta^{(l)} \cdot \mathrm{PPFD}_0}\right) \\
\nu_0^{(l)} &= r_0^{(l)} \times \exp\left(k_\mathrm{T}^{(l)} T_{\mathrm{a}_0}\right) \\
y_0^{(l)} &\sim N(\mu_0^{(l)} - \nu_0^{(l)}, \sigma^{2(l)}),
\end{aligned}
\tag{3.8}
$$

where (l) is not an exponent, but indicates a specific sample. Other terms are as defined for Eq. 3.6. The m samples were used to build up the posterior predictive distribution. In this way posterior predictions of GPP (μ_0) and NEE (y_0) were obtained. Note that the uncertainty in the posterior predictions of GPP arose due to uncertainty in the posterior estimates of $\boldsymbol{\beta}$. Uncertainty in the posterior prediction of NEE also considered the uncertainty arising due to the residual error.

Prediction was performed for each 10-day sample for $m = 30\,000$ samples (3 chains and 10 000 samples per chain). These were then summarized (median

and 95 % credible interval) to obtain the posterior predictive inference for NEE and GPP for each 10-day block. These 95 % credible intervals show the uncertainty. Hence the actual values of NEE and GPP are likely to be in this interval, but not necessarily at the median. We reported the number of half-hourly NEE measurements that lie inside and outside of 95 % credible intervals of the corresponding half-hourly modelled NEE distributions. In this way, we checked whether realistic credible intervals were obtained. Validation against a separate or hold-out dataset was in principle possible, but was not necessary in this study, because we did not use the NRH model to predict at blocks outside the range of the data. Moreover, we did not use the posterior $\boldsymbol{\beta}$ values outside the blocks where they were fitted.

3.3 Results and discussion

3.3.1 Performance of MCMC

We examined the trace plots of the three Markov chains for each β_i and τ_e obtained for each 10-day block for both choices of informative and non-informative prior distributions. Trace plots for one 10-day block (1 May to 10 May 2009) are shown in Fig. A3.3. We observed a proper mixing of the three Markov chains, indicating the convergence of three Markov chains to a stationary distribution that could be used for inference. The Gelman–Rubin PSRF was close to 1 (Table A3.1) for each β_i and τ_e, providing further support for the convergence of the Markov chains. The post burn-in samples were used for inference for each 10-day block in the growing season of 2009.

Fig. 3.2 shows the posterior prediction of half-hourly NEE for a 10-day block (1 May to 10 May 2009) for the choice of informative and non-informative prior distributions. The half-hourly NEE was summarized by the median and the 2.5 and 97.5 % iles (i.e., 95 % credible intervals). Out of 338 available half-hourly NEE measurements in this 10-day block, 6 % laid outside the 95 % credible intervals for both choices of prior distribution. This showed that the coverage of the 95 % credible interval was appropriate. There was no substantial difference in the shape of the percentiles curve between the choices of prior distribution. This indicated that the choice of informative or non-informative priors did not influence the posterior prediction of NEE. Similar results were observed for other 10-day blocks. Over the entire 2009 growing season 94 % of the 7126 available half-hourly NEE measurements were bracketed by the 95 % credible intervals for posterior predicted NEE. The choice of informative or non-informative priors did not lead to any substantial difference in the posterior predicted median or 95 % credible intervals.

The 10-day block shown in Fig. 3.2 shows that the posterior predicted median of NEE was positive during the day and negative during the night. This is to be expected owing to the lack of photosynthesis at night. However, at night the 95 % credible interval spanned zero implying that, when prediction uncertainty is considered, the actual predicted NEE *might* be positive. This is not possible physically, but is an artefact of the statistical approach. Since

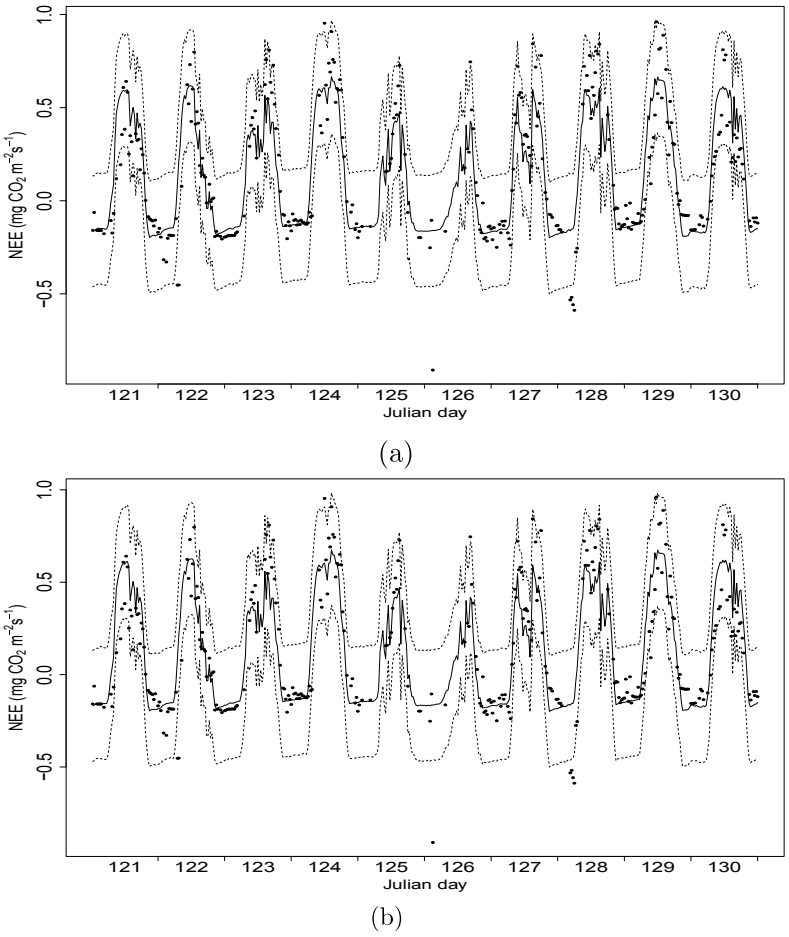

Figure 3.2 Median (solid lines) and 95 % credible intervals (dashed lines) of the posterior distribution of NEE together with half-hourly NEE measurements (solid points) for a 10-day block (1 May to 10 May 2009, Julian days 121 to 130): **(a)** when using informative prior distributions, **(b)** when using non-informative prior distributions.

this is a non-linear regression-type problem the uncertainty in the prediction arises due to both the uncertainty in the estimated regression parameters, $\boldsymbol{\beta}$ and the residual uncertainty. This residual uncertainty was assumed to follow a normal distribution with zero mean and precision, τ_e, and reflects the scatter of the observations round the posterior median prediction. Following our discussion above, this correctly represents the uncertainty in prediction. A consequence of this was that that the prediction intervals were wide and the predictions were potentially positive during the night. This could potentially be addressed by introducing further constraints into the model to allow τ_e to vary temporally (e.g., Hamm et al., 2012). We leave that as a topic for future research whilst noting that our dataset is not very large and we have already fitted a complicated model.

3.3.2 Uncertainty in partitioned GPP at half-hourly and daily time step

Fig. 3.3 shows the histograms of the posterior distribution of half-hourly and daily-summed GPP for Julian days 121 (1 May) and 196 (15 July) for the choice of both informative and non-informative prior distributions. These allow visualization of the uncertainty within a day and between days for late spring and mid-summer. Clearly the predictions resulting from informative and non-informative priors were similar. For both days higher values of GPP were observed in the afternoon compared to the morning on both Julian days. This reflected the increase in GPP predictions with increasing PPFD from morning to afternoon. The assimilation of carbon was also expected to increase from the start of the growing season to the peak (summer time) of the growing season. It was clear that higher values in GPP were predicted on Julian day 196 compared to Julian day 121 for both morning and afternoon. Seasonal variation in daily GPP was also observed in the daily sum of GPP, which increased from 7–9 $\mathrm{g\,C\,m^{-2}\,d^{-1}}$ on Julian day 121 to 10.5–12.5 $\mathrm{g\,C\,m^{-2}\,d^{-1}}$ on Julian day 196. Variation in daily GPP during the 2009 growing season for the choice of informative priors is shown in Fig 3.4. The same plot for the choice of non-informative priors is shown in Fig. A3.4.

We tested whether within the posterior half-hourly GPP distributions, the non-rectangular hyperbolic relationship of GPP with PPFD had been preserved. Fig. 3.5 shows, for an example 10-day block (Julian days 121–130), posterior GPP versus PPDF. The resulting curve shows that the non-rectangular hyperbolic relationship was indeed preserved, and GPP values initially rose and reached a plateau with increasing PPFD. This is important since our daily GPP estimates were obtained by summing half-hourly values. Since the range of PPDF values during the day is large and the relationship between PPFD and GPP non-linear, a realistic representation of the light response curve of GPP is important.

We concluded that the posterior predictions of half-hourly and daily GPP were reliable. We used the posterior distribution of the NRH parameters to predict half-hourly NEE and the 95 % credible intervals bracketed 94 % of the available half-hourly NEE measurements (Sect. 3.3.1 and Fig. 3.2). This indicated that our posterior predictions accurately captured the uncertainty in the measured NEE values. We used the same posterior distributions of the NRH parameters to estimate uncertainty in half-hourly GPP. Therefore, we expect that the underlying uncertainty in half-hourly GPP was also accurate.

3.3.3 Posterior distributions of $\boldsymbol{\beta}$

Figs. 3.6 and 3.7 show the temporal profile (mean and 95 % credible interval) for $\boldsymbol{\beta}$ for each 10-day block for informative and non-informative prior $\boldsymbol{\beta}$ distributions respectively.

A clear seasonal pattern in the posterior distribution of α and A_{max} was observed. When using non-informative priors, spikes in the 97.5 % iles for A_{max} were observed at 41, 47, and 59 $\mathrm{mg\,CO_2\,m^{-2}\,s^{-1}}$ (Fig. 3.7e) for three 10-day blocks (Julian days 91–100, 281–290, and 291–300). These values

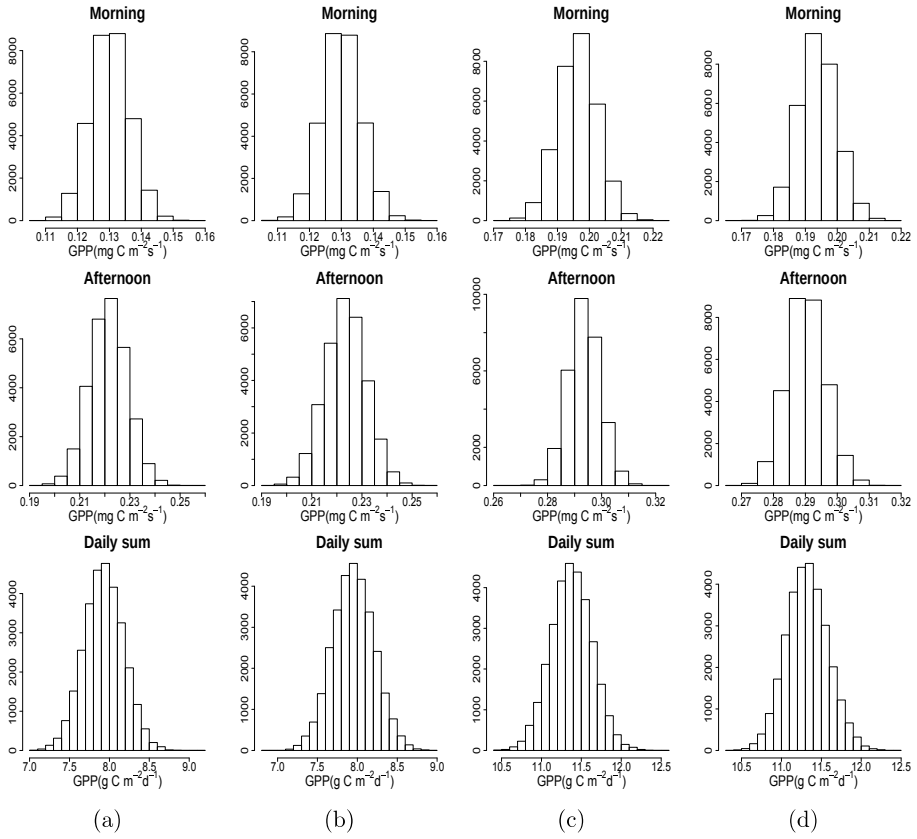

Figure 3.3 Histograms of half hourly GPP (Morning and afternoon) and daily sum of GPP when using: **(a)** informative priors on Julian day 121 (1 May 2009), **(b)** non-informative priors on Julian day 121, **(c)** informative priors on Julian day 196 (15 July 2009), **(d)** non-informative priors on Julian day 196. The morning and afternoon time belong to half-hour 8:00 CET to 8:30 CET and 13:00 CET to 13:30 CET respectively. The y axis is frequency; CET is Central European Time.

are physically unrealistic (see Sect. 3.2.4.2). When using informative priors, the same three 10-day blocks also showed spikes in the 97.5 % iles for $A_{\max}$ (Fig. 3.6e); however these spikes were much smaller and were physically realistic. For other 10-day blocks, both choices of prior yielded comparable posterior distributions of $A_{\max}$ (Figs. 3.6e and 3.7f) with uncertainty less than that of the informative and non-informative prior distributions (Fig. 3.1c and Sect. 3.2.4.1). The posterior distributions of α, r_0, and k_{T} were similar for both choices of prior distribution. The choice of non-informative prior yielded wider credible intervals for θ compared to the choice of informative priors (Figs. 3.6b and 3.7b).

We calculated the sum of daily GPP for each of the above mentioned 10-day blocks (91–100, 281–290, and 291–300) for both choices of prior (Fig. A3.5). We found no significant difference in the range of GPP for

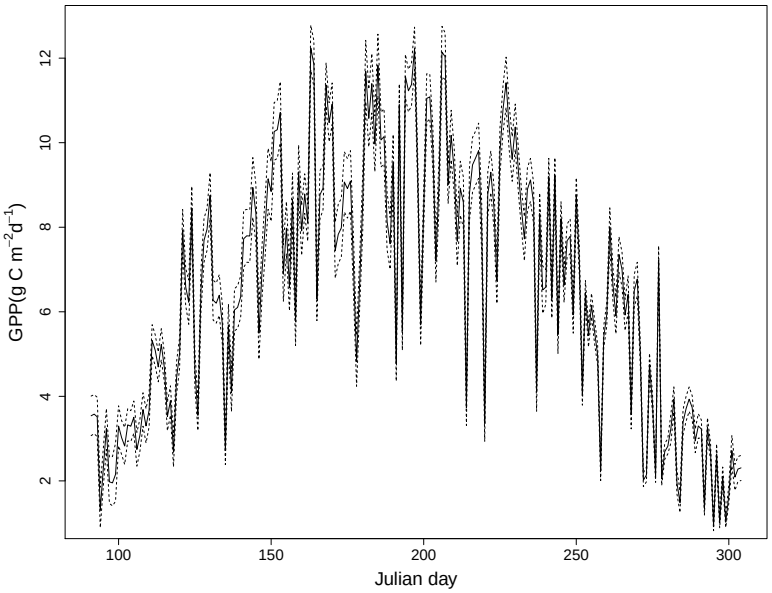

Figure 3.4 Median (solid line) and 95% credible intervals (dashed lines) of daily GPP distributions during the growing season of 2009 (1st April to 31st October 2009, Julian days 91 to 304) for the choice of informative prior distributions.

each block. For example, the range of daily-summed values for 10-day block 281–290 was 26–38 g C m^{-2} d^{-1} for both choices of prior. This indicated that the unrealistic spikes in the posterior distributions of $A_{\max}$ did not affect the prediction of GPP. This led us to evaluate the sensitivity of GPP to $A_{\max}$. We fixed the value of the NRH parameters α, θ, r_0, and k_{T} at their mean. We varied $A_{\max}$ from 0 to 100 mg CO_2 m^{-2} s^{-1} at an interval of 0.5. We estimated the value of GPP at each interval using Eq. 3.2. $A_{\max}$ was varied from 0 to 100 mg CO_2 m^{-2} s^{-1} so that it could cover the spikes in the posterior distributions of $A_{\max}$ (Fig. 3.7e).

The plot of $A_{\max}$ against GPP (Fig. 3.8) revealed that GPP varied strongly up to $A_{\max} = 5$ mg CO_2 m^{-2} s^{-1}. After this value GPP saturated. The underlying reason is the fact that in light limited conditions, i.e., $A_{\max} \gg \alpha \times$ PPFD, Eq. 3.2 reduces to $P_a = \alpha \times$ PPFD and hence P_a and thus GPP becomes independent of $A_{\max}$. This explains why the GPP posterior predictions were not affected by the unrealistic values of $A_{\max}$ occurring in periods of low light intensities. The choice of prior distribution therefore played a minimal role in the prediction of GPP. The use of informative priors, however, constrained the estimation of the posterior distributions of the parameters.

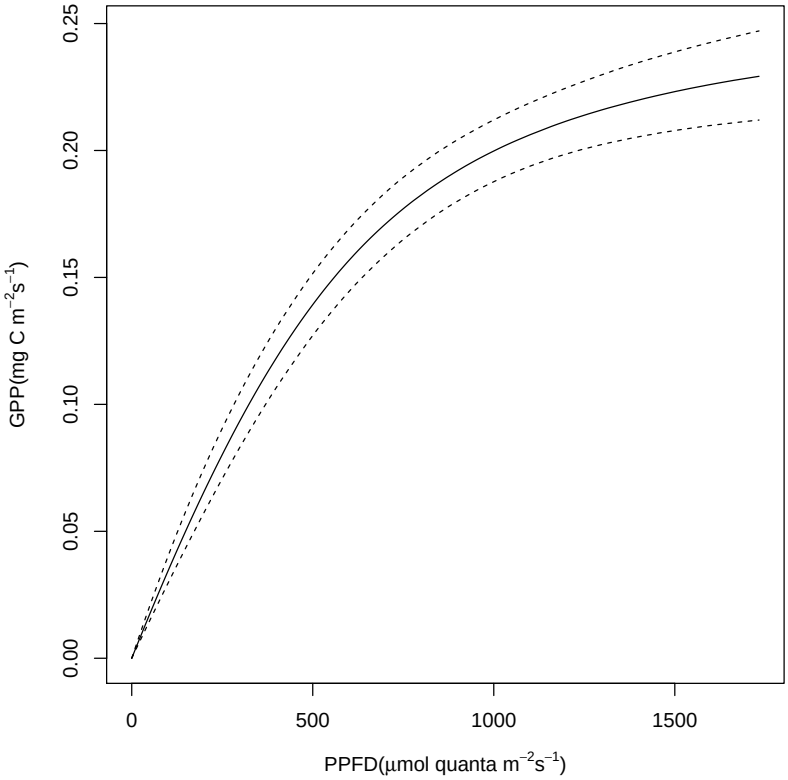

Figure 3.5 Median (solid line) and 95 % credible intervals (dashed lines) of half-hourly gross primary production (GPP) with photosynthetic photon flux density (PPFD) for a 10-day block (1 May to 10 May 2009, Julian days 121 to 130) for the choice of informative prior distributions.

3.3.4 Some issues and limitations of this study in estimating uncertainty using the NRH model

The Bayesian approach applied to the NRH model is a solid method to quantify the model parameters and their uncertainty. The 10-day block although suited for the purpose of this study, is insufficient to incorporate the effects of more rapid changes (day to day) in soil moisture and nutrient levels in the NRH model. In principle, these rapid changes could be incorporated by daily estimation of the NRH parameters (Aubinet et al., 2012; Gilmanov et al., 2013), although this could not be achieved in this study due to the lack of continuous high quality, half-hourly NEE data. The temporal variation in soil moisture and nutrient level for the study site should be investigated further. This may help to select an optimum block size where the within-block variation is limited. The availability of continuous high quality NEE data, however, may impose further constraints on the selection of an optimum block size.

The residual term ε_i in Eq 3.6 contains the model representation error and

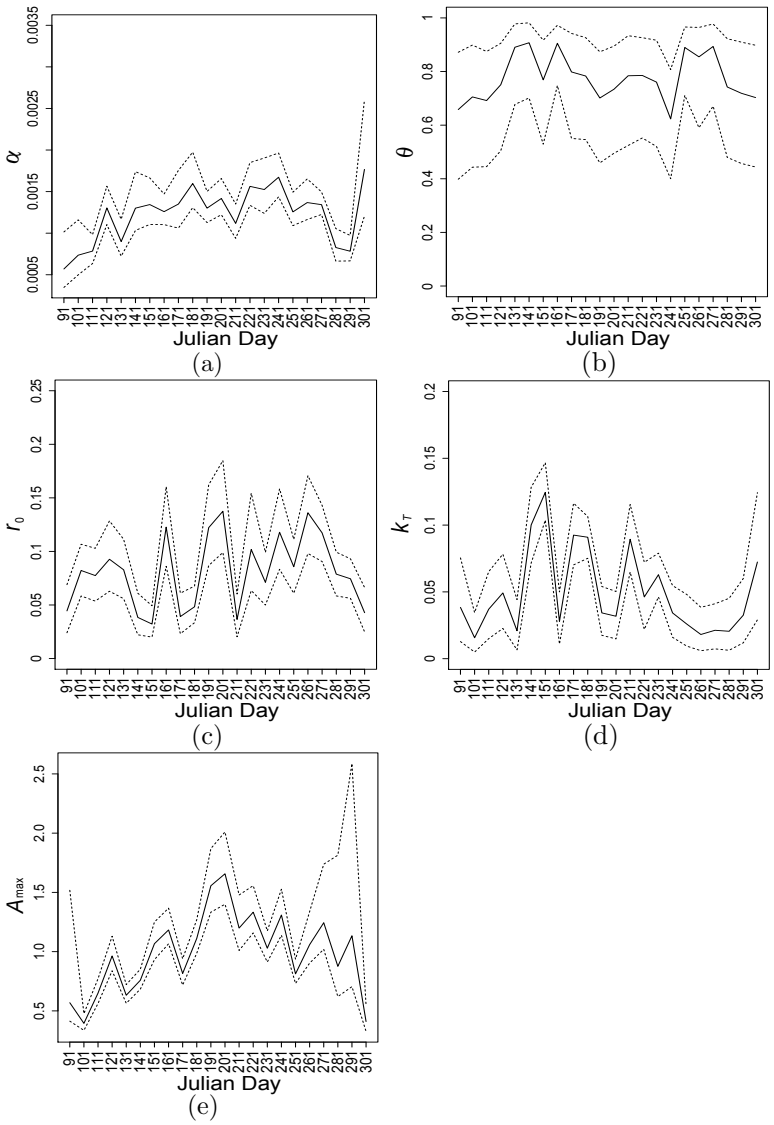

Figure 3.6 Median (solid lines) and 95 % credible intervals (dashed lines) of the posterior distributions of the NRH parameters when using informative prior distributions for each 10-day block during the growing season in 2009. The x axis is the first Julian day of each 10-day block. The y axis represents NRH parameter. Information about the NRH parameters is given in Table 3.1.

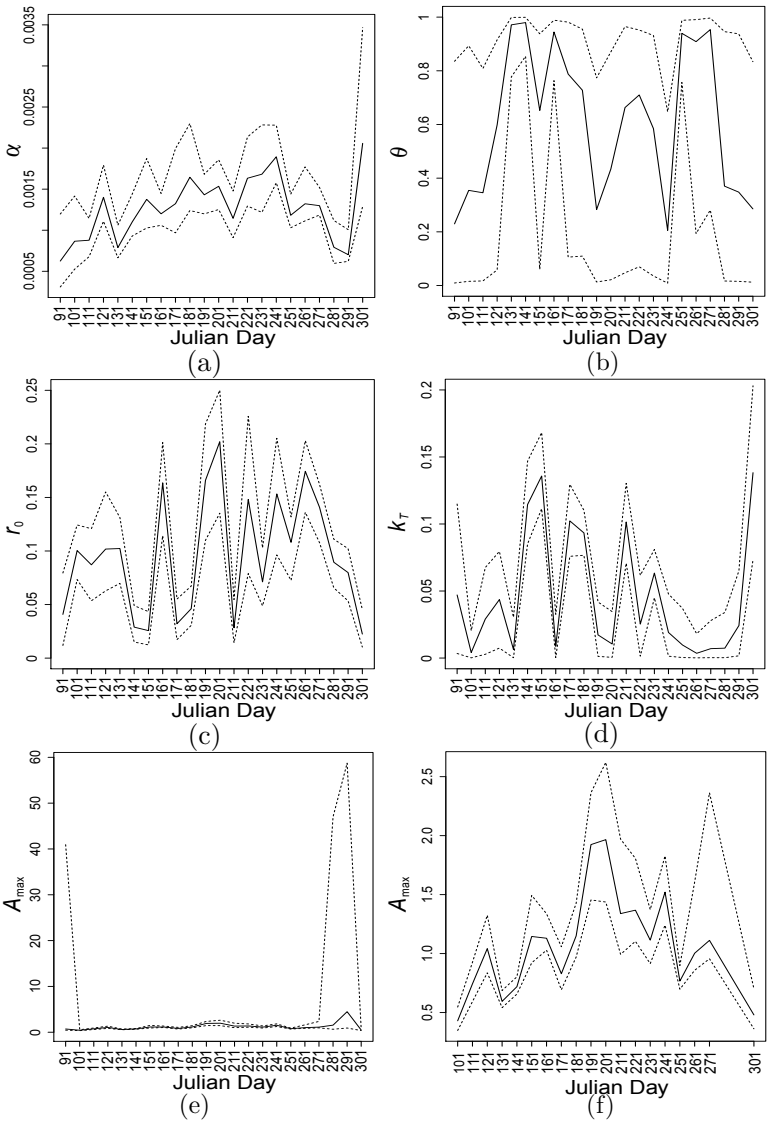

Figure 3.7 As Fig. 3.6 when using non-informative prior distributions. To help visualization of $A_{\max}$ we have added a subfigure **(f)** with the spikes removed (i.e., without the blocks of Julian days 91–100, 281–290, and 291–300).

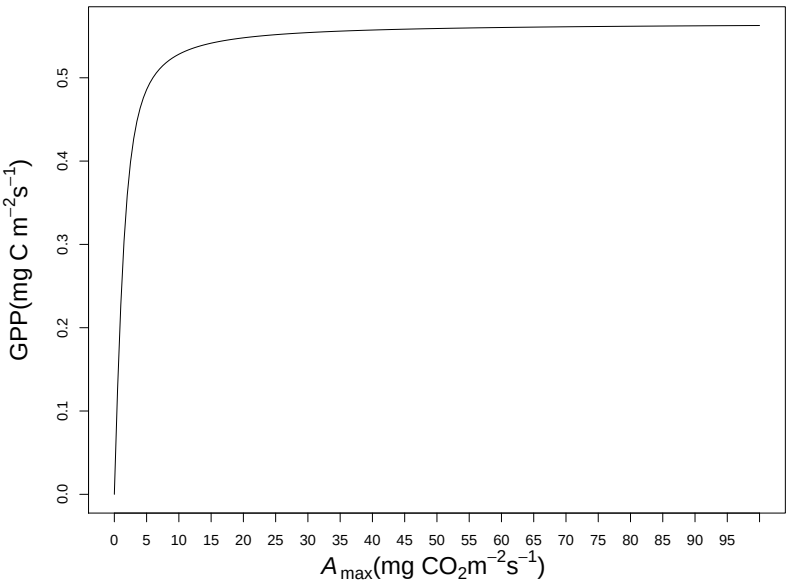

Figure 3.8 Variation of gross primary production (GPP) with the variation of photosynthetic capacity (A_{max}) from 0 to 100 $\mathrm{mg\,CO_2\,m^{-2}\,s^{-1}}$. The values of quantum yield (α), degree of curvature (θ), ecosystem respiration at reference temperature (r_0), and temperature sensitive paramete (k_{T}) are fixed at 0.7, 0.0022, 0.1, 0.07 respectively. Air temperature (T_{a}) and photosynthetic photon flux density (PPFD) are fixed at 10 °C and 900 $\mu\mathrm{mol\,quanta\,m^{-2}\,s^{-1}}$.

the random measurement error. We were unable to separate ε_i into these two components. It is possible to calculate the random measurement error using the paired-measurement approach (Richardson et al., 2006b). Richardson et al. (2008) compared the random measurement error in NEE to ε_i, and concluded that ε_i is mainly due to the random measurement error. We assumed the same to hold for our study, although we could not evaluate this using the paired-measurement approach. Model representation errors included, for example, the fact that we have not parameterized respiration separately for day and night, or separately for vegetation and soil. Vegetation respiration depends also upon other factors, such as irradiance (Sun et al., 2015), photorespiration (because it is nearly proportional to GPP) and produced CO_2 that remains in the trees (Teskey et al., 2008). It is not feasible to model all these processes separately. Thus our model can be expected to contain some representation errors.

Systematic errors also result in uncertainty in NEE measurements (Moncrieff et al., 1996; Aubinet et al., 2012). We have applied the Foken classification system (Sect. 3.2.1) to filter out the low quality NEE measurements that contain high systematic errors. This reduced the effect of systematic errors on the posterior prediction of NRH parameters and on the model residuals. A source of systematic error that we could not account for was storage of CO_2 below the measurement height during stable conditions at

night (Goulden et al., 1996). The turbulent mixing after sunrise may cause hysteresis in the light response curve between morning and late afternoon hours. This hysteresis will contribute to the scatter in the model fit, and thus to the uncertainty in the estimated parameters.

The implementation of the NRH model assumed that PPFD and T_a were known without error and all uncertainty was attributed to the response variable (NEE). This assumption is usual in statistical regression modelling, but is unlikely to be correct in this case. There is scope to incorporate information about uncertainty in PPFD and T_a, although this would lead to a more complicated model. Future research could examine whether relaxing this assumption would improve the model.

We focused in the growing season in 2009. This short period was chosen to illustrate the implementation of the Bayesian approach to quantify the uncertainty in half-hourly partitioned GPP using the NRH model. The study could be extended towards multiple years, allowing a multi-year comparison although that was outside the scope of our methodological focus. Further, different models have been investigated previously to partition GPP (Richardson et al., 2006a; Desai et al., 2008). Any model is a source of uncertainty in itself because it cannot account for every process. The scope of this study can therefore be further widened by addressing multiple established ways of partitioning GPP and thus analysing uncertainty associated with these.

Beer et al. (2010) partitioned GPP from NEE both using the rectangular hyperbola (RH) light-response curve (Lasslop et al., 2010) and a conventional night-time data based approach (Reichstein et al., 2005) for many FLUXNET sites, and further used the partitioned GPP to calibrate five highly diverse diagnostic models for GPP to produce the distribution of global GPP. Although the present study focused on better understanding the uncertainty in partitioning GPP using NRH light-response curve, future research can build on our findings and extend our approach to other sites and years.

3.4 Conclusions

The study concluded that the choice of informative and non-informative prior distributions of the NRH model parameters led to similar posterior distributions for both GPP and NEE. Obtaining informative priors is time consuming because the values of each parameter are not explicitly mentioned in the literature. Informative priors also require the acquisition of information on species or site specific values of photosynthetic capacity at light saturation (A_{max}) and ecosystem respiration at reference temperature (r_0) parameter. As an alternative, non-informative priors can be obtained with proper constraints using minimum information on the NRH parameters such as the positivity of A_{max}. Therefore, non-informative priors can be used for any species type irrespective of study sites. These findings are valuable to conduct uncertainty analysis across a larger sample of sites with different GPP characteristics, e.g., by obtaining NEE and other meteorological data from the FLUXNET data base. The downside of non-informative prior is the production of spikes

in the posterior of $A_{\max}$ for some days in this study. Therefore, if such values are of interest in a particular study (e.g., photosynthetic nitrogen use efficiency that relies on the ratio of $A_{\max}$ and leaf nitrogen) then informative prior should be used.

The estimates of the NRH model parameters were obtained for 10-day blocks. The values of the posterior parameters and their variation over time could provide further understanding of how the forest responds to factors not included in the model, such as soil moisture, nutrition or tree age.

Quantifying uncertainty estimates as empirical distributions in half-hourly gross primary production (GPP) was implemented in the Bayesian framework using the non-rectangular hyperbola (NRH) model. These uncertainty estimates were provided at daily time steps. The approach could be extended to include the uncertainty in meteorological forcing, in particular photosynthetic photon flux density and air temperature. The distributions in half-hourly GPP can be further used to obtain distributions at any desired time steps, such as 8-day and monthly. The uncertainty in GPP estimated in this study can be used further to quantify the propagated uncertainty in the validation of satellite GPP products such as MODIS 17 or process-based simulators such as BIOME-BGC. Although we focussed on quantifying the uncertainty in GPP partitioning, our approach could also be used to either estimate R_{eco} or fill missing NEE data and this will be achieved in the future study.

3.5 Appendices

Appendix A

Potential scale reduction factor

The Gelman-Rubin potential scale reduction factor (PSRF) diagnostic uses an analysis of variance approach to evaluate convergence (Brooks and Gelman, 1998). Let m be the number of Markov chains and n be the length of each chain. For a parameter β, the simulations can be labelled as $\beta_{ij}(i = 1, 2, ..., n; j = 1, 2, ..., m)$. Within-chain variance (W) is calculated as the mean of the variances of each chain as:

$$W = \frac{1}{m}\sum_{j=1}^{m} s_j^2, \text{ where } s_j^2 = \frac{1}{n-1}\sum_{i=1}^{n}(\beta_{ij} - \overline{\beta}_{.j})^2, \ \overline{\beta}_{.j} = \frac{1}{n}\sum_{i=1}^{n}\beta_{ij}. \quad \text{(A3.1)}$$

Between-chain variance (B) is based on $n \times m$ samples pooled together:

$$B = \frac{n}{m-1}\sum_{j=1}^{m}(\overline{\beta}_{.j} - \overline{\beta}_{..})^2, \text{ where } \overline{\beta}_{..} = \frac{1}{m}\sum_{j=1}^{m}\overline{\beta}_{.j}. \quad \text{(A3.2)}$$

The variance of the stationary distribution is estimated as a weighted average of W and B:

$$\widehat{\mathrm{Var}}(\beta) = \frac{n-1}{n}W + \frac{1}{n}B. \quad \text{(A3.3)}$$

The potential scale reduction factor (PSRF) is estimated as:

$$\widehat{R} = \sqrt{\frac{\widehat{\mathrm{Var}}(\beta)}{W}}. \quad \text{(A3.4)}$$

If the PSRF is close to 1, this can be concluded that each of m Markov chains of n simulated observations of β is close to the target distribution. For practical purpose the convergence is assumed if PSRF<1.05 (Lunn et al., 2000). We estimated PSRF for each non-rectangular hyperbola (NRH) parameter and precision of likelihood (τ_e) using CODA package (Plummer et al., 2015) for the R Programming Language and Environment (R Core Team, 2014). NRH parameters are degree of curvature (θ) , quantum yield (α), photosynthetic capacity at light saturation (A_{max}), ecosystem respiration at reference temperature (r_0),and temperature sensitive parameter (k_T).

The PSRF is estimated with uncertainty as Markov chain lengths are finite, therefore CODA package reports the lower (50%) and the upper (97.5%) quantiles of PSRF for each NRH parameter.

Gelman-Rubin-Brooks plot to identify burn-in period

Gelman-Rubin-Brooks (GRB) plot shows the evolution of PSRF as the number of iterations increases(Brooks and Gelman, 1998). We identified the appropriate length of the burn-in for both informative and non-informative prior distributions using the following steps:

1. We generated three Markov chains for each 10-day block. Trace plots of each β_i were generated by WinBUGS and were examined to evaluate whether the Markov chains converged approximately.
2. The Gelman-Rubin-Brooks (GRB) plot was then generated for each NRH parameter and τ_e to diagnose the convergence. The GRB plot was generated using he CODA package. Markov chains were divided into bins. The first bin contained samples from 1:50 iterations, the second bin from 1:50+n ($n = 10$ in CODA), the third contains sample from 1:(50+2n) and so on. The lower (50%) and the upper (97.5%) quantiles of Gelman-Rubin potential scale reduction factor (PSRF) or shrink factor (Eq. A3.4) is calculated for each bin and for each NRH parameter and τ_e that is plotted against bins to generate the GRB plot. A convergence is diagnosed if both quantiles approach 1 ($1 \leq \text{PSRF} \leq 1.05$). We analysed all 154 GRB plots (22 10-day blocks $\times$ 7 estimated parameters) for both informative and non-informative priors.
3. For each GRB plot, we identified the number of iterations after which the lower and upper quantiles of PSRF become close to 1. The number of iterations varied from 500 to 6000 when informative priors were used and from 2000 to 15000 when non-informative priors were used. We adopted the upper limits 6000 and 15000 as burn-in periods to ensure that Markov chains converged to stationary distributions for any NRH parameter and τ_e and for any 10-day block.

We presented below the GRB plot of each NRH parameter only for that 10 days block where we identified the maximum number of iterations for the convergence. Fig. A3.1 shows the GRB plots in the case of informative prior distributions of the NRH parameters. It can be observed that 50^{th} (median) and 97.5^{th} percentile of PSRF become close to 1 ($1 \leq \text{PSRF} \leq 1.05$) after 6000 iterations for the NRH parameters α and θ ("theta" and "alfa" respectively in the figure). This shows the convergence of Markov chains after 6000 iterations. For other NRH parameters, Markov chains converge before 6000.

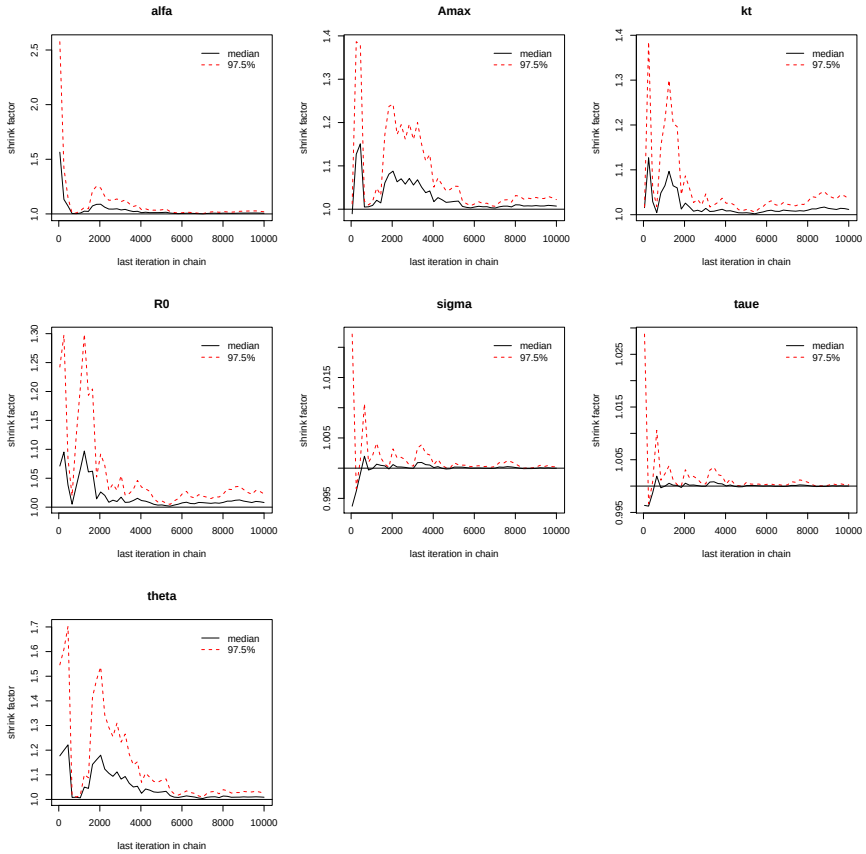

Figure A3.1 Gelman-Rubin-Brooks (GRB) plot of each NRH parameter for 8^{th} September to 17^{th} September 2009 (Julian days 251 to 260) for the choice of informative prior distributions. "alfa","Amax","kt","R0",and "theta" correspond to α, θ, A_{max}, r_0, k_{T}, and τ_{e} respectively. "sigma" and "taue" correspond to standard deviation (σ) and precision (τ_{e}) of the normal distribution of likelihood. Note that $\tau_e = 1/\sigma^2$. Information about the NRH parameters is given in Table 3.1.

Fig. A3.2 shows the GRB plots in the case of non-informative prior distributions of the NRH parameters. It can be observed that 50^{th} (median) and 97.5^{th} percentile of PSRF become close to 1 ($1 \leq \text{PSRF} \leq 1.05$) after 15000 iterations for the NRH parameter θ ("theta" in the figure). This shows the convergence of Markov chains after 15000 iterations. For other NRH parameters, Markov chains converge before 15000.

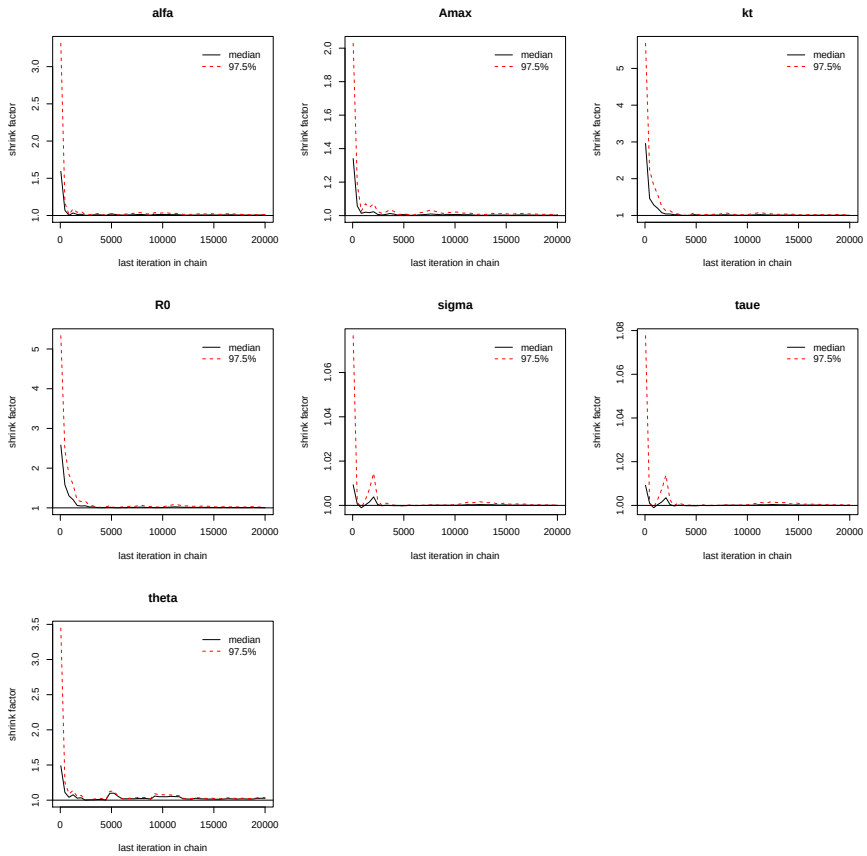

Figure A3.2 Gelman-Rubin-Brooks (GRB) plot of each non-rectangular hyperbola (NRH) parameter for 21^{st} May to 30^{th} September 2009 (Julian days 141 to 150) for the choice of non-informative prior distributions. "alfa","Amax","kt","R0",and "theta" correspond to α, θ, A_{max}, r_0, k_T, and τ_e respectively. "sigma" and "taue" correspond to standard deviation (σ) and precision (τ_e) of the normal distribution of likelihood. Note that $\tau_e = 1/\sigma^2$. Information about the NRH parameters is given in Table 3.1.

Trace plots for the NRH parameters after burn-in periods

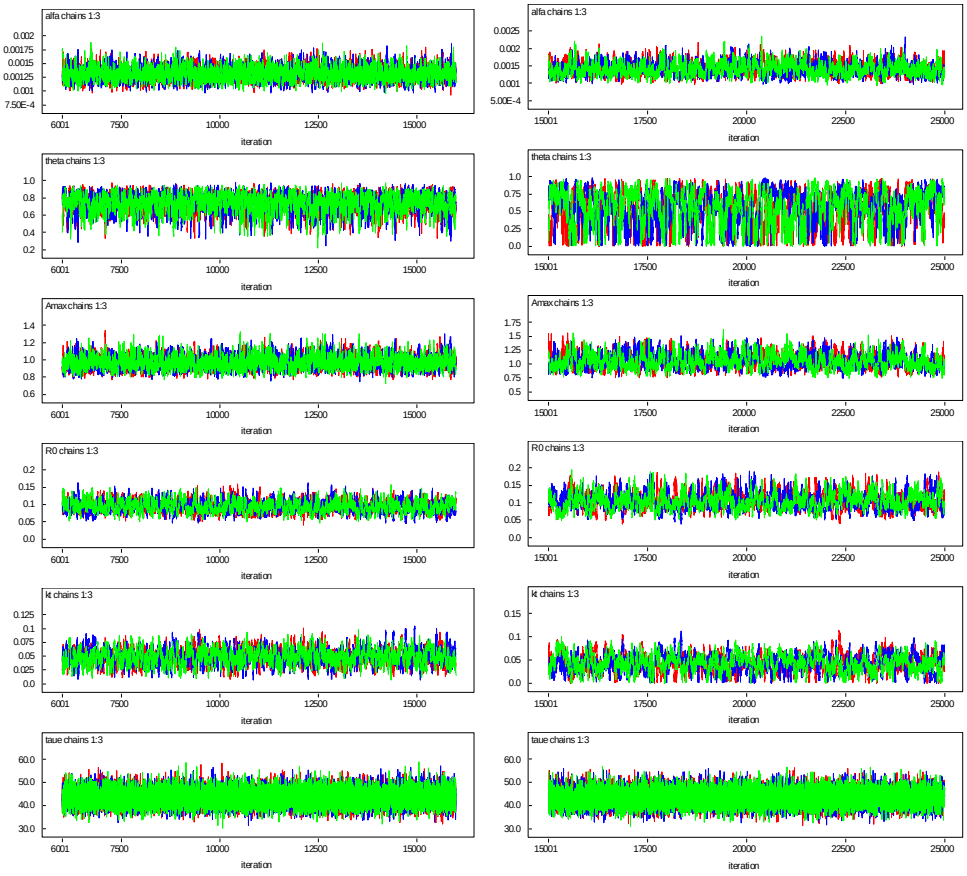

a Trace plots for informative prior distributions **b** Trace plots for non-informative prior distributions

Figure A3.3 Trace plots of three Markov chains of 10000 post burn-in iterations for each NRH parameter and precision of τ_e for a 10-day block (1^{st} May to 10^{th} May 2009, Julian days 121 to 130). alfa, theta, Amax, R0, kt, and taue correspond to α, θ, A_{max}, r_0, k_T and τ_e respectively. Information about the NRH parameters is given in Table 3.1.

PSRF for the NRH parameters after burn-in period

Table A3.1 50 and 97.5 percentile of potential scale reduction factor (PSRF) calculated for quantum yield (α), degree of curvature (θ) , photosynthetic capacity at light saturation (A_{max}), ecosystem respiration at reference temperature (r_0),and temperature sensitive parameter (k_{T}) and precision of likelihood (τ_{e}) after burn-in period for the choice of informative and non-informative prior distributions for a 10-day block (1^{st} May to 10^{th} May 2009, Julian days 121 to 130).

	Informative prior distributions		Non-informative prior distributions	
	50%	97.5%	50%	97.5%
α	1.00	1.00	1.00	1.01
θ	1.00	1.00	1.00	1.01
A_{max}	1.00	1.00	1.00	1.00
r_0	1.00	1.00	1.00	1.00
k_{T}	1.00	1.00	1.00	1.00
τ_{e}	1.00	1.00	1.00	1.00

Variation in daily gross primary production (GPP) during growing season

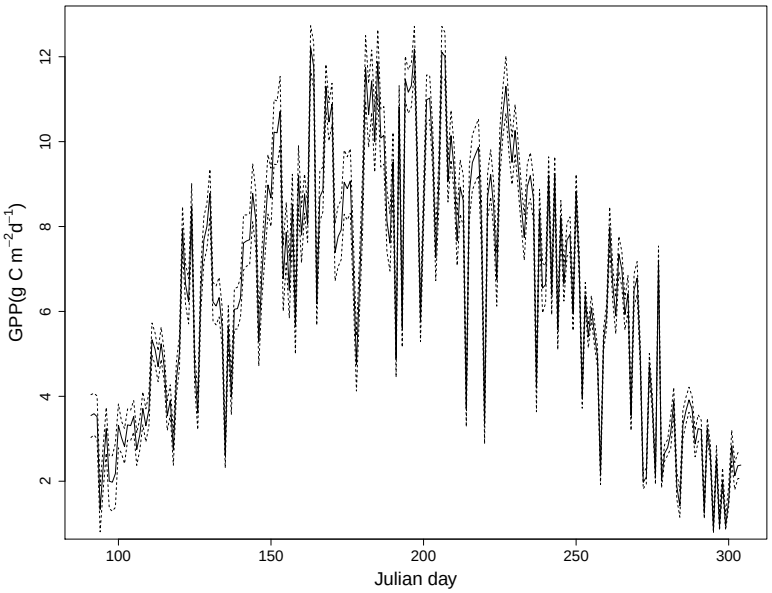

Figure A3.4 Median (solida line) and 95% credible intervals (dashed lines) of daily GPP distributions during the growing season of 2009 (1^{st} April to 31^{st} October 2009, Julian days 91 to 304) for the choice of non-informative prior distribution.

Histogram of 10 days sum of daily GPP

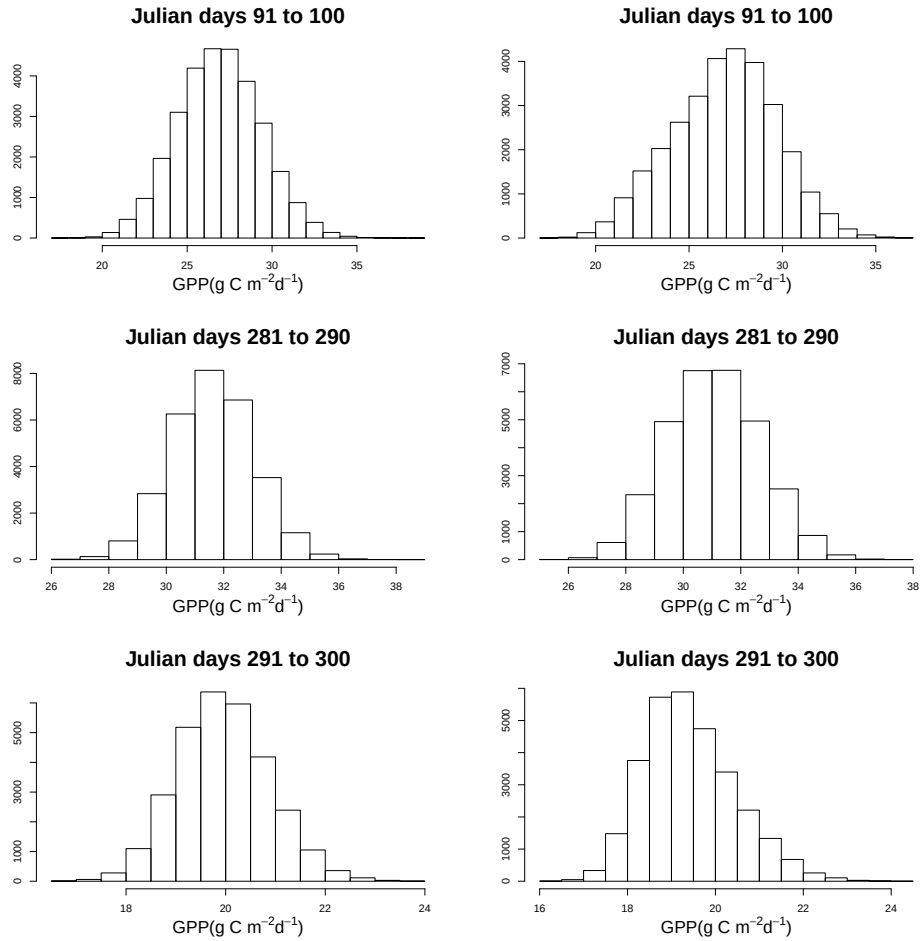

a For informative prior distributions **b** For non-informative prior distributions

Figure A3.5 Distributions of sum of daily GPP for each of three 10-day blocks 91-100, 281-290, and 291-300.

Appendix B: Model file for WinBUGS

Model file specification for informative prior distributions of non-rectangular hyperbola (NRH) model parameters:

```
model
{
for(i in 1:n)
{
## normal distribution on likelihood with precision ''taue'' (τe).
y[i] ~ dnorm(mu[i], taue)
## likelihood
mu[i] <-(0.5/theta)*(alfa*x1[i]+Amax-sqrt(pow((alfa*x1[i]+
Amax),2)-4*alfa*Amax*theta*x1[i]))-R0*exp(kt*x2[i])
}
## gamma distribution on ''taue''
taue ~ dgamma(0.001,0.001)
## calculation of standard deviation ''sigma'' from precision ''taue''
sigma <- 1/sqrt(taue)
## informative priors of NRH parameters
alfa ~ dnorm(0.0022,2295684.114)
theta ~ dbeta(10,3)
Amax ~ dgamma(4,2.5)
kt ~ dgamma(4,120)
R0 ~ dbeta(2,64)
}
```

Model file specification for non-informative prior distributions of NRH model parameters:

```
model
{
for(i in 1:n)
{
y[i] ~ dnorm(mu[i], taue)
mu[i] <-(0.5/theta)*(alfa*x1[i]+Amax-sqrt(pow((alfa*x1[i]+
Amax),2)-4*alfa*Amax*theta*x1[i]))-R0*exp(kt*x2[i])
}
taue ~ dgamma(0.001,0.001)
sigma <- 1/sqrt(taue)
## non-informative priors of NRH parameters with constraints
alfa ~ dnorm(0,0.001)I(0,)
theta ~ dnorm(0,0.001)I(0,1)
Amax ~ dnorm(0,0.001)I(0,)
kt ~ dnorm(0,0.001)I(0,)
```

```
R0 ~ dnorm(0,0.001)I(0,)
}
```

Where n is number of data points, y is half-hourly NEE data, x1 is half-hourly photosynthetic photon flux density (PPFD), x2 is half-hourly air temperature (T_a). alfa, theta, Amax, kt, and R0 correspond to NRH parameter α (quantum yield), θ (degree of curvature), A_{max} (photosynthetic capacity), r_0 (ecosystem respiration at reference temperature), k_T (temperature sensitive parameter) respectively.

Bayesian integration of flux tower data into BIOME-BGC

4

This chapter has been published as a discussion paper: Raj, R., Hamm, N. A. S., van der Tol, C., Stein, A., 2016. Bayesian integration of flux tower data into process-based simulator for quantifying uncertainty in simulated output. Geoscientific Model Development Discussion, 1-32, doi:10.5194/gmd-2016-216.

Abstract

Parameters of a process-based forest growth simulator are difficult or impossible to obtain from field observations. Reliable estimates can, however, be obtained using calibration against observations of output and state variables. In this study, we present a Bayesian framework to calibrate the widely used process-based simulator BIOME-BGC against estimates of gross primary production (GPP) data. We used GPP partitioned from flux tower measurements of a net ecosystem exchange over a 55 year old Douglas fir stand as an example. The uncertainties of both the BIOME-BGC parameters and the simulated GPP were estimated. The calibrated parameters leaf and fine root turnover (LFRT), ratio of fine root carbon to leaf carbon (FRC:LC), ratio of carbon to nitrogen in leaf ($C:N_{leaf}$), canopy water interception coefficient (W_{int}), fraction of leaf nitrogen in Rubisco (FLNR), and soil rooting depth (SD) characterize the photosynthesis and carbon and nitrogen allocation in the forest. The calibration improved the root mean square error and enhanced Nash-Sutcliffe efficiency between simulated and flux tower daily GPP compared to the uncalibrated BIOME-BGC. Nevertheless, the seasonal cycle for flux tower GPP was not reproduced exactly, and some overestimate in spring and underestimates in summer remained after calibration. Further analysis showed that, although simulated GPP was time dependent due to carbon allocation, it still followed the variability of the meteorological forcing closely. We hypothesized that the phenology exhibited a seasonal cycle that was not accurately reproduced by the simulator. We investigated this by allowing the parameter values to vary month-by-month. Time varying parameters substantially improved the simulated GPP as compared to GPP obtained with constant parameters. The time varying estimation also revealed a seasonal change in parameter values that determine phenology, and in parameters that determine soil water availability. It was concluded that Bayesian calibration approach can reveal features of the modelled physical processes, and identify aspects of the process simulator that are too rigid.

Keywords: Process-based simulator, BIOME-BGC, gross primary production, Bayesian calibration, uncertainty estimation.

4.1 Introduction

Forest ecosystems play an important role in the global carbon cycle by controlling atmospheric CO_2 level. Knowledge of gross primary production (GPP) for forest ecosystems is indispensable for the estimation of forest carbon storage. Process-based forest simulators (PBS) evaluate forest ecosystem activity by simulating different physiological plant responses to climatic conditions, atmospheric properties and plant structures (Constable and Friend, 2000; Running, 1994).

A PBS requires input parameters that distinguish different vegetation types by their physiological and morphological characteristics. Implementation of a PBS for specific sites is complicated by the large number of parameters for plants, the soil and the atmosphere. Field measurements of PBS parameters are difficult or impossible leading to incomplete knowledge of site specific parameters for the occurring species. In practice practitioners often rely on the literature for values of the PBS parameters (Mäkelä et al., 2000; Hartig et al., 2012).

A systematic adjustment of PBS parameters are required within the margins of the uncertainty so that the simulated outputs (e.g., GPP) satisfy pre-agreed criteria. This adjustment of a simulator parameters is called calibration. Calibration is often performed to obtain single optimized values of the parameters without the quantification of uncertainty in the parameters and the simulated outputs. Quantification of uncertainty is important for both scientific and practical purposes (Bastin et al., 2013; He et al., 2014; Hamm et al., 2015b).

The Bayesian framework provides a coherent method for calibrating a PBS (van Oijen et al., 2005; Reinds et al., 2008; van Oijen et al., 2011) and involves the identification of uncertainty in the parameters from the available information. This uncertainty is expressed as the prior probability distributions of the parameters. Independent observations of the variables corresponding to the PBS outputs (e.g., GPP) are used to update the prior probability distributions by means of Bayes rule. This updating generates the posterior probability distributions of the parameters, which can be summarized as medians and 95% credible intervals as the quantification of uncertainty. Hence the Bayesian framework combines prior probability distributions of the parameters and the observations to quantify uncertainty in the parameters and the PBS outputs.

In this study, a widely used simulator BIOME-BGC (Thornton, 1998) was calibrated in a Bayesian framework for the single output variable, GPP. A systematic search of the literature was used to construct the prior probability distributions on the BIOME-BGC parameters (Raj et al., 2014). A time series of daily flux tower GPP, which had been partitioned from the flux tower measurements of net ecosystem exchange, provided independent observations of GPP (Raj et al., 2016). We used flux tower GPP to update the priors of BIOME-BGC parameters. BIOME-BGC simulates GPP at daily time-step and it updates its memory between days (White et al., 2000; Thornton, 2010). This memory corresponds to the mass (amount of carbon) stored in different components of the vegetation, litter, and soil. This study further

investigated the effect of BIOME-BGC memory to reproduce the seasonal cycle of GPP by means of Bayesian calibration.

The objective of this study was to quantify the uncertainty in BIOME-BGC input parameters and simulated GPP by integrating flux tower GPP into BIOME-BGC in a Bayesian framework. We obtained the posterior BIOME-BGC parameters: (a) that do not vary over the entire study period; and (b) that vary at the monthly time-steps. The monthly variation in posterior parameters allowed us to 'overrule' the simulated mass storage by those of a simulation with different parameter values. This enabled us to evaluate which part of the memory of the BIOME-BGC needs improvement.

4.2 Site description

Calibration of BIOME-BGC was performed at the Speulderbos forest site, which is located at $52^o15'08''$ N, $05^o41'25''$ E within a large forested area in the Netherlands. There is a flux tower within a dense 2.5 ha Douglas fir stand, which is a type of evergreen needleleaf species. The stand was planted in 1962. The vegetation, soil, and climate of this site have been thoroughly described elsewhere (Steingrover and Jans, 1994; van Wijk et al., 2001; Su et al., 2009; Raj et al., 2014).

4.3 Methods

4.3.1 Data and simulators

4.3.1.1 The BIOME-BGC simulator

BIOME-BGC simulates biogeochemical processes including carbon, water and nitrogen fluxes within the vegetation, litter and soil compartment of terrestrial ecosystem at a daily time steps (Running and Hunt, 1993; Thornton et al., 2002). Evapotranspiration (ET), photosynthesis and respiration (autotrophic and heterotrophic) are the main processes simulated by BIOME-BGC. Simulation of daily ET is based on the Penman-Monteith equation (McNaughton and Jarvis, 1983; Monteith and Unsworth, 2008), which simulates ET as a function of incoming radiation, vapour pressure deficit (VPD) and the conductance associated with the evaporative surface. The photosynthetic routine uses Farquhar's biochemical model to estimate GPP (Farquhar et al., 1980; Thornton et al., 2002), which is the overall fixation of carbon. GPP is estimated independently for the sunlit and shaded canopy fractions. Final GPP is the sum of the contributions of the sunlit and shaded canopy fractions. GPP is a function of temperature, vapour pressure deficit, soil water content, solar radiation, atmospheric CO_2 concentration, leaf area index and leaf nitrogen concentration (Churkina and Running, 1998). The photosynthesis routine adds carbon to the system, which is removed from the system through respiration. Respiration routine computes autotrophic respiration as the sum of maintenance and growth respiration. Maintenance respiration is calculated as a function of leaf and root nitrogen concentration and tissue temperature.

Growth respiration is the proportion of total new carbon allocated to growth. Heterotrophic respiration is the release of carbon through the process of decomposition of both litter and soil.

BIOME-BGC requires site characteristics, daily meteorological data, and ecophysiological parameters as inputs. The site characteristics include soil texture (percentage of sand, silt, and clay), elevation, latitude, shortwave albedo, wet and dry atmospheric deposition of nitrogen, symbiotic and asymbiotic fixation of nitrogen, and the effective soil rooting depth. We took the site characteristics data at Speulderbos from Raj et al. (2014). The meteorological data include daily minimum temperature (Tmin), daily maximum temperature (Tmax), the average daytime temperature (Tday), daily total precipitation, the daylight average shortwave radiant flux density (srad), the daylight average vapour pressure deficit (VPD) and the daylength from sunrise to sunset. We collected half-hourly temperature, prcp, srad, and relative humidity (RH) for each day in 2009 from the Speulderbos flux tower and daily values were obtained by the half hourly measurements. We derived VPD from relative humidity (RH) using the procedure described in Monteith and Unsworth (1990). BIOME-BGC requires 35 ecophysiological parameters for evergreen needleleaf forest/species (Table 4.1) and we obtained the prior uncertainty (expressed as a probability distribution) in each parameter for Speulderbos from Raj et al. (2014).

4.3.1.2 Flux tower GPP data

We used daily observed data of net ecosystem exchange NEE to predict GPP at Speulderbos for the growing season (April to October) of 2009. To predict GPP, half-hourly GPP were separated from flux tower measurements of half-hourly net ecosystem exchange at Speulderbos site using non-rectangular hyperbola (NRH) model (Gilmanov et al., 2003). The estimation of the NRH model parameters was performed in a Bayesian framework that yielded posterior distributions of the NRH parameters and posterior predictions of GPP and its associated uncertainty (see Raj et al., 2016, for details). NEE was measured every half hour, leading to half-hourly predictions of GPP. These half-hourly values were summed to yield daily values of GPP and its associated uncertainty.

4.3.2 Bayesian modelling

4.3.2.1 Bayes rule

Bayesian calibration begins with Bayes rule (Gelman et al., 2013):

$$p(\boldsymbol{\theta}|\mathbf{z}) = \frac{p(\mathbf{z}|\boldsymbol{\theta})p(\boldsymbol{\theta})}{p(\mathbf{z})} \propto \text{likelihood} \times \text{prior}. \tag{4.1}$$

The terms in Eq. 4.1 are:

- $p(\boldsymbol{\theta})$ is the prior probability density function (pdf) of the PBS parameters (e.g., FLNR, soil depth), contained in the vector $\boldsymbol{\theta}$;

- $p(\mathbf{z}|\boldsymbol{\theta})$ is the conditional probability of observing the data $\mathbf{z}$ given $\boldsymbol{\theta}$ and is called the likelihood function. The vector $\mathbf{z}$ contains the independent observations of GPP, separated from NEE (see Sect. 4.3.1.2);
- $p(\mathbf{z})$ is the normalization constant, which is independent of $\boldsymbol{\theta}$;
- $p(\boldsymbol{\theta}|\mathbf{z})$ is the posterior pdf of $\boldsymbol{\theta}$ given the observed data.

The likelihood function is determined by the probability distribution of the residuals $\mathbf{e} = (e_1, e_2, ..., e_n)$, which are the difference between $\mathbf{y} = (y_1, y_2, .., y_n)$ and $p(\mathbf{z})$:

$$e_t = z_t - y_t, \quad t = 1, 2, ..., n \tag{4.2}$$

where $\mathbf{y}$ denotes the simulated GPP (i.e., the output from the PBS). The residuals include the observation error and the simulator inadequacy, which arises due to the fact that the simulated output does not represent the true value of the process even if $\boldsymbol{\theta}$ are known with no uncertainty (Kennedy and O'Hagan, 2001).

The posterior pdf in Eq. 4.1 cannot be obtained analytically for most practical problems. Inference is performed using the unnormalized density (Gelman et al., 2013) using Markov chain Monte Carlo (MCMC) simulation (Metropolis et al., 1953; Hastings, 1970; Gelfand and Smith, 1990; Vrugt et al., 2009; Gelman et al., 2013; Vrugt, 2016), as described in Sect. 4.3.2.2.

4.3.2.2 DiffeRential Evolution Adaptive Metropolis (DREAM)

We adopted the DREAM algorithm proposed by Vrugt et al. (2008, 2009) to implement MCMC. DREAM stands for DiffeRential Evolution Adaptive Metropolis. DREAM runs N different Markov chains in parallel for each θ_j. Let the vector of simulator parameters $\boldsymbol{\theta} = (\theta_1, \theta_2, \theta_3, ..., \theta_d)$. The current state of the i^{th} chain is given by single d-dimensional parameter vector $\boldsymbol{\theta}^{(i)}$. The N Markov chains make N such vectors $\boldsymbol{\theta}^{(1)}$, $\boldsymbol{\theta}^{(2)}$,....., $\boldsymbol{\theta}^{(N)}$. The following steps explain briefly the DREAM algorithms.

1. For each chain i ($i = 1, 2, ..., N$), an arbitrary starting point $\boldsymbol{\theta}^{(i)}$ from the prior pdf of the parameters are sampled.
2. A simulator is run at the starting points and and the likelihood $p(\mathbf{z}|\boldsymbol{\theta}^{(i)})$ ($i = 1, 2, ..., N$) is obtained. The density $p(\boldsymbol{\theta}^{(i)}|\mathbf{z})$ is then obtained for each chain:

$$\begin{aligned} p(\boldsymbol{\theta}^{(i)}|\mathbf{z}) &= p(\boldsymbol{\theta}^{(i)}) \times p(\mathbf{z}|\boldsymbol{\theta}^{(i)}) \\ &= \left\{ p(\theta_1^{(i)}) \cdot p(\theta_2^{(i)}) \cdot .... \cdot p(\theta_d^{(i)}) \right\} \times p(\mathbf{z}|\boldsymbol{\theta}^{(i)}) \end{aligned} \tag{4.3}$$

   The choice of likelihood and prior pdf of $\boldsymbol{\theta}$ for BIOME-BGC are explained in Sect. 4.3.3.2 and 4.3.3.1.
3. For i = 1,2,3,.....,N:
   a) A candidate point $\boldsymbol{\theta}^{(i)*}$ in chain i is generated from the randomly chosen pairs of chains:

$$\boldsymbol{\theta}^{(i)*} = \boldsymbol{\theta}^{(i)} + (\mathbf{1}_d + \boldsymbol{\lambda}_d)\gamma(\delta, d) \left(\sum_{k=1}^{\delta} \boldsymbol{\theta}^{(k)} - \sum_{l=1}^{\delta} \boldsymbol{\theta}^{(l)} \right) + \boldsymbol{\zeta}_d \tag{4.4}$$

and

$$\gamma = 2.38/\sqrt{2\delta d}$$

where δ is the number of chain pairs used to generate the candidate point, $\boldsymbol{\theta}^{(k)}$ and $\boldsymbol{\theta}^{(l)}$ are randomly selected from the state of other chains; $k, l \in (1, 2, .., N)$ and $k \neq l \neq i$. The values of $\boldsymbol{\lambda}_d$ and $\boldsymbol{\zeta}_d$ are sampled from the uniform distribution $U(-b, b)$ and the normal distribution $\mathcal{N}(0, c)$ respectively. The typical default values of $\delta = 3$, $b = 1$, and $c = 10^{-6}$. γ is the jump-size, whose value depends on δ and d. DREAM implements a randomized subspace sampling, i.e., all dimensions of $\boldsymbol{\theta}^{(i)}$ are not updated jointly and some dimensions of $\boldsymbol{\theta}^{(i)*}$ are reset to those of $\boldsymbol{\theta}^{(i)}$. The value of γ is, therefore, obtained with d', the number of dimensions updated jointly.

b) The simulator is run at the candidate point $\boldsymbol{\theta}^{(i)*}$ and the density $p(\boldsymbol{\theta}^{(i)*}|\mathbf{z}) = p(\boldsymbol{\theta}^{(i)*}) \times p(\mathbf{z}|\boldsymbol{\theta}^{(i)*})$.

c) The Metropolis ratio is given as $p(\mathbf{z}|\boldsymbol{\theta}^{(i)*})/p(\mathbf{z}|\boldsymbol{\theta}^{(i)})$

d) The candidate point $\boldsymbol{\theta}^{(i)*}$ is accepted if the Metropolis ratio is larger than an acceptance criterion, which is a random number generated from the uniform distribution between 0 and 1. This may allow acceptance of $\boldsymbol{\theta}^{(i)*}$ with a lower likelihood than the current candidate point.

e) If the candidate point is accepted: $\boldsymbol{\theta}^{(i)} = \boldsymbol{\theta}^{(i)*}$, otherwise it remains at $\boldsymbol{\theta}^{(i)}$.

4. All N Markov chains evolve in parallel for T times by repeating Step 3. In order to perform inference using the Markov chains it is important that the chains have converged to a stationary distribution that is independent of their initial values. This is evaluated using diagnostic statistics and diagnostic plots, as described in Sect. 4.3.3.3. Unconverged chains chains are discarded as "burn-in" and the post burn-in samples are then used to conduct inference on each θ_j. The post burn-in samples are then used to conduct inference on each θ_j. For example median and 95 % credible interval can be obtained over these samples. A simulator is run on the posterior distributions of $\boldsymbol{\theta}$ to get the uncertainty in the simulated output (e.g., GPP for BIOME-BGC).

   The choice of N, T, and burn-in period are discussed in Sect. 4.3.3.3. The convergence diagnostic of Markov chains are also explained further in Sect. 4.3.3.3.

4.3.3 Implementation of DREAM for BIOME-BGC

4.3.3.1 Prior distributions of the BIOME-BGC parameters

The computational load of Bayesian calibration of a simulator can be reduced by excluding those input parameters that have negligible influence on the simulated output (Xenakis et al., 2008; van Oijen et al., 2013; Minunno et al.,

2013). BIOME-BGC requires 35 ecophysiological parameters for evergreen needleleaf species (Table 4.1), each having a varying degree of influence on the simulated GPP. Raj et al. (2014) conducted variance-based sensitivity analysis (VBSA) of BIOME-BGC at Speulderbos to investigate the sensitivity of simulated GPP to the ecophysiological parameters and the effective soil rooting depth. They treated soil rooting depth as a parameter. For VBSA, they identified the uncertainty in each ecophysiological parameter and the soil depth in the form of pdfs. They found that GPP is mainly sensitive to 5 ecophysiological parameters and the soil rooting depth, while others were found to have negligible influence on simulated GPP. In this study, we included these 6 input parameters (highlighted in Table 4.1) for calibration, whose prior pdfs were assumed identical to that identified by Raj et al. (2014). Other input parameters were fixed at the mean value of the distribution provided by Raj et al. (2014).

4.3.3.2 The likelihood

Recall from Sect. 4.3.2.1 that the likelihood is determined by the pdf of the residuals, $e_t = z_t - y_t$ (Eq. 4.2). Hence, the likelihood function evaluates how well the BIOME-BGC simulated GPP, $\mathbf{y}$, is able to reproduce the data, $\mathbf{z}$. The likelihood function typically defined assuming that the residuals are independent and identically normally distributed (van Oijen et al., 2005; Svensson et al., 2008; Reinds et al., 2008; Braakhekke et al., 2013; Starrfelt and Kaste, 2014). This assumes that the simulator models perfectly the temporal profile of GPP leaving no residual temporal correlation in the residuals from the time series. This assumption may not be correct.

BIOME-BGC simulates the time series of GPP at daily time steps. We relaxed the assumption that the temporal profile of simulated GPP perfectly follows the flux tower GPP and modelled the temporal correlation in the residuals. We adopted a likelihood that assumes the residuals follow an autoregressive process of order one (Vrugt, 2016), given as:

$$p_{\log}(\mathbf{z}|\boldsymbol{\theta}) = -\frac{n}{2}\log(2\pi) + \frac{1}{2}\log\left(1-\phi^2\right) - \frac{1}{2}\left(1-\phi^2\right)\hat{\sigma}_1^{-2}e_1^2 - \sum_{t=2}^{n}\log(\hat{\sigma}_t) - \frac{1}{2}\sum_{t=2}^{n}\left(\frac{e_t - \phi e_{t-1}}{\hat{\sigma}_t}\right)^2 \tag{4.5}$$

where ϕ and $\hat{\sigma}$ are nuisance parameters that are inferred jointly with $\boldsymbol{\theta}$. The parameter $|\phi| < 1$ accounts for the temporal correlation in the residuals, $\mathbf{e}$ and $\phi = 0$ means that there is no temporal correlation. We evaluated whether the posterior distribution ϕ were different from zero (Sect. 4.4.1).

Eq. 4.5 gives the likelihood on the logarithmic scale. This improves numerical stability by avoiding rounding errors in the computation. n is the length of the vectors $\mathbf{z}$ and $\mathbf{y}$.

Table 4.1 35 ecophysiological parameters needed to run BIOME-BGC for Douglas fir (evergreen needleleaf species). Mean values/distributions were taken from Raj et al. (2014). The ecophysiological parameters highlighted in bold and the soil rooting depth were included in a Bayesian calibration. U(min, max), $\mathcal{N}$(mean, standard deviation), B(shape1, shape2) represent uniform, normal, and beta distribution respectively.

Ecophysiological parameter	Symbol	Unit	Mean value/distribution†
Leaf and fine root turnover	**LFRT**	1 yr^{-1}	$U(0.196, 0.5)^{\dagger}$
Annual live wood turnover fraction	LWT	1 yr^{-1}	0.70
Annual whole-plant mortality fraction	WPM	1 yr^{-1}	0.005
Annual fire mortality fraction	FM	1 yr^{-1}	0.005
new fine root C : new leaf C	**FRC:LC**	kg C (kg C)$^{-1}$	$U(0.78, 2.16)^{\dagger}$
new stem C : new leaf C	SC:LC	kg C (kg C)$^{-1}$	2.391
new live wood C : new total wood C	LWC:TWC	kg C (kg C)$^{-1}$	0.071
new croot C : new stem C	CRC:SC	kg C (kg C)$^{-1}$	0.262
Current growth proportion	CGP	Prop.	0.5
C:N of leaves	**C:N$_{\mathbf{leaf}}$**	kg C (kg N)$^{-1}$	$\mathcal{N}(26.731, 3.731)^{\dagger}$
C:N of leaf litter, after retranslocation	C:N$_{\mathrm{lit}}$	kg C (kg N)$^{-1}$	31.625
C:N of fine roots	C:N$_{\mathrm{fr}}$	kg C (kg N)$^{-1}$	54.8
C:N of live wood	C:N$_{\mathrm{lw}}$	kg C (kg N)$^{-1}$	54.8
C:N of dead wood	C:N$_{\mathrm{dw}}$	kg C (kg N)$^{-1}$	1029.5
Leaf litter labile proportion	L$_{\mathrm{lab}}$	Unitless	0.644
Leaf litter cellulose proportion	L$_{\mathrm{cel}}$	Unitless	0.201
Leaf litter lignin proportion	L$_{\mathrm{lig}}$	Unitless	0.155
Fine root labile proportion	FR$_{\mathrm{lab}}$	Unitless	0.527
Fine root cellulose proportion	FR$_{\mathrm{cel}}$	Unitless	0.378
Fine root lignin proportion	FR$_{\mathrm{lig}}$	Unitless	0.095
Dead wood cellulose proportion	DW$_{\mathrm{cel}}$	Unitless	0.772
Dead wood lignin proportion	DW$_{\mathrm{lig}}$	Unitless	0.228
Canopy water interception coefficient	$\boldsymbol{W}_{\mathbf{int}}$	1 LAI^{-1} day^{-1}	$\mathcal{N}(0.04, 0.02)^{\dagger}$
Canopy light extinction coefficient	k	Unitless	0.453
All-sided to projected leaf area ratio	LAI$_{\mathrm{all:proj}}$	LAI LAI^{-1}	2.572
Canopy average specific leaf area	SLA	m^2 (kg C)$^{-1}$	14.65
Ratio of shaded SLA:sunlit SLA	SLA$_{\mathrm{shd:sun}}$	SLA SLA^{-1}	2.0
Fraction of leaf N in Rubisco	**FLNR**	Unitless	$B(25.67, 756.28)^{\dagger}$
Maximum stomatal conductance	g_{smax}	m s^{-1}	0.0051
Cuticular conductance	g_{cut}	m s^{-1}	0.000051
Boundary layer conductance	g_{bl}	m s^{-1}	0.075
Leaf water potential: start of conductance reduction	LWP$_{\mathrm{i}}$	Mpa	-0.647
Leaf water potential: complete conductance reduction	LWP$_{\mathrm{f}}$	Mpa	-2.487
Vapor pressure deficit: start of conductance reduction	VPD$_{\mathrm{i}}$	Pa	610.0
Vapor pressure deficit: complete conductance reduction	VPD$_{\mathrm{f}}$	Pa	3130.0
Site characteristic			
Effective soil Depth	**SD**	meter	$U(0.4, 2)^{\dagger}$

4.3.3.3 Posterior prediction of BIOME-BGC parameters and GPP

We implemented DREAM algorithm in MATLAB version R2015b. The DREAM toolbox was provided by its developer, Jasper A. Vrugt, University of California, Davis, USA. Technical details of the DREAM toolbox are provided by Vrugt (2016).

We used $N = 10$ Markov chains with $T = 15000$ iterations for each chain. This produced 150000 ($N \times T$) posterior samples for each θ_j ($j = 1, 2, .., 6$ for selected BIOME-BGC parameters for calibration). Gelman et al. (2013) and Vrugt et al. (2009) recommend discarding the first 50% of the samples as a burn-in; however, we discarded 10000 samples, in order to reduce the computation cost. This resulted in 50000 ($N \times (T - \text{burn-in})$) post burn-in samples for each θ_j. The convergence of these post burn-in samples was evaluated using the Gelman–Rubin diagnostic (Gelman and Rubin, 1992) and through visual examination of the trace plots. The Gelman–Rubin potential scale reduction factor (PSRF) compares the between-chain and within-chain variance of the parallel Markov chains. A PSRF close to 1 indicates that the chains have converged.

The post burn-in samples created 50000 vectors of $\boldsymbol{\theta}$. BIOME-BGC was run at each parameter vector using daily meteorological data of 2009 and the daily simulated GPP (posterior prediction of GPP) was evaluated and stored. This produced the distribution of daily GPP, which was summarized by the median and the 2.5 and 97.5 percentile (i.e., 95 % credible interval). The 95 % credible interval showed the uncertainty in the daily simulated GPP. We compared these 95 % credible intervals and medians over the growing season with that of flux tower GPP.

We conducted two experiments to obtain the posterior samples of $\boldsymbol{\theta}$:

1. Experiment 1: We used daily flux tower GPP for five months in the growing season (April to August 2009) to calibrate BIOME-BGC for the growing season. For calculation of the log-likelihood using Eq. 4.5, we set $n = 153$, equal to the number of days in April to August. Note that we did not include the daily flux tower GPP for September and October in the calibration and we used these data for validation of the calibrated BIOME-BGC. In this experiment, the obtained posterior samples of $\boldsymbol{\theta}$ were used to simulate GPP and the associated uncertainty for each day in 2009.
2. Experiment 2: We used daily flux tower GPP for one month only, e.g., April, in the growing season to calibrate BIOME-BGC. For the likelihood calculation, we set $n = 30$, equal to the number of days in April. The obtained posterior distributions of $\boldsymbol{\theta}$ were used to simulate daily GPP with the associated uncertainty for 2009. We then extracted the daily simulated GPP (with the associated uncertainty) of April only and discarded the other months in 2009. Likewise, we obtained the simulated GPP and the associated uncertainty for the other six months (May to October 2009) in the growing season. Experiment 2 resulted in seven different posterior samples of $\boldsymbol{\theta}$.

For both experiments, we followed the same procedure explained in the paragraph 2 and 3 of this section.

4.3.3.4 Statistical evaluation of BIOME-BGC simulated GPP

We determined the performance of the calibration using two criteria that evaluate efficiency with which the calibrated BIOME-BGC reproduces the flux tower GPP. Both criteria provide a single measure of BIOME-BGC efficiency in simulating daily GPP over the selected period. The first criterion was the root mean square error (RMSE) between the simulated and flux tower GPP:

$$\mathrm{RMSE} = \sqrt{\frac{1}{n}\sum_{t=1}^{n}(z_t - y_t)^2} \tag{4.6}$$

where n is the number of daily flux tower GPP (z_t) and the simulated GPP (y_t). RMSE has the units of GPP. A low value of RMSE indicates the high accuracy. The second criterion was the Nash-Sutcliffe efficiency (NSE) (Nash and Sutcliffe, 1970):

$$\mathrm{NSE} = 1 - \frac{\sum_{t=1}^{n}(z_t - y_t)^2}{\sum_{t=1}^{n}(z_t - \overline{z})^2} \tag{4.7}$$

where $\overline{z}$ is the mean of the observations (flux tower GPP). NSE can range from $-\infty$ to 1. An NSE value close to 1 indicates high accuracy in the simulation of GPP. Following Dumont et al. (2014), we assumed that a NSE ≥ 0.5 indicates adequate accuracy in the simulated GPP.

We evaluated the performance of BIOME-BGC for the following cases:

1. For Experiment 1, we obtained RMSE and NSE for the two periods: calibration period of five months (April to August) and the validation period of two months (September and October). For each period, the calculations were made for 2.5 percentiles, 97.5 percentiles, and medians. Note that the RMSE and NSE are typically evaluated at the median of the posterior predictive distribution; however, this does not evaluate the posterior uncertainty (Hamm et al., 2015a). Therefore we also calculated the RMSE and NSE for the 2.5 and 97.5 percentiles of the posterior predictive distribution of BIOME-BGC simulated GPP ($y_{2.5}$ and $y_{97.5}$) against the same percentiles for the posterior predictive distribution of flux tower GPP ($z_{2.5}$ and $z_{97.5}$).
2. For Experiment 2, we obtained RMSE and NSE for the same two periods and percentiles as stated in point 1 (above), to make a direct comparison with the results of Experiment 1.
3. To show the performance of uncalibrated BIOME-BGC, we obtained the daily simulated GPP with 95% credible intervals at the prior distributions of six selected parameters (Table 4.1). We sampled from these prior distributions to obtain 50000 parameter vectors. BIOME-BGC was run at these parameter vectors to yield the prior predictor of BIOME-BGC simulated GPP. We calculated the RMSE and NSE for the same two periods and percentiles as stated in point 1, to make a direct comparison with Experiments 1 and 2.

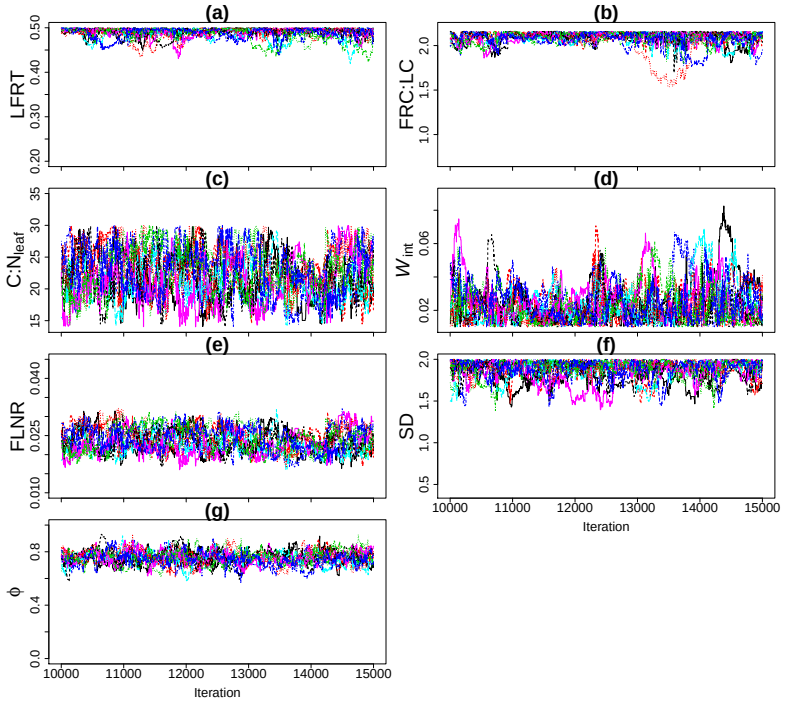

Figure 4.1 Trace plot of each calibrated BIOME-BGC parameter and ϕ for Experiment 1. Information about the BIOME-BGC parameters is given in Table 4.1.

4.4 Results

4.4.1 Convergence of the Markov chains

The value of Gelman–Rubin PSRF was close to one for each θ_j obtained in both experiments (Table 4.2). Figs. 4.1a to 4.1f show the trace plots of each θ_j for Experiment 1. Visual inspection of the trace plots indicated that all ten Markov chains were mixed properly with each other. For Experiment 2, we also observed the convergence of the Markov chains for each θ_j in each month of the growing season (trace plots not shown here). The visual and statistical diagnostic demonstrated that each θ_j had explored its range and the obtained samples from the converged chains were the samples from the posterior distribution.

Fig. 4.1g shows the trace plot of ϕ, accounting for the temporal correlation in the error residuals (Sect. 4.3.3.2), for Experiment 1. We observed $\phi \neq 0$ and its value ranged from 0.56 to 0.93 with a mean at 0.75. The non-zero values of ϕ indicated that the residuals are temporarily correlated, thus supporting our choice of likelihood function (Eq. 4.5). For Experiment 2, non-zero values of ϕ were also obtained in each month.

Table 4.2 Gelman–Rubin potential scale reduction factor (PSRF) of each BIOME-BGC parameter selected for calibration and ϕ for experiment 1 and 2.

	PSRF							
	Experiment 1	Experiment 2						
Julian days → Parameter ↓	91-243	91-120	121-151	152-181	182-212	213-243	244-273	274-304
LFRT	1.05	1.03	1.01	1.03	1.03	1.04	1.03	1.01
FRC:LC	1.09	1.02	1.01	1.01	1.04	1.06	1.02	1.01
$C:N_{leaf}$	1.04	1.02	1.02	1.01	1.04	1.04	1.03	1.03
$W_{\mathbf{int}}$	1.02	1.01	1.01	1.02	1.06	1.03	1.03	1.01
FLNR	1.04	1.04	1.02	1.01	1.05	1.06	1.02	1.01
SD	1.04	1.03	1.02	1.02	1.03	1.1	1.02	1.02
ϕ	1.02	1.03	1.01	1.01	1.03	1.03	1.01	1.01

4.4.2 Posterior distribution of BIOME-BGC parameters

Fig. 4.2 shows the temporal profile of median and 95% credible interval of each θ_j over the growing season for Experiment 2. The median and 95% interval for Experiment 1 is constant, since this did not vary over time. For both experiments, we observed that the uncertainty in the posterior distribution of each θ_j was reduced compared to the prior distribution, indicating that $\boldsymbol{\theta}$ were constrained by the flux tower GPP observations. These uncertainties were higher in Experiment 2 than that of Experiment 1. The upper quantiles (97.5%) of the posterior distributions of the parameters LFRT, FRC:LC, and SD were found close to the maximum values of the corresponding prior distributions for both experiments. The uniform priors of these parameters (Table 4.1) possibly imposed an upper boundary in the posteriors. We chose to keep these maximum values since the choices, given in Table 4.1, were based on the realistic ranges of LFRT, FRC:LC, and SD for Dougls-fir at Speulderbos.

For Experiment 2, the uncertainties in LFRT, FRC:LC, W_{int}, and SD were higher at the start and end of the growing season compared to other months. The uncertainties in these parameters were lowest during the peak of the growing season (July and August). The values of LFRT, FRC:LC, and SD increased during the peak of the growing season and became close to that obtained in Experiment 1 and then started decreasing. The opposite trend was observed for W_{int}. The uncertainty in $C:N_{leaf}$ for any month obtained in Experiment 2 was comparable and within the range of that obtained in experiment 1. We did not find significant variation in the trend of FLNR obtained in Experiment 2 during the growing season; however, higher uncertainty in FLNR was observed compared to Experiment 1.

4.4.3 Evaluation of calibrated BIOME-BGC for Experiment 1

We evaluated the performance of calibrated BIOME-BGC by comparing the daily simulated posterior GPP and the daily posterior flux tower GPP, for the calibration period of April to August (Fig. 4.3) and the validation period of September and October (Fig. 4.4). The daily simulated and flux tower GPP were summarized by the median and 95% credible interval. The temporal profile of these medians and credible intervals were plotted against that of

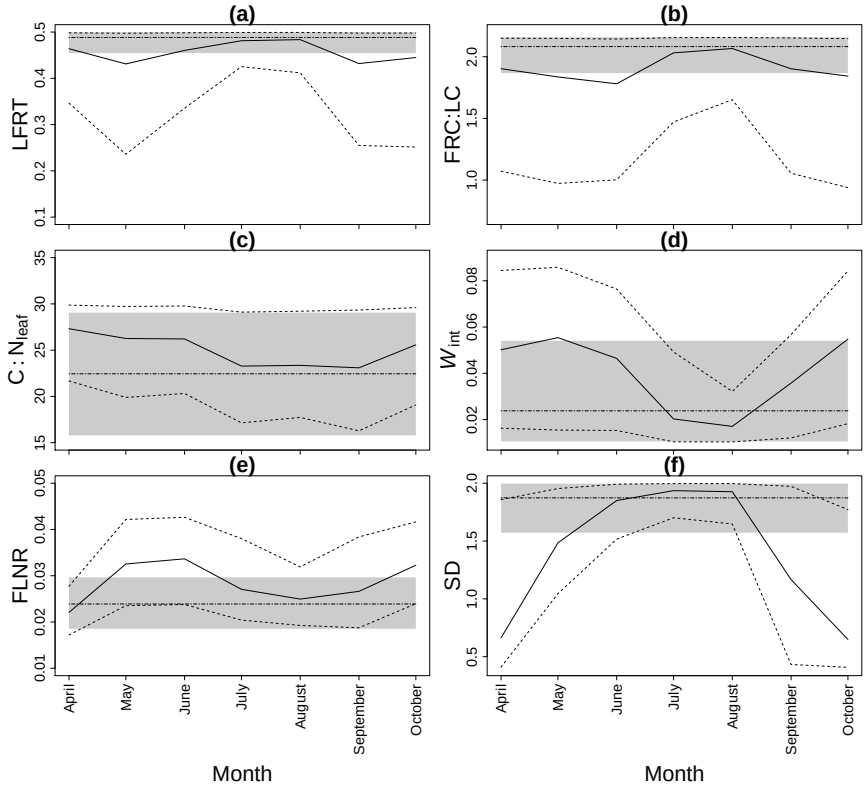

Figure 4.2 Median (solid lines) and 95% credible intervals (dashed lines) of the posterior distributions of each calibrated BIOME-BGC parameter obtained from Experiment 2 for each month during the growing season of 2009. The grey shade and dotted-dashed line represent median and 95% credible intervals obtained for Experiment 1. The range of the y-axis represents the prior uncertainty in BIOME-BGC parameters. Information about the BIOME-BGC parameters is given in Table 4.1.

flux tower GPP. Evaluation of the BIOME-BGC before and after calibration (Experiment 1) based on the statistical criteria (RMSE and NSE) is shown in Table 4.3. The periods for which these criteria were obtained are explained in Sect. 4.3.3.4.

Overall, posterior predicted daily GPP was close to flux tower GPP during the calibration period (Fig. 4.3), although the separation between these two temporal profiles in April (Julian day 91 to 120) was large compared to other months (Julian day 121 to 242) in the growing season. For the validation period, the simulated GPP closely followed the flux tower GPP (Fig. 4.4).

The posterior predicted BIOME-BGC GPP was improved compared with the prior predicted BIOME-BGC, as indicated by the drop of RMSE for the median as well as the 2.5 and 97.5 percentile for both calibration and validation periods (Table 4.3). The NSE criterion was also improved after calibration (NSE > 0.5), whereas before calibration, the value of NSE was negative. The enhancement in NSE and the drop of RMSE give statistical

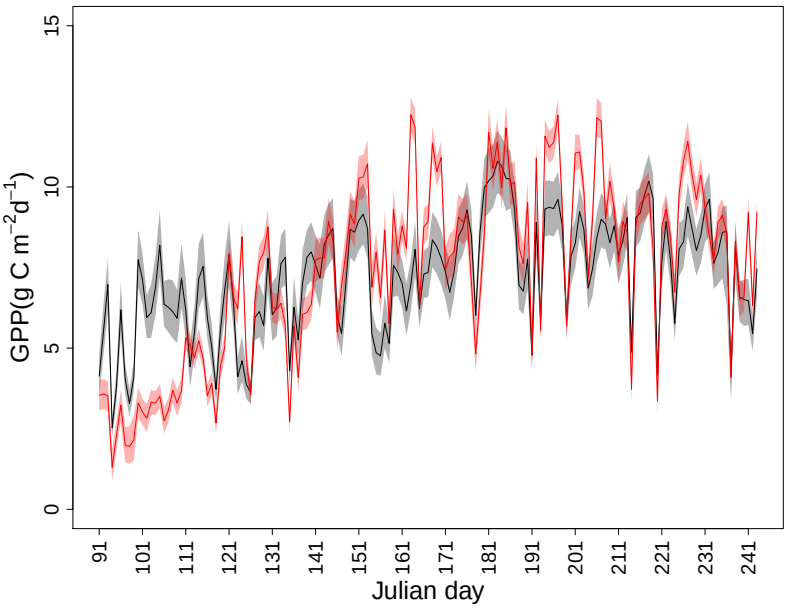

Figure 4.3 Temporal profile of the daily posterior predicted BIOME-BGC GPP, obtained for Experiment 1, and the daily posterior predicted flux tower GPP for the calibration period of five months (April to August, Julian days 91 to 243). The medians and 95% credible intervals of BIOME-BGC GPP are represented by the black line and grey shade respectively. The medians and 95% credible intervals of flux tower GPP are represented by the red line and red shade respectively.

Table 4.3 Root mean square error (RMSE) and Nash-Sutcliffe efficiency (NSE) between the posterior predicted BIOME-BGC and flux tower GPP for different experiments (see Sect. 4.3.3.4).

		2.5%		Median		97.5%	
	Period	RMSE	NSE	RMSE	NSE	RMSE	NSE
Before calibration	April to August	5.06	-2.53	3.74	-0.85	4.26	-1.3
	September-October	2.23	-0.15	1.22	0.68	2.64	-0.42
Experiment 1	April to August	1.84	0.53	1.81	0.57	1.85	0.57
	September-October	0.91	0.81	0.83	0.85	0.79	0.87
Experiment 2	April to August	1.3	0.77	1.24	0.8	1.45	0.73
	September-October	0.94	0.79	0.84	0.85	0.92	0.83

evidence of the improvement in the daily simulated GPP after calibration.

4.4.4 Relation of posterior simulated GPP with meteorological variables

Most of the variability of daily BIOME-BGC output was due to the meteorological input data. Fig. 4.5 illustrates this by showing the seasonal variation of the medians of the daily posterior predicted GPP, obtained from Experiment 1, together with Tday, VPD, srad, and precipitation. Tday, VPD, and srad were correlated strongly with each other and the posterior predicted GPP followed the pattern of these input variables. In general

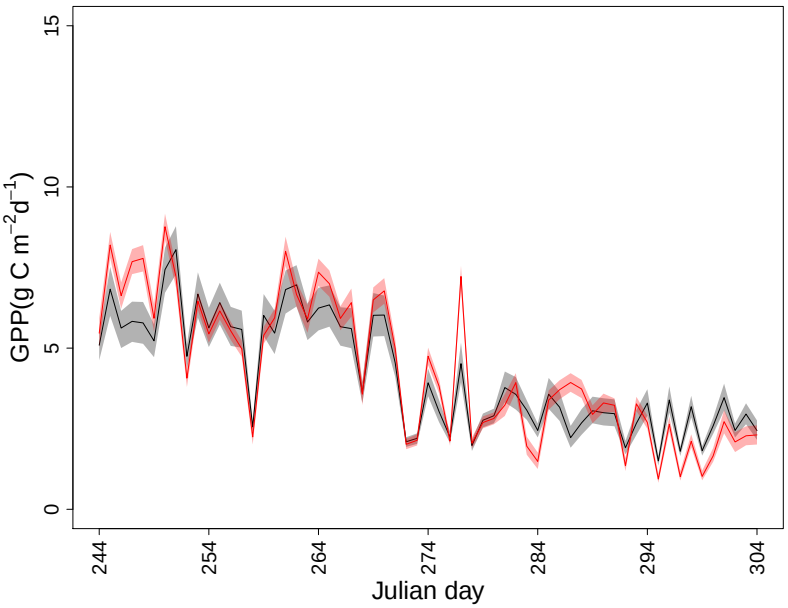

Figure 4.4 Temporal profile of the daily posterior predicted BIOME-BGC GPP, obtained from Experiment 1, and the daily posterior predicted flux tower GPP for the validation period of two months (September and October, Julian days 244 to 304). Other details as for Fig. 4.3.

between days, we observed that the increase in Tday, VPD, and srad increased GPP and vice-versa. The daily simulated GPP had a strong positive correlation with Tday, with a correlation coefficient $r = 0.85$. GPP showed less positive correlation with VPD and srad, compared to Tday, with $r = 0.71$ and $r = 0.66$ respectively. A negative, but weak ($>$ -0.5), correlation was found between GPP and precipitation with $r = -0.22$. This is due to the negative correlation that rainfall has with srad, VPD and Tday, whereas the effect on GPP is usually not immediate due to the replenishment of the soil water reservoir.

Because BIOME-BGC simulates the seasonal phenology, the daily simulated GPP on a particular Julian day is not temporarily independent. GPP depends on the history of the meteorological data. To verify this, we swapped the meteorological data of Julian days 91-166 with those of days 167-242, ran BIOME-BGC with the swapped meteorological data with the posterior samples of $\boldsymbol{\theta}$ (obtained from Experiment 1) and then reversed the generated output of GPP back into the original order. Fig. 4.6 compares the temporal profile of the medians of $\mathrm{GPP}_{\mathrm{sp}}$ (GPP swapped) with those obtained from Eperiment 1 (Sect. 4.4.3) with the meteorological data in the correct order. If only the meteorological data of a particular day and the input parameters would be responsible for daily simulation, the temporal profile of $\mathrm{GPP}_{\mathrm{sp}}$ and $\mathrm{GPP}_{\mathrm{exp1}}$ should have matched exactly; however, this is not the case. We observed a difference in daily $\mathrm{GPP}_{\mathrm{sp}}$ and $\mathrm{GPP}_{\mathrm{exp1}}$. The swapping of

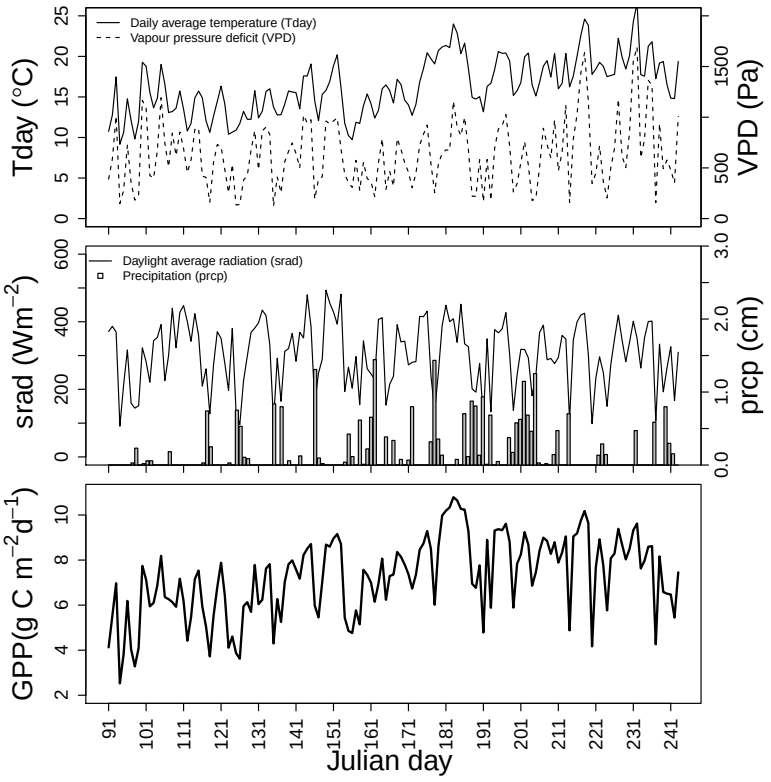

Figure 4.5 Variation of the posterior median of BIOME-BGC GPP, obtained from Experiment 1, with the daily meteorological variables during the growing season of 2009. The meteorological variables are Tday (average daytime temperature), VPD (vapour pressure deficit), prcp (daily total precipitation), srad (daylight average shortwave radiant flux density).

meteorological data led to an over- and underestimation of daily GPP_{sp} with a maximum of 1.4 and 1.8 g C m^{-2} s^{-1} respectively. This indicated clearly that the daily simulated GPP was temporarily dependent and did not depend only on the meteorological data and the input parameters for a given day. This temporal dependency was due to the update of the BIOME-BGC storage terms between days.

4.4.5 Posterior simulated GPP for Experiment 2

Combining the daily simulations of each month provided the temporal profile of the medians and 95% credible intervals of the daily simulated posterior GPP over the growing season. Fig. 4.7 shows this temporal profile (black line and grey shade) from April to August. We observed that the posterior predicted GPP had a better fit to the flux tower GPP, compared to Experiment 1 (Fig. 4.3). Particularly, the posterior predicted GPP of April (Julian days 91 to 120) followed the flux tower GPP more closely than Experiment 1. We

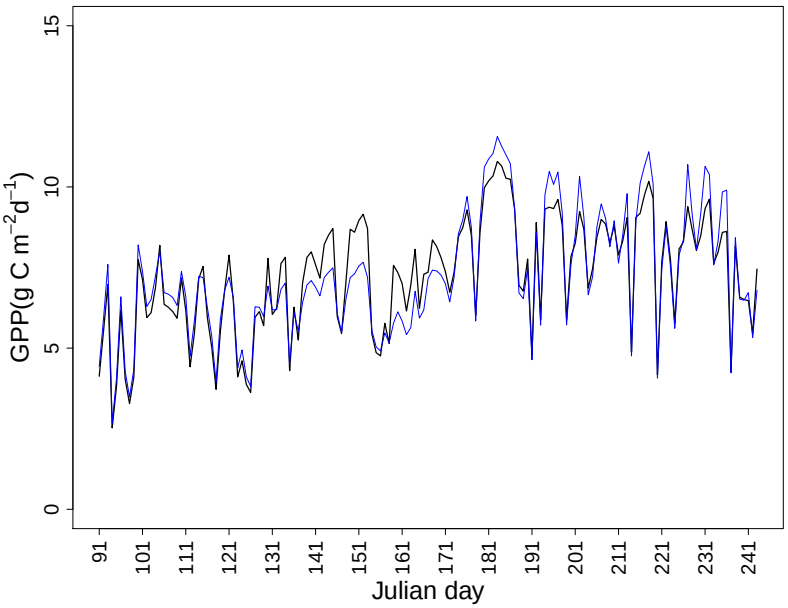

Figure 4.6 Temporal profile of the daily posterior median BIOME-BGC GPP, obtained in Experiment 1, at meteorological data with correct sequence (black line) and where the meteorological data were swapped between Julian days 91-166 with 167-242 (blue line). The order of simulated GPP were corrected for swapping.

found further enhancement in the NSE compared to Experiment 1 for the median, 2.5, and 9.5 percentile over the period of April to August (Table 4.3) where the values of NSE became closer to 1. A drop in RMSE was also observed. For the period of September and October (temporal profile not shown here), however, the NSE and RMSE were the same as for Experiment 1. These results indicated an improvement in the posterior predicted GPP compared to that obtained from Experiment 1, but at the expense of a higher degree of freedom.

4.5 Discussion

4.5.1 Simulatoin of GPP using BIOME-BGC

To explain our results, we identified the processes within BIOME-BGC that are controlled by the six calibrated parameters and relate to the simulation of GPP (Fig. 4.8). These processes are implemented by different routines. The routines, however, are controlled not only by these six parameters, but also generate intermediate outputs, as shown in Fig. 4.8. We only highlight those routines that were relevant to the simulation of GPP. We refer the reader to Thornton (2010) for a detailed explanation of the routines.

BIOME-BGC simulates the daily development of plant carbon pools (White et al., 2000). The development of carbon pools is governed by the daily

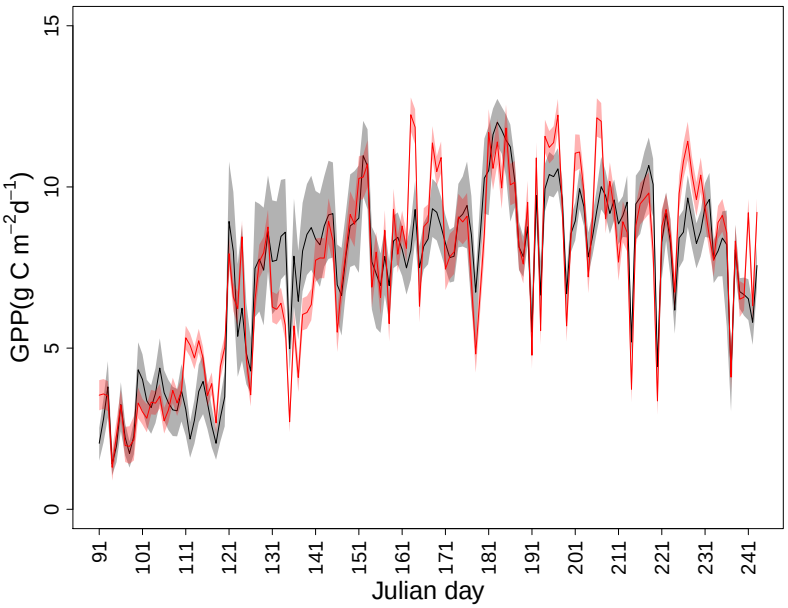

Figure 4.7 Temporal profile of the daily posterior predicted BIOME-BGCC GPP, obtained from Experiment 2, and the daily posterior predicted flux tower GPP for months (April to August, Julian days 91 to 243). Other details as for Fig. 4.3.

update of BIOME-BGC memory of mass of carbon stored in different components of the plant. The simulated development of plant carbon pools on a particular day is dependent on the previous days. BIOME-BGC converts the carbon stored in the leaf pool (leaf C) into an equivalent leaf area index (LAI). The development of leaf C controls the development of LAI in the radiation transfer routine. Leaf C relates to the loss of leaf biomass, which is expressed as the parameter LFRT. The parameter FRC:LC is also responsible for the development of leaf C and then LAI. In the precipitation routine, W_{int}, together with LAI, determines the amount of precipitation intercepted by the canopy, which in turns controls the amount of water that reaches the soil. The soil psi routine calculates the volumetric water content in the soil as the ratio of soil water to SD. Thereafter, soil water potential is derived as a function of volumetric water content. The soil water potential acts as a multiplier in the evapotranspiration routine to simulate stomatal closure and the leaf scale conductance to water vapour per unit leaf area.

The photosynthesis routine converts the conductance to water vapour to the conductance for CO_2, which measures the rate of passage of CO_2 into the leaf stomata. The parameter C:N_{leaf} together with LAI determines the leaf nitrogen content from the carbon pool in the photosynthesis routine and the day leaf maintenance respiration per unit leaf area in the respiration routine. The leaf scale conductance to CO_2, leaf nitrogen content, day leaf maintenance respiration and the parameter FLNR are further used in the Farquhar model, implemented in the photosynthesis routine, to simulate

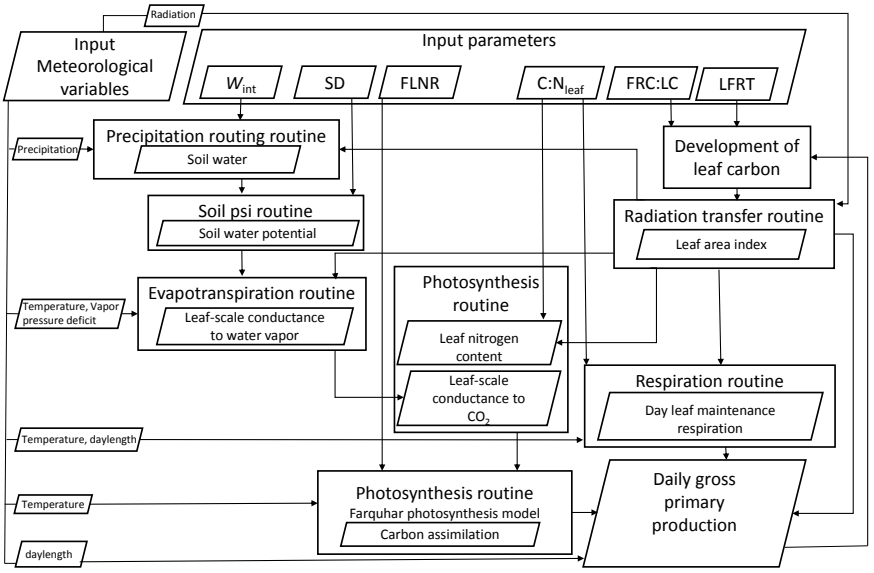

Figure 4.8 The BIOME-BGC internal routines that simulate gross primary production (GPP), controlled by the meteorological data and the six calibrated parameters. Rectangular boxes represent the BIOME-BGC routines and the parallelograms represent the input and output of the routine. Information about the BIOME-BGC parameters is given in Table 4.1.

the carboxylation capacity (V_{cmax}) and thus the carbon assimilation. The assimilated carbon is then added to the day leaf maintenance respiration and then multiplied by the LAI and daylength to simulate the daily GPP. The respiration routine also calculates the maintenance respiration of root and stem (not shown in Fig. 4.8) together with leaf. The respiration terms are summed and then subtracted from GPP to obtain available carbon for allocation, which further updates leaf C. Finally, Fig. 4.8 indicates which meteorological variables are used in a given routine, although we have not described their specific role.

We presented the link between six calibrated parameters and the BIOME-BGC internal routines so that we could explain our results considering the development of the state variables, principally such as LAI and V_{cmax}. LAI and V_{cmax} exhibit a seasonal cycle and affect the seasonality of simulated GPP. This is explored further in Sect. 4.5.2.

4.5.2 BIOME-BGC calibration

BIOME-BGC accounts for dynamic for carbon stocks in the vegetation by means of allocation, hence it uses parameters that are constant for the year of simulation. Consider Experiment 1. The memory of BIOME-BGC is updated between days (Sect. 4.5.1), and Biome-BGC takes care of the simulation of time-varying state variables such as leaf area index (LAI) and carboxylation capacity (V_{cmax}) used in Farquhar's model. Therefore, the daily simulated

GPP are temporarily dependent, which was highlighted experimentally in our study by the swapping of meteorological variables between Julian days 91-166 and 167-242 (Fig. 4.6). The posterior predicted GPP closely followed the posterior predicted flux tower GPP even for those months (September and October) which were not included in the calibration (Fig. 4.4), although this was not perfect as shown by the fact that $\phi \neq 0$. If the simulator would properly capture the temporal development of GPP we would expect that $\phi = 0$, even after allowing for some uncertainty in the prediction. The fact that the residuals showed temporal autocorrelation indicated that the representation of dynamic processes within the simulator could be improved.

Experiment 1 showed that BIOME-BGC was able to reproduce closely the posterior predicted flux tower GPP. Further, the Bayesian calibration allowed daily GPP simulation as well as quantification of the associated uncertainty (Figs. 4.3 and 4.4). Furthermore, the apparent overprediction of daily simulated GPP, compared to flux tower GPP, for the month of April raised questions: (a) on the reliability of simulated GPP for those months that were not included in this study; and (b) whether the seasonal cycle of all of the state variables was simulated realistically. These questions led us to estimate the time varying posterior distributions of parameters in Experiment 2. We recognize that this contradicts the specified use of BIOME-BGC since it: (a) violates the requirement of constant parameters; and (b) affects the update of the state variables over time. Nevertheless, the experiment did allow more flexibility to vary the parameters over time, with consequences for the update of state variables and the posterior prediction of GPP.

Consider Experiment 2. Note that BIOME-BGC actually simulated daily GPP for a whole year with the posterior distributions of the parameters of each month. We selected only the daily simulated GPP of that month to which the posterior distributions belong and we discarded the other eleven months of simulations. The temporal profile in Fig. 4.7 is the combinations of daily simulated GPP of each month in the growing season (Sect. 4.3.3.3 and 4.4.5). We observed an improvement (Fig. 4.7), particularly in the month of April, in the daily posterior predicted GPP compared to Experiment 1 (Fig. 4.3). This improvement was also clear in Table 4.3 which shows an increase in the NSE and decrease in the RMSE for Experiment 2 compared to Experiment 1. The calibration approach adopted in Experiment 2 was more flexible and led to increased prediction accuracy despite contradicting the BIOME-BGC design.

Experiment 2 showed variation in the six calibrated parameter over the growing season (Fig. 4.2), particularly W_{int}, SD , FRC:LC, and LFRT. These variations were also in-line with the seasonal variation in GPP. For example, maintaining the high GPP rates during the peak of the growing season (July and August), required more soil water, which was obtained by decreasing the parameters W_{int}, in turn affecting the water intercepted by the canopy (precipitation routing routine in Fig. 4.8), and increasing the soil rooting depth (SD). The parameters FRC:LC and LFRT also increased and both affected GPP through LAI. The variation in FLNR and C:N_{leaf}, which together determined V_{cmax}, also changed month-by-month (Fig. 4.8). These results indicated that Biome-BGC, with the six parameters that we calibrated,

may be able to accurately simulate the seasonal cycle of some state variables, but may be too rigid to simulate all state updates. The result was that the posterior predictive distribution of the parameters varied month-by-month with consequences for the posterior predicted BIOME-BGC GPP. Specifically the predictions improved (lower RMSE, higher NSE) relative to Experiment 1. To our knowledge, this aspect has not been discussed in earlier work on the calibration of BIOME-BGC (Maselli et al., 2008; Ueyama et al., 2010; Yan et al., 2014).

In this study we performed our calibration based on six parameters (LFRT, FRC:LC, C:N_{leaf}, W_{int}, FLNR, and SD) whereas BIOME-BGC has 35 parameters in total. A calibration based on 35 parameters was not feasible computationally so, in line with other authors (e.g., Minunno et al., 2013), we chose a subset of the parameters. We defend our choice of parameters based on our previous experimental results, which showed that annual total GPP was most sensitive to these parameters (Raj et al., 2014) at Speulderbos. Nevertheless, GPP may be sensitive to other parameters at finer spatial scales. Computational developments and the flexibility of the DREAM algorithm may allow more parameters to be calibrated, so this should be explored further in future.

4.6 Conclusions

This study presented a calibration of BIOME-BGC. We illustrated the framework at the Speulderbos forest site, the Netherlands. Our study led to the following conclusions:

1. Quantification of uncertainty in the simulated GPP is not integrated into BIOME-BGC, although Monte Carlo approaches allow exploration of uncertainty due to uncertain parameters. The Bayesian framework allowed quantification of uncertainty in both the estimated parameters and the predicted GPP, through the posterior (predictive) distribution. The uncertainty is important in the sense that it helps to determine how much confidence can be placed in the results of forest carbon related studies based on GPP. A calibration based on optimization of BIOME-BGC parameters, as done in earlier studies, can not capture the associated uncertainty in the simulated GPP.

2. We modelled the temporal correlation in the residuals through the nuisance parameter, ϕ, in the likelihood function. Our results supported the use of temporal correlation in the residuals for the inference of the posterior parameter distributions of BIOME-BGC. This showed that BIOME-BGC did not properly simulate the temporal profile of GPP. Hence the calibration also gave greater insight into the simulator. Future research should identify the cause of this limitation.

3. We used the calibration results to gain further insights into the functioning of BIOME-BGC through analysis of the time varying posterior parameter distributions. Our study revealed that the constant distributions of BIOME-BGC parameters were not adequate to simulate

the seasonality in daily GPP. The seasonality was captured more precisely by using time varying parameters. This reinforces our previous conclusion. The implications of temporal correlation and time-varying parameters should receive attention from the BIOME-BGC modelling community.

4. We implemented our calibration using the DREAM algorithm and its freely available MATLAB toolbox. DREAM offers considerable computational advantages and flexibility compared to other MCMC implementations and is gaining increased usage. It shows promise for biogeochemical and other environmental simulation applications. Specifically future research could calibrate more parameters.

Synthesis

5

5.1 Positioning the research

Forests, as an important terrestrial carbon sink, play a significant role to partially offset the emission of excess CO_2 produced by anthropogenic activities. They may serve as a low cost option for carbon sequestration. Gross primary production (GPP) is an important characteristics of forest vegetation for carbon sequestration, because GPP is the overall rate of atmospheric CO_2 fixation (uptake of carbon) by plants via photosynthesis. Part of this carbon uptake is lost through plant respiration, whereas the remaining part is used to produce new biomass. Quantification of GPP together with the continuous monitoring of its temporal variations at local and regional scale are, therefore, indispensable to obtain reliable data for indicating the strength of forests to sequester carbon. The method that was adopted in this dissertation, for quantification of GPP at the local scale, serves as a building block for its quantification at the regional scale in the sense that the method, implemented at one local forest site, can be adopted for other forest sites. This has two implications. First, the method should be efficient so that it quantifies GPP with accuracy together with its associated uncertainty. This is important in the sense that it helps to determine how much confidence can be placed in quantified GPP. The efficiency of the adopted method at local scale further ensures that the accuracy of GPP is high at regional scales. Second, the method should be flexible so that only changes in required input information are sufficient for its adaptation at various forest sites. Therefore in this dissertation, a complete method at local scale was explored.

GPP can be quantified using two sources: (a) forest process-based simulators (PBS), such as BIOME-BGC, which are designed to capture the critical interactions between climate conditions and forest ecosystem processes; and (b) flux towers that have been established for many years to measure the net ecosystem exchange (NEE) of CO_2 from which GPP can be partitioned using flux partitioning models. Both sources provide an opportunity to quantify and monitor GPP at the local scale. Maintaining and running a flux tower is, however, difficult and economically expensive activities. Moreover, the quality of NEE data is affected by many factors, such as rain drops on the sensors, instrument failure, and footprint heterogeneity. No such problems occur when running a PBS. In addition, a PBS can be run at time scales beyond the limit of direct measurements. This means that a PBS can simulate GPP at those points in time when the flux tower was not existent and when there is a big gap in the series of NEE measurements due to inadequate quality. In countries like India, where the flux towers are installed within a dense forests, sudden shutdown of flux tower occurred in the past due to the wild animal attack and sometimes due to failure of solar power. This has resulted into big gaps in NEE data. For those periods of shutdown, PBS can be considered as an opportunity for quantifying GPP.

Simulation of GPP by PBS at a high accuracy, however, depends upon how well the parameterization is achieved. One can measure the parameters directly in the field, but this approach is not practical because it is

time consuming and expensive work and it requires the measurements of several parameters. Further, several parameters are not physically measurable. BIOME-BGC has 35 parameters for evergreen needleleaf forest/species. Proper parameterization is required to obtain accurate simulations of GPP. Calibration of a PBS is important in order to obtain reliable estimates of the input parameters. Calibration of a PBS using a Bayesian statistical method can estimate the parameters with the associated uncertainty. The implication is that uncertainty in the input parameters can be propagated through PBS to simulate GPP with the associated uncertainty. A Bayesian statistical method, however, relies on meaningful assumptions for the prior distributions to ensure appropriate values of the prior beliefs about the parameters. The beliefs are updated against the measured data of the simulated output to obtain the posterior estimates of parameters.

A solution that was helpful in this dissertation was to update the prior beliefs in PBS parameters and the simulated output by means of GPP partitioned from NEE data using a non-rectangular hyperbola (NRH) flux partitioning model. Reliable estimation of the parameters of flux partitioning model is necessary, because partitioned GPP and their seasonal pattern depend upon the parameters. A Bayesian statistical analysis can also play an important role if the prior belief about the parameters of the flux partitioning model is available. Moreover, prior beliefs in PBS parameters also provide an opportunity to conduct a sensitivity analysis of PBS so that the complexity of a Bayesian statistical method could be simplified by updating only those parameters that are most influential on the simulated GPP. This dissertation provided a relevant method for integrating flux tower GPP into BIOME-BGC simulator using a Bayesian statistical method for the accurate simulation of GPP with the associated uncertainty.

The methods proposed in this dissertation are flexible in the sense that flux tower GPP data and the prior beliefs about the parameters of a PBS can be replaced for other species at different forest sites. Implementation of a Bayesian statistical method for calibrating a PBS is computationally expensive because it is necessary to run the PBS thousands of times until reliable posterior distributions of the parameters are obtained. A successful implementation also depends on the handling of large parameter samples obtained from prior and posterior distribution of parameters, and large amount of simulated outputs resulting from thousands of PBS runs. Furthermore, flux partitioning requires the handling of large amount of NEE data that are measured at high temporal frequency of half-hour.

The Bayesian statistical method may be more difficult to implement at the regional scale, both computationally and due to the data requirements for calibration. There may be forest sites where there are no flux towers. At these sites, however, recent advances in remotely sensed data, including derived fluorescence, which are highly correlated with GPP, may provide an effective solution to constrain the PBS parameters and simulated GPP. This offers considerable possibilities, but will necessitate the development and application of methods to quality assure such heterogeneous data. Further, at the regional scale Bayesian methods will be required to handle large amount of data both spatially and temporally, and thousands of PBS runs at different

forest sites. This may tremendously increase the computational time required to apply Bayesian methods. Statistical emulation of PBS is one approach to reduce the computation burden. Further, increasingly faster computers with large memory and the capability of parallel computing, together with the development of cloud computing services, provide a promising way to accelerate the process so that the regional quantification of GPP with high accuracy and the associated uncertainty could be achieved using the methods proposed in this dissertation.

5.2 Research findings and conclusions

1. *Objectives 1: to define prior belief of the BIOME-BGC parameters as a prior probability distributions, and to implement variance-based sensitivity analysis (VBSA) of BIOME-BGC to reveal the most influential parameters on the simulated gross primary production (GPP) as well as net primary production (NPP).*

   An extensive literature review for each BIOME-BGC parameter was carried out in order to construct the prior distributions of each of the 35 parameters needed for evergreen needleleaf forest/species. The field inventory data, if they were available at the study site, were also included. These prior distributions allowed me to conduct VBSA of BIOME-BGC. The results showed that GPP and NPP were highly sensitive to the following parameters: fraction of leaf nitrogen in Rubisco, the ratio of fine root carbon to leaf carbon, the ratio of carbon to nitrogen in leaf, the leaf and fine root turnover, the water interception coefficient and soil depth. GPP and NPP were particularly sensitive to the ratio of fine root carbon to leaf carbon that is responsible for leaf area index development.

   The study concluded that comprehensive and extensive literature search including field inventory data wherever possible should be adopted to construct a prior probability distributions of BIOME-BGC parameters. This defined the full range of input parameters that is a prerequisite in variance-based sensitivity analysis of BIOME-BGC and further in the calibration of BIOME-BGC using a Bayesian statistical method. The importance of undertaking a global VBSA revealed a significant influence of a parameter water interception coefficient (W_{int}) on GPP and NPP, which were not found in any other sensitivity analysis study based on one-at-a-time sensitivity analysis that did not examine the simulator behaviour over the full parameter space. My third paper (chapter 4) showed that my approach presented an efficient way of reducing the complexity of calibrating the BIOME-BGC simulator by considering only the key influential input parameters. Calibration can be further supported by prior belief of the input parameters in the form of prior probability distributions.

2. *Objective 2: To partition GPP with the associated uncertainty from flux tower measurements of net ecosystem exchange (NEE) using a non-*

rectangular hyperbola (NRH) model and Bayesian statistical method.

This study also adopted an extensive literature search to define the prior probability distributions (informative prior distributions) of parameters, which were necessary to fit the NRH model to NEE data using a Bayesian statistical method for the partitioning of GPP. The posterior distributions of the NRH parameters were obtained for every 10-day period. The 10-day period was chosen to obtain time varying parameters that incorporates indirectly the temporal changes in the factors such as canopy structure, soil moisture and ecosystem nutrient levels that affect GPP. The NRH model did not include these factors directly. Hence, although these factors were not included, the time varying NRH parameters did account for them. The posterior distributions of NRH parameters allowed me to partition GPP with the associated uncertainty at half-hourly time steps. These half-hourly time series were further summed to obtain partitioned GPP at daily time steps. This study also defined non-informative prior distributions and conducted the whole analysis as was done with informative prior distributions of the NRH parameters.

The study concluded that partitioned half-hourly and daily GPP data with the associated uncertainties were accurate because the same posterior distributions of the NRH parameters accurately captured the uncertainty in the measured NEE data. The accuracy in partitioned GPP was important so that it could be used further in a proper calibration of BIOME-BGC. The study further concluded that the choice of informative and non-informative prior distributions of the NRH model parameters led to partitioned GPP with similar associated uncertainty. Therefore, non-informative priors could be used for any species type irrespective of study sites. These findings are valuable to conduct uncertainty analysis across a larger sample of sites with different GPP characteristics. In addition, the study concluded that the distributions in half-hourly GPP can be summed to obtain distributions at any desired time steps, such as 8-day and monthly. These can be used further to quantify the propagated uncertainty in the validation of satellite GPP products such as MODIS 17.

3. *Objective 3: to implement a Bayesian statistical method to integrate a flux tower GPP into BIOME-BGC to quantify the reliable estimate of parameters as a posterior distribution, and simulated GPP with the associated uncertainty, and to investigate the effect of time varying BIOME-BGC parameters on the simulated GPP.*

   Knowledge of prior distributions of BIOME-BGC parameters and which parameter to target in a calibration were obtained from the study to achieve objective 1. The calibration was performed against daily simulation of GPP and daily flux tower GPP (obtained from the study to achieve objective 2). The estimated parameters, which were constant over the year, were used to simulate daily GPP with the associated uncertainty. The results showed that the calibration improved the GPP simulations and they closely followed the flux tower GPP, compared

to the uncalibrated BIOME-BGC. However, the seasonal cycle for flux tower GPP was not exactly reproduced, and some overestimates in spring (April) and underestimates in summer (August) remained after calibration. I hypothesized that the phenology exhibited a seasonal cycle that was not accurately reproduced by the BIOME-BGC. I investigated this by allowing the parameter values to vary month-by-month. Time varying parameters substantially improved the simulated GPP as compared to GPP obtained with constant or time invariant parameters. The time varying estimation also revealed a seasonal change in parameter values that determine LAI, and in parameters that determine soil water availability.

This study concluded that calibrated BIOME-BGC using a Bayesian statistical method was able to reproduce closely the flux tower GPP with the quantification of uncertainty. Such quantification in simulated GPP is not in the integral routine of BIOME-BGC. This study revealed that the time invariant BIOME-BGC parameters were not adequate to simulate the seasonality in daily GPP. The seasonality could be capture more precisely by using time varying parameters as obtained at monthly time steps in this study.

Overall, I focused on obtaining forest GPP with its related accuracy using a Bayesian statistical method by integrating two sources: the BIOME-BGC simulator and flux tower GPP, and this was achieved in this dissertation.

5.3 Recommendations

My dissertation proposes a complete method for the improved simulations of gross primary production (GPP) with the associated uncertainty by the process-based simulator BIOME-BGC. Despite that the proposed method is complete, it was limited to a single tree species Douglas-fir at the Speulderbos site in the Netherlands. The proposed method can be further extended to many forest sites containing multiple species with different GPP characteristics, e.g., by obtaining prior information on the inputs for different tree species and by obtaining net ecosystem exchange (NEE) data from the global databases, such as FLUXNET, of flux tower measurements of NEE. Collection of necessary input information, however, may be more complicated than for the current site where the data have been systematically collected during the past decades.

Different flux towers are installed within different forest ecosystems with one dominating tree species. Partitioning of GPP from NEE data at various flux tower sites can also take benefit from the findings of this dissertation that showed that non-informative prior distributions of the parameters of NRH flux partitioning model can be used for any species type. The non-informative priors can be obtained with minimum effort as compared to informative priors. Partitioning of GPP at various flux tower sites will provide relevant data to the modelling community to validate and calibrate different process-based simulators at various sites. Such simulator-data

comparison will provide an opportunity to highlight areas in space or time of the poor process representations of the simulator and this will further guide to simulator improvement.

Bibliography

Aber, J. D., Melillo, J. M., 1980. Litter decomposition: Measuring relative contributions of organic-matter and nitrogen to forest soils. Canadian Journal of Botany 58 (4), 416–421.

Allison, F. E., Mirphy, R. M., Klein, C. J., 1963. Nitrogen requirements for the decomposition of various kinds of finely ground woods in soil. Soil Science 96 (3), 187–190.

Aubinet, M., Vesala, T., Papale, D., 2012. Eddy Covariance: A Practical Guide to Measurement and Data Analysis, 1st Edition. Springer, Dordrecht, The Netherlands.

Baldocchi, D. D., 2003. Assessing the eddy covariance technique for evaluating carbon dioxide exchange rates of ecosystems: past, present and future. Global Change Biology 9 (4), 479–492.

Barclay, H. J., 1998. Conversion of total leaf area to projected leaf area in lodgepole pine and douglas-fir. Tree Physiology 18 (3), 185–193.

Bastin, L., Cornford, D., Jones, R., Heuvelink, G. B. M., Pebesma, E., Stasch, C., Nativi, S., Mazzetti, P., Williams, M., 2013. Managing uncertainty in integrated environmental modelling: The UncertWeb framework. Environmental Modelling & Software 39, 116–134.

Beer, C., Reichstein, M., Tomelleri, E., Ciais, P., Jung, M., Carvalhais, N., Rdenbeck, C., Arain, M. A., Baldocchi, D., Bonan, G. B., Bondeau, A., Cescatti, A., Lasslop, G., Lindroth, A., Lomas, M., Luyssaert, S., Margolis, H., Oleson, K. W., Roupsard, O., Veenendaal, E., Viovy, N., Williams, C., Woodward, F. I., Papale, D., 2010. Terrestrial gross carbon dioxide uptake: Global distribution and covariation with climate. Science 329 (5993), 834–838.

Blackman, F. F., 1905. Optima and limiting factors. Annals of Botany 19 (2), 281–296.

Bonan, G. B., Levis, S., Kergoat, L., Oleson, K. W., 2002. Landscapes as patches of plant functional types: An integrating concept for climate and ecosystem models. Global Biogeochemical Cycles 16 (2), 5–1–5–23.

Bond-Lamberty, B., Gower, S. T., Ahl, D. E., Thornton, P. E., 2005. Reimplementation of the BIOME-BGC model to simulate successional change. Tree Physiology 25 (4), 413–424.

Braakhekke, M. C., Wutzler, T., Beer, C., Kattge, J., Schrumpf, M., Ahrens, B., Schöning, I., Hoosbeek, M. R., Kruijt, B., Kabat, P., Reichstein, M., 2013. Modeling the vertical soil organic matter profile using Bayesian parameter estimation. Biogeosciences 10 (1), 399–420.

Brooks, S. P., Gelman, A., 1998. General methods for monitoring convergence of iterative simulations. Journal of Computational and Graphical Statistics 7 (4), 434–455.

Bulmer, M. G., 1979. Principles of statistics. Dover Publications, New York, USA.

Campolongo, F., Cariboni, J., Saltelli, A., 2007. An effective screening design for sensitivity analysis of large models. Environmental Modelling & Software 22 (10), 1509–1518.

Canadell, J. G., Kirschbaum, M. U. F., Kurz, W. A., Sanz, M.-J., Schlamadinger, B., Yamagata, Y., 2007. Factoring out natural and indirect human effects on terrestrial carbon sources and sinks. Environmental Science & Policy 10 (4), 370–384.

Cannell, M. G. R., Thornley, J. H. M., 1998. Temperature and CO_2 responses of leaf and canopy photosynthesis: a clarification using the non-rectangular hyperbola model of photosynthesis. Annals of Botany 82 (6), 883–892.

Chiesi, M., Chirici, G., Marchetti, M., Hasenauer, H., Moreno, A., Knohl, A., Matteucci, G., Pilegaard, K., Granier, A., Longdoz, B., Maselli, F., 2016. Testing the applicability of BIOME-BGC to simulate beech gross primary production in Europe using a new continental weather dataset. Annals of Forest Science 73 (3), 713–727.

Chiesi, M., Maselli, F., Moriondo, M., Fibbi, L., Bindi, M., Running, S. W., 2007. Application of BIOME-BGC to simulate Mediterranean forest processes. Ecological Modelling 206 (1-2), 179–190.

Churkina, G., Running, S. W., 1998. Contrasting climatic controls on the estimated productivity of global terrestrial biomes. Ecosystems 1 (2), 206–215.

Cienciala, E., Tatarinov, F. A., 2006. Application of BIOME-BGC model to managed forests: 2. Comparison with long-term observations of stand production for major tree species. Forest Ecology and Management 237 (1-3), 252–266.

Cole, D., Rapp., M., 1981. Elemental cycling in forest ecosystems. In: Reichle, D. (Ed.), Dynamic properties of forest ecosystems. Vol. 23. Cambridge University Press, USA, pp. 341–409.

Cole, D. W., Gessel, S. P., Dice, S., 1981. Productivity of forest ecosystems studied during the IBP: the woodlands data set. In: Reichle, D. E. (Ed.), Dynamics Properties of Forest Ecosystems. Cambridge University Press, Cambridge, pp. 567–672.

Cole, D. W., Gessel, S. P., Dice, S. F., 1968. Distribution and cycling of nitrogen, phosphorus, potassium and calcium in a second-growth Douglas fir ecosystem. In: Young, H. (Ed.), Primary productivity and mineral

cycling in natural ecosystems. University of Maine Press, Orono, ME, pp. 197–232.

Constable, J. V. H., Friend, A. L., 2000. Suitability of process-based tree growth models for addressing tree response to climate change. Environmental Pollution 110 (1), 47–59.

Cregg, B. M., 1994. Carbon allocation, gas-exchange, and needle morphology of *Pinus ponderosa* genotypes known to differ in growth and survival under imposed drought. Tree Physiology 14, 883–898.

Davidson, E. A., Janssens, I. A., Luo, Y., 2006. On the variability of respiration in terrestrial ecosystems: moving beyond Q10. Global Change Biology 12 (2), 154–164.

Deblonde, G., Penner, M., Royer, A., 1994. Measuring leaf-area index with the LICOR LAI 2000 in pine stands. Ecology 75 (5), 1507–1511.

Dekker, S. C., 2000. Modelling and monitoring forest evapotranspiration. Behaviour, concepts and parameters. Ph.D. thesis, Institute for Biodiversity and Ecosystem Dynamics, University of Amsterdam, The Netherlands.

Desai, A. R., Richardson, A. D., Moffat, A. M., Kattge, J., Hollinger, D. Y., Barr, A., Falge, E., Noormets, A., Papale, D., Reichstein, M., Stauch, V. J., 2008. Cross-site evaluation of eddy covariance GPP and RE decomposition techniques. Agricultural and Forest Meteorology 148 (6–7), 821–838.

Dice, S., 1970. The biomass and nutrient flux in a second growth Douglas fir ecosystem. Ph.D. thesis, University of Washington, Seattle, WA.

Domec, J.-C., Lachenbruch, B., Pruyn, M. L., Spicer, R., 2012. Effects of age-related increases in sapwood area, leaf area, and xylem conductivity on height-related hydraulic costs in two contrasting coniferous species. Annals of Forest Science 69 (1), 17–27.

Drew, A. P., Running, S. W., 1975. Comparison of two techniques for measuring surface area of conifer needles. Forest Science 21 (3), 231–232.

Du, Z., Nie, Y., He, Y., Yu, G., Wang, H., Zhou, X., 2015. Complementarity of flux-and biometric-based data to constrain parameters in a terrestrial carbon model. Tellus B 67.

Dumont, B., Leemans, V., Mansouri, M., Bodson, B., Destain, J. P., Destain, M. F., 2014. Parameter identification of the STICS crop model, using an accelerated formal MCMC approach. Environmental Modelling & Software 52, 121–135.

Duyzer, J. H., Dorsey, J. R., Gallagher, M. W., Pilegaard, K., Walton, S., 2004. Oxidized nitrogen and ozone interaction with forests. II: Multi-layer process-oriented modelling results and a sensitivity study for Douglas fir. Quarterly Journal of the Royal Meteorological Society 130 (600), 1957–1971.

Edmonds, R. L., 1987. Decomposition rates and nutrient dynamics in small-diameter woody litter in four forest ecosystems in Washington, U.S.A. Canadian Journal of Forest Research 17 (6), 499–509.

Farquhar, G. D., von Caemmerer, S., Berry, J. A., 1980. A biochemical model of photosynthetic CO_2 assimilation in leaves of C_3 species. Planta 149 (1), 78–90.

Fassnacht, K. S., Gower, S. T., Norman, J. M., McMurtrie, R. E., 1994. A comparison of optical and direct methods for estimating foliage surface area index in forests. Agricultural and Forest Meteorology 71, 183–207.

Fogel, R., 1983. Root turnover and productivity of coniferous forests. Plant and Soil 71, 75–85.

Foken, T., Göckede, M., Mauder, M., Mahrt, L., Amiro, B., Munger, W., 2005. Post-field data quality control. In: Lee, X., Massman, W., Law, B. (Eds.), Handbook of Micrometeorology. Vol. 29 of Atmospheric and Oceanographic Sciences Library. Springer, Dordrecht, The Netherlands, Ch. 9, pp. 181–208.

Fujimori, T., Kawanabe, S., Saito, H., Grier, C. C., Shidei, T., 1976. Biomass and primary production in forests of three major vegetation zones of the northwestern United States. Journal of the Japanese Forestry Society 58 (10), 360–373.

Gelfand, A. E., Smith, A. F. M., 1990. Sampling-based approaches to calculating marginal densities. Journal of the American Statistical Association 85 (410), 398–409.

Gelman, A., Carlin, J. B., Stern, H. S., Dunson, D. B., Vehtari, A., Rubin, D. B., 2013. Bayesian Data Analysis, 3rd Edition. CRC press, Boca Raton.

Gelman, A., Rubin, D. B., 1992. Inference from iterative simulation using multiple sequences. Statistical Science 7 (4), 457–511.

Gholz, H. L., 1982. Environmental limits on aboveground net primary production. Leaf area, and biomass in vegetation zones of the Pacific Northwest. Ecology 63 (2), 469–481.

Gholz, H. L., Fitz, F. K., Waring, R., 1976. Leaf area differences associated with old-growth forest communities in the western Oregon Cascades. Canadian Journal of Forest Research 6 (1), 49–57.

Gholz, H. L., Grier, C. C., Campbell, A. G., Brown, A. T., 1979. Equations for estimating biomass and leaf area of plants in the Pacific Northwest. Tech. rep., Oregon State University, Corvallis.

Gilmanov, T. G., Aires, L., Barcza, Z., Baron, V. S., Belelli, L., Beringer, J., Billesbach, D., Bonal, D., Bradford, J., Ceschia, E., Cook, D., Corradi, C., Frank, A., Gianelle, D., Gimeno, C., Gruenwald, T., Guo, H., Hanan, N., Haszpra, L., Heilman, J., Jacobs, A., Jones, M. B., Johnson, D. A., Kiely, G., Li, S., Magliulo, V., Moors, E., Nagy, Z., Nasyrov, M., Owensby, C., Pinter, K., Pio, C., Reichstein, M., Sanz, M. J., Scott, R., Soussana, J. F., Stoy, P. C., Svejcar, T., Tuba, Z., Zhou, G., 2010. Productivity, respiration, and light-response parameters of World grassland and agroecosystems derived from flux-tower measurements. Rangeland Ecology & Management 63 (1), 16–39.

Gilmanov, T. G., Verma, S. B., Sims, P. L., Meyers, T. P., Bradford, J. A., Burba, G. G., Suyker, A. E., 2003. Gross primary production and light response parameters of four Southern Plains ecosystems estimated using long-term CO_2-flux tower measurements. Global Biogeochemical Cycles 17 (2), 1071.

Gilmanov, T. G., Wylie, B. K., Tieszen, L. L., Meyers, T. P., Baron, V. S., Bernacchi, C. J., Billesbach, D. P., Burba, G. G., Fischer, M. L., Glenn, A. J., Hanan, N. P., Hatfield, J. L., Heuer, M. W., Hollinger, S. E., Howard, D. M., Matamala, R., Prueger, J. H., Tenuta, M., Young, D. G., 2013. CO_2 uptake and ecophysiological parameters of the grain crops of midcontinent North America: Estimates from flux tower measurements. Agriculture, Ecosystems & Environment 164, 162–175.

Goulden, M. L., Munger, J. W., Fan, S.-M., Daube, B. C., Wofsy, S. C., 1996. Measurements of carbon sequestration by long-term eddy covariance: methods and a critical evaluation of accuracy. Global Change Biology 2 (3), 169–182.

Gower, S. T., Vogt, K. A., Grier, C. C., 1992. Carbon dynamics of Rocky Mountain Douglas-fir: Influence of water and nutrient availability. Ecological Monographs 62 (1), 43–65.

Grier, C., Cole, D., Dyrness, C., Fredriksen, R., 1974. Nutrient cycling in 37- and 450-year-old Douglas-fir ecosystems. Tech. rep., Integrated Research in the Coniferous Forest Biome, University of Washington, Seattle.

Grier, C. C., Logan, R. S., 1977. Old-growth *Pseudotsuga menziesii* communities of a Western Oregon watershed: Biomass distribution and production budgets. Ecological Monographs 47 (4), 373–400.

Hagen, S. C., Braswell, B. H., Linder, E., Frolking, S., Richardson, A. D., Hollinger, D. Y., 2006. Statistical uncertainty of eddy fluxbased estimates of gross ecosystem carbon exchange at Howland Forest, Maine. Journal of Geophysical Research: Atmospheres 111 (D8), D08S03.

Hamm, N. A. S., Atkinson, P. M., Milton, E. J., 2012. A per-pixel, non-stationary mixed model for empirical line atmospheric correction in remote sensing. Remote Sensing of Environment 124, 666–678.

Hamm, N. A. S., Finley, A. O., Schaap, M., Stein, A., 2015a. A spatially varying coefficient model for mapping air quality at the European scale. Atmospheric Environment 102, 393–405.

Hamm, N. A. S., Hall, J. W., Anderson, M. G., 2006. Variance-based sensitivity analysis of the probability of hydrologically induced slope instability. Computers & Geosciences 32 (6), 803–817.

Hamm, N. A. S., Soares Magalhães, R. J., Clements, A. C. A., 2015b. Earth observation, spatial data quality and neglected tropical diseases. PLoS Neglected Tropical Diseases 9 (12), e0004164.

Harmon, M. E., Baker, G. A., Spycher, G., Greene, S. E., 1990. Leaf-litter decomposition in the *Picea/Tsuga* forests of Olympic National Park, Washington, U.S.A. Forest Ecology and Management 31, 55–66.

Hartig, F., Dyke, J., Hickler, T., Higgins, S. I., O'Hara, R. B., Scheiter, S., Huth, A., 2012. Connecting dynamic vegetation models to data – an inverse perspective. Journal of Biogeography 39 (12), 2240–2252.

Hastings, W. K., 1970. Monte Carlo sampling methods using Markov chains and their applications. Biometrika 57 (1), 97–109.

He, H., Liu, M., Xiao, X., Ren, X., Zhang, L., Sun, X., Yang, Y., Li, Y., Zhao, L., Shi, P., Du, M., Ma, Y., Ma, M., Zhang, Y., Yu, G., 2014. Large-scale estimation and uncertainty analysis of gross primary production in Tibetan alpine grasslands. Journal of Geophysical Research: Biogeosciences 119 (3), 466–486.

Hessl, A. E., Milesi, C., White, M. A., Peterson, D. L., Keane, R. E., 2004. Ecophysiological parameters for Pacefic Northwest trees. Tech. rep., United States Department of Agriculture, Forest Service, Pacific Northwest Research Station, Portland.

Hlásny, T., Barcza, Z., Barka, I., Merganičová, K., Sedmák, R., Kern, A., Pajtík, J., Balázs, B., Fabrika, M., Churkina, G., 2014. Future carbon cycle in mountain spruce forests of Central Europe: Modelling framework and ecological inferences. Forest Ecology and Management 328, 55–68.

Hobbie, S. E., Oleksyn, J., Eissenstat, D. M., Reich, P. B., 2010. Fine root decomposition rates do not mirror those of leaf litter among temperate tree species. Oecologia 162 (2), 505–513.

Homma, T., Saltelli, A., 1996. Importance measures in global sensitivity analysis of nonlinear models. Reliability Engineering & System Safety 52 (1), 1–17.

Houborg, R., Cescatti, A., Migliavacca, M., 2012. Constraining model simulations of GPP using satellite retrieved leaf chlorophyll. In: IEEE International Geoscience and Remote Sensing Symposium (IGARSS). IEEE, pp. 6455–6458.

Houborg, R., Cescatti, A., Migliavacca, M., Kustas, W. P., 2013. Satellite retrievals of leaf chlorophyll and photosynthetic capacity for improved modeling of GPP. Agricultural and Forest Meteorology 177, 10–23.

Ichii, K., Hashimoto, H., Nemani, R., White, M., 2005. Modeling the interannual variability and trends in gross and net primary productivity of tropical forests from 1982 to 1999. Global and Planetary Change 48 (4), 274–286.

Imvitthaya, C., Honda, K., Lertlum, S., Tangtham, N., 2011. Calibration of a biome-biogeochemical cycles model for modeling the net primary production of teak forests through inverse modeling of remotely sensed data. Journal of Applied Remote Sensing 5 (1), 053516–053516.

IPCC, 2013. Summary for policymakers. In: Stocker, T. F., Qin, D., Plattner, G. K., Tignor, M., Allen, S. K., Boschung, J., Nauels, A., Xia, Y., Bex, V., Midgley, P. M. (Eds.), Climate Change 2013: The Physical Science Basis. Contribution of Working Group I to the Fifth Assessment Report of the Intergovernmental Panel on Climate Change. Cambridge University Press, Cambridge, United Kingdom and New York, NY, USA., pp. 1–27.

Johnson, I. R., 2013. PlantMod: exploring the physiology of plant canopies. IMJ Software, Melbourne, Australia.

Johnson, I. R., Thornley, J. H. M., Frantz, J. M., Bugbee, B., 2010. A model of canopy photosynthesis incorporating protein distribution through the canopy and its acclimation to light, temperature and CO_2. Annals of Botany 106 (5), 735–749.

Jung, M., Verstraete, M., Gobron, N., Reichstein, M., Papale, D., Bondeau, A., Robustelli, M., Pinty, B., 2008. Diagnostic assessment of European gross primary production. Global Change Biology 14 (10), 2349–2364.

Kennedy, M. C., O'Hagan, A., 2001. Bayesian calibration of computer models. Journal of the Royal Statistical Society: Series B (Statistical Methodology) 63 (3), 425–464.

Kennedy, M. C., OHagan, A., 2001b. Supplementary details on bayesian calibration of computer models. Report, University of Sheffield, Sheffield, U.K.

Keyes, M. R., Grier, C. C., 1981. Above- and below-ground net production in 40-year-old Douglas-fir stands on low and high productivity sites. Canadian Journal of Forest Research 11 (3), 599–605.

Klaassen, W., Bosveld, F., de Water, E., 1998. Water storage and evaporation as constituents of rainfall interception. Journal of Hydrology 212 213, 36–50.

Kondo, M., Ichii, K., Ueyama, M., Mizoguchi, Y., Hirata, R., Saigusa, N., 2013. The role of carbon flux and biometric observations in constraining a terrestrial ecosystem model: a case study in disturbed forests in East Asia. Ecological Research 28 (5), 893–905.

Körner, C., 1995. Leaf diffusive conductances in the major vegetation types of the Globe. In: Schulze, E. D., Caldwell, M. M. (Eds.), Ecophysiology of Photosynthesis. Vol. 100 of Springer Study Edition. Springer-Verlag, New York, Ch. 22, pp. 463–490.

Landsberg, J. J., Waring, R. H., 1997. A generalised model of forest productivity using simplified concepts of radiation-use efficiency, carbon balance and partitioning. Forest Ecology and Management 95 (3), 209–228.

Lasslop, G., Reichstein, M., Papale, D., Richardson, A. D., Arneth, A., Barr, A., Stoy, P., Wohlfahrt, G., 2010. Separation of net ecosystem exchange into assimilation and respiration using a light response curve approach: critical issues and global evaluation. Global Change Biology 16 (1), 187–208.

Lewis, J. D., McKane, R. B., Tingey, D. T., Beedlow, P. A., 2000. Vertical gradients in photosynthetic light response within an old-growth Douglas-fir and western hemlock canopy. Tree Physiology 20 (7), 447–456.

Li, X., Liang, S., Yu, G., Yuan, W., Cheng, X., Xia, J., Zhao, T., Feng, J., Ma, Z., Ma, M., Liu, S., Chen, J., Shao, C., Li, S., Zhang, X., Zhang, Z., Chen, S., Ohta, T., Varlagin, A., Miyata, A., Takagi, K., Saiqusa, N., Kato, T., 2013. Estimation of gross primary production over the terrestrial ecosystems in China. Ecological Modelling 261:262, 80–92.

Long, S. P., Zhu, X.-G., Naidu, S. L., Ort, D. R., 2006. Can improvement in photosynthesis increase crop yields? Plant, Cell & Environment 29 (3), 315–330.

Lunn, D., Jackson, C., Best, N., Thomas, A., Spiegelhalter, D., 2013. The BUGS Book - A Practical Introduction to Bayesian Analysis. CRC Press, Boca Raton.

Lunn, D., Thomas, A., Best, N., Spiegelhalter, D., 2000. WinBUGS - A Bayesian modelling framework: Concepts, structure, and extensibility. Statistics and Computing 10 (4), 325–337.

Luyssaert, S., Inglima, I., Jung, M., Richardson, A. D., Reichstein, M., Papale, D., Piao, S. L., Schulze, E. D., Wingate, L., Matteucci, G., Aragao, L., Aubinet, M., Beer, C., Bernhofer, C., Black, K. G., Bonal, D., Bonnefond, J. M., Chambers, J., Ciais, P., Cook, B., Davis, K. J., Dolman, A. J., Gielen, B., Goulden, M., Grace, J., Granier, A., Grelle, A., Griffis, T., GrNwald, T., Guidolotti, G., Hanson, P. J., Harding, R., Hollinger, D. Y., Hutyra, L. R., Kolari, P., Kruijt, B., Kutsch, W., Lagergren, F., Laurila, T., Law, B. E., Le Maire, G., Lindroth, A., Loustau, D., Malhi, Y., Mateus, J., Migliavacca, M., Misson, L., Montagnani, L., Moncrieff, J., Moors, E., Munger, J. W., Nikinmaa, E., Ollinger, S. V., Pita, G., Rebmann, C., Roupsard, O., Saigusa, N., Sanz, M. J., Seufert, G., Sierra, C., Smith, M. L., Tang, J., Valentini, R., Vesala, T., Janssens, I. A., 2007. CO_2 balance of boreal, temperate, and tropical forests derived from a global database. Global Change Biology 13 (12), 2509–2537.

Mahecha, M. D., Reichstein, M., Carvalhais, N., Lasslop, G., Lange, H., Seneviratne, S. I., Vargas, R., Ammann, C., Arain, M. A., Cescatti, A., Janssens, I. A., Migliavacca, M., Montagnani, L., Richardson, A. D., 2010. Global convergence in the temperature sensitivity of respiration at ecosystem level. Science 329, 838–840.

Mäkelä, A., Landsberg, J., Ek, A. R., Burk, T. E., Ter-Mikaelian, M., Ägren, G. I., Oliver, C. D., Puttonen, P., 2000. Process-based models for forest ecosystem management: current state of the art and challenges for practical implementation. Tree Physiology 20 (5–6), 289–298.

Marcelis, D., 2011. Satellite-Born Monitoring of Gross Primary Productivity: In a Temperate Coniferous Forest by using MODIS Data and the Photochemical Reflectance Index. LAMBERT Academic Publishing, Germany.

Maselli, F., Chiesi, M., Fibbi, L., Moriondo, M., 2008. Integration of remote sensing and ecosystem modelling techniques to estimate forest net carbon uptake. International Journal of Remote Sensing 29 (8), 2437–2443.

McNaughton, K. G., Jarvis, P. G., 1983. Predicting effects of vegetation changes on transpiration and evaporation. Water deficits and plant growth 7, 1–47.

Meinzer, F., 1982. The effect of vapor pressure on stomatal control of gas exchange in Douglas fir (*Pseudotsuga menziesii*) saplings. Oecologia 54 (2), 236–242.

Metropolis, N., Rosenbluth, A. W., Rosenbluth, M. N., Teller, A. H., Teller, E., 1953. Equation of state calculations by fast computing machines. The Journal of Chemical Physics 21 (6), 1087–1092.

Minet, J., Laloy, E., Tychon, B., Franois, L., 2015. Bayesian inversions of a dynamic vegetation model at four European grassland sites. Biogeosciences 12 (9), 2809–2829.

Minunno, F., van Oijen, M., Cameron, D. R., Pereira, J. S., 2013. Selecting parameters for Bayesian calibration of a process-based model: A methodology based on canonical correlation analysis. SIAM/ASA Journal on Uncertainty Quantification 1 (1), 370–385.

Mohren, G. M. J., 1987. Simulation of forest growth, applied to Douglas fir stands in the Netherlands. Ph.D. thesis, Wageningen Agriculture university, The Netherlands.

Mohren, G. M. J., van de Veen, J. R., 1995. Forest growth in relation to site conditions. Application of the model FORGRO to the Solling spruce site. Ecological Modelling 83 (1), 173–183.

Moncrieff, J. B., Malhi, Y., Leuning, R., 1996. The propagation of errors in long-term measurements of land-atmosphere fluxes of carbon and water. Global Change Biology 2 (3), 231–240.

Monteith, J. L., Unsworth, M. H., 1990. Principles of Environmental Physics, 2nd Edition. Edward Arnold, Sevenoaks, UK.

Monteith, J. L., Unsworth, M. H., 2008. Principles of Environmental Physics, 3rd Edition. Academic Press, Burlington, Massachusetts.

Morris, M. D., 1991. Factorial sampling plans for preliminary computational experiments. Technometrics 33 (2), 161–174.

Mummery, D., Battaglia, M., 2004. Significance of rainfall distribution in predicting eucalypt plantation growth, management options, and risk assessment using the process-based model CABALA. Forest Ecology and Management 193 (1-2), 283–296.

Mustafa, Y., 2012. Improving forest growth estimation : Bayesian networks for integrating satellite images and process-based forest growth models. Ph.D. thesis, University of Twente, The Netherlands.

Nash, J. E., Sutcliffe, J. V., 1970. River flow forecasting through conceptual models part i A discussion of principles. Journal of hydrology 10 (3), 282–290.

Nobel, P. S., 2009. Physicochemical and Environmental Plant Physiology, 4th Edition. Academic Press, Canada.

Oakley, J., 2002. Eliciting Gaussian process priors for complex computer codes. Journal of the Royal Statistical Society: Series D 51 (1), 81–97.

Oakley, J. E., O'Hagan, A., 2007. Uncertainty in prior elicitations: a non-parametric approach. Biometrika 94 (2), 427–441.

Odongo, V., Hamm, N., Milton, E., 2014. Spatio-temporal assessment of Tuz Gölü, Turkey as a potential radiometric vicarious calibration site. Remote Sensing 6 (3), 2494–2513.

Odongo, V. O., Onyando, J. O., Mutua, B. M., van Oel, P. R., Becht, R., 2013. Sensitivity analysis and calibration of the modified universal soil loss equation (MUSLE) for the upper Malewa catchment, Kenya. International Journal of Sediment Research 28 (3), 368–383.

Ogren, E., 1993. Convexity of the photosynthetic light-response curve in relation to intensity and direction of light during growth. Plant Physiology 101 (3), 1013–1019.

Olszyk, D. M., Johnson, M. G., Tingey, D. T., Rygiewicz, P. T., Wise, C., VanEss, E., Benson, A., Storm, M. J., King, R., 2003. Whole-seedling biomass allocation, leaf area, and tissue chemistry for Douglas-fir exposed to elevated CO_2 and temperature for 4 years. Canadian Journal of Forest Research 33 (2), 269–278.

Panshin, A. J., Zeeuw, C. d., Brown, H. P., 1964. Textbook of Wood Technology, 2nd Edition. McGraw-Hill, New York.

Peng, C., Liu, J., Dang, Q., Apps, M. J., Jiang, H., 2002. TRIPLEX: a generic hybrid model for predicting forest growth and carbon and nitrogen dynamics. Ecological Modelling 153 (1-2), 109–130.

Plummer, M., Best, N., Cowles, K., Vines, K., Sarkar, D., Bates, D., Almond, R., 2015. Package coda. Accessed January 25, 2015.
URL `http://cran.r-project.org/web/packages/coda/coda.pdf`

Portillo-Estrada, M., Korhonen, J. F. J., Pihlatie, M., Pumpanen, J., Frumau, A. K. F., Morillas, L., Tosens, T., Niinemets, U., 2013. Inter- and intra-annual variations in canopy fine litterfall and carbon and nitrogen inputs to the forest floor in two European coniferous forests. Annals of Forest Science 70 (4), 367–379.

Potter, C. S., Randerson, J. T., Field, C. B., Matson, P. A., Vitousek, P. M., Mooney, H. A., Klooster, S. A., 1993. Terrestrial ecosystem production: A process model based on global satellite and surface data. Global Biogeochemical Cycles 7 (4), 811–841.

R Core Team, 2014. R: A Language and Environment for Statistical Computing. R Foundation for Statistical Computing, Vienna, Austria.
URL `http://www.R-project.org/`

Rabinowitch, E. I., 1951. Photosynthesis and related processes. Soil Science 72 (6), 482.

Raj, R., Hamm, N. A. S., van der Tol, C., Stein, A., 2014. Variance-based sensitivity analysis of BIOME-BGC for gross and net primary production. Ecological Modelling 292, 26–36.

Raj, R., Hamm, N. A. S., van der Tol, C., Stein, A., 2016. Uncertainty analysis of gross primary production partitioned from net ecosystem exchange measurements. Biogeosciences 13 (5), 1409–1422.

Reich, P. B., Ellsworth, D. S., Walters, M. B., Vose, J. M., Gresham, C., Volin, J. C., Bowman, W. D., 1999. Generality of leaf trait relationships: A test across six biomes. Ecology 80 (6), 1955–1969.

Reichstein, M., Falge, E., Baldocchi, D., Papale, D., Aubinet, M., Berbigier, P., Bernhofer, C., Buchmann, N., Gilmanov, T., Granier, A., Grünwald, T., Havránková, K., Ilvesniemi, H., Janous, D., Knohl, A., Laurila, T., Lohila, A., Loustau, D., Matteucci, G., Meyers, T., Miglietta, F., Ourcival, J.-M., Pumpanen, J., Rambal, S., Rotenberg, E., Sanz, M., Tenhunen, J., Seufert, G., Vaccari, F., Vesala, T., Yakir, D., Valentini, R., 2005. On the separation of net ecosystem exchange into assimilation and ecosystem respiration: review and improved algorithm. Global Change Biology 11 (9), 1424–1439.

Reinds, G. J., van Oijen, M., Heuvelink, G. B. M., Kros, H., 2008. Bayesian calibration of the VSD soil acidification model using European forest monitoring data. Geoderma 146 (3 - 4), 475–488.

Reyer, C., Lasch, P., Mohren, G. M. J., Sterck, F. J., 2010. Inter-specific competition in mixed forests of Douglas-fir (*Pseudotsuga menziesii*) and common beech (*Fagus sylvatica*) under climate change - a model-based analysis. Annals of Forest Science 67 (8), 805–805.

Ricciuto, D. M., Davis, K. J., Keller, K., 2008. A bayesian calibration of a simple carbon cycle model: The role of observations in estimating and reducing uncertainty. Global Biogeochemical Cycles 22 (2), GB2030.

Richards, K. R., Stokes, C., 2004. A review of forest carbon sequestration cost studies: A dozen years of research. Climatic Change 63 (1), 1–48.

Richardson, A. D., Braswell, B. H., Hollinger, D. Y., Burman, P., Davidson, E. A., Evans, R. S., Flanagan, L. B., Munger, J. W., Savage, K., Urbanski, S. P., Wofsy, S. C., 2006a. Comparing simple respiration models for eddy flux and dynamic chamber data. Agricultural and Forest Meteorology 141, 219–234.

Richardson, A. D., Hollinger, D. Y., 2005. Statistical modeling of ecosystem respiration using eddy covariance data: Maximum likelihood parameter estimation, and Monte Carlo simulation of model and parameter uncertainty, applied to three simple models. Agricultural and Forest Meteorology 131 (3–4), 191–208.

Richardson, A. D., Hollinger, D. Y., Burba, G. G., Davis, K. J., Flanagan, L. B., Katul, G. G., Munger, J. W., Ricciuto, D. M., Stoy, P. C., Suyker, A. E., Verma, S. B., Wofsy, S. C., 2006b. A multi-site analysis of random error in tower-based measurements of carbon and energy fluxes. Agricultural and Forest Meteorology 136 (1–2), 1–18.

Richardson, A. D., Mahecha, M. D., Falge, E., Kattge, J., Moffat, A. M., Papale, D., Reichstein, M., Stauch, V. J., Braswell, B. H., Churkina, G., Kruijt, B., Hollinger, D. Y., 2008. Statistical properties of random CO_2 flux measurement uncertainty inferred from model residuals. Agricultural and Forest Meteorology 148 (1), 38–50.

Ripullone, F., Grassi, G., Lauteri, M., Borghetti, M., 2003. Photosynthesisnitrogen relationships: interpretation of different patterns between *Pseudotsuga menziesii* and *Populus* × *euroamericana* in a mini-stand experiment. Tree Physiology 23 (2), 137–144.

Ruimy, A., Jarvis, P., Baldocchi, D., Saugier, B., 1995. CO_2 fluxes over plant canopies and solar radiation: A review. Advances in Ecological Research 26, 1–68.

Ruimy, A., Saugier, B., Dedieu, G., 1994. Methodology for the estimation of terrestrial net primary production from remotely sensed data. Journal of Geophysical Research-Atmospheres 99 (D3), 5263–5283.

Running, S. W., 1994. Testing Forest-BGC ecosystem process simulations across a climatic gradient in Oregon. Ecological Applications 4 (2), 238–247.

Running, S. W., Gower, S. T., 1991. Forest-bgc, a general model of forest ecosystem processes for regional applications. ii. dynamic carbon allocation and nitrogen budgets. Tree Physiology 9 (1–2), 147–160.

Running, S. W., Hunt, E. R., 1993. Generalization of a forest ecosystem process model for other biomes, BIOME-BGC, and an application for global-scale models. In: Ehleringer, J. R., Field, C. B. (Eds.), Scaling physiological processes: Leaf to globe. Academic Press, Inc. New York, pp. 141–158.

Running, S. W., Nemani, R. R., Heinsch, F. A., Zhao, M., Reeves, M., Hashimoto, H., 2004. A continuous satellite-derived measure of global terrestrial primary production. BioScience 54 (6), 547–560.

Saltelli, A., Chan, K., Scott, E. M. (Eds.), 2000. Sensitivity Analysis. Wiley, Chichester.

Saltelli, A., Ratto, M., Andres, T., Campolongo, F., Cariboni, J., Gatelli, D., Saisana, M., Tarantola, S., 2008. Global Sensitivity Analysis: The Primer. John Wiley & Sons, Ltd, Chichester.

Santantonio, D., Hermann, K. K., Overton, W. S., 1977. Root biomass studies in forest ecosystems. Pedobiologia 17, 1–31.

Sedjo, R. A., 2001. Forest carbon sequestration: some issues for forest investments. Resources for the Future, Washington, DC, USA, 01-34.

Simpson, D., Butterbach-Bahl, K., Fagerli, H., Kesik, M., Skiba, U., Tang, S., 2006. Deposition and emissions of reactive nitrogen over European forests: A modelling study. Atmospheric Environment 40 (29), 5712–5726.

Skillman, J. B., 2008. Quantum yield variation across the three pathways of photosynthesis: not yet out of the dark. Journal of Experimental Botany 59 (7), 1647–1661.

Sobol', I. M., 1993. Sensitivity analysis for non-linear mathematical models. Mathematical Modelling Computational Experiment 1, 407–414.

Sollins, P., Grier, C. C., McCorison, F. M., Cromack, K., J., Fogel, R., Fredriksen, R. L., 1980. The internal element cycles of an old-growth Douglas-fir ecosystem in Western Oregon. Ecological Monographs 50 (3), 261–285.

Starrfelt, J., Kaste, O., 2014. Bayesian uncertainty assessment of a semi-distributed integrated catchment model of phosphorus transport. Environmental Science: Processes & Impacts 16 (7), 1578–1587.

Stavins, R. N., Richards, K. R., 2005. The cost of U. S. forest-based carbon sequestration. Tech. rep., Pew Center on Global Climate Change, Arlington, VA.

Steingrover, E. G., Jans, W. W. P., 1994. Physiology of forest-grown Douglas r trees: Effect of air pollution and drought. Tech. Rep. 94/3, IBN DLO, Institute for Forestry and Nature Research, Wageningen, the Netherlands.

Stoy, P. C., Katul, G. G., Siqueira, M. B. S., Juang, J.-Y., Novick, K. A., Uebelherr, J. M., Oren, R., 2006. An evaluation of models for partitioning eddy covariance-measured net ecosystem exchange into photosynthesis and respiration. Agricultural and Forest Meteorology 141 (1), 2–18.

Su, Z., Timmermans, W. J., van der Tol, C., Dost, R., Bianchi, R., Gomez, J. A., House, A., Hajnsek, I., Menenti, M., Magliulo, V., Esposito, M., Haarbrink, R., Bosveld, F., Rothe, R., Baltink, H. K., Vekerdy, Z., Sobrino, J. A., Timmermans, J., van Laake, P., Salama, S., van der Kwast, H., Claassen, E., Stolk, A., Jia, L., Moors, E., Hartogensis, O., Gillespie, A., 2009. Eagle 2006- Multi-purpose, multi-angle and multi-sensor in-situ and airborne campaigns over grassland and forest. Hydrology and Earth System Sciences 13 (6), 833–845.

Sun, J., Guan, D., Wu, J., Jing, Y., Yuan, F., Wang, A., Jin, C., 2015. Day and night respiration of three tree species in a temperate forest of northeastern China. iForest - Biogeosciences and Forestry 8 (1), 25–32.

Sutton, M., Reis, S. (Eds.), 2011. The nitrogen cycle and its influence on the European greenhouse gas balance. NERC/Centre for Ecology & Hydrology, Edinburgh, UK, Integrated Project funded under the 6th Framework Programme 2006-2011.

Svensson, M., Jansson, P.-E., Gustafsson, D., Kleja, D. B., Langvall, O., Lindroth, A., 2008. Bayesian calibration of a model describing carbon, water and heat fluxes for a Swedish boreal forest stand. Ecological Modelling 213 (3-4), 331–344.

Swank, W. T., Schreuder, H. T., 1974. Comparison of three methods of estimating surface area and biomass for a forest of young eastern white pine. Forest Science 20 (1), 91–100.

Tatarinov, F. A., Cienciala, E., 2006. Application of BIOME-BGC model to managed forests: 1. Sensitivity analysis. Forest Ecology and Management 237, 267–279.

Teskey, R. O., Saveyn, A., Steppe, K., McGuire, M. A., 2008. Origin, fate and significance of co_2 in tree stems. New Phytologist 177 (1), 17–32.

Thomson, A. M., Csar Izaurralde, R., Smith, S. J., Clarke, L. E., 2008. Integrated estimates of global terrestrial carbon sequestration. Global Environmental Change 18 (1), 192–203.

Thornley, J. H. M., 2002. Instantaneous canopy photosynthesis: Analytical expressions for sun and shade leaves based on exponential light decay down the canopy and an acclimated non-rectangular hyperbola for leaf photosynthesis. Annals of Botany 89 (4), 451–458.

Thornley, J. H. M., Johnson, I. R., 2000. Plant and crop modelling. In: A Mathematical approach to Plant and Crop Physiology. The Blackburn Press, Caldwell, New Jersey.

Thornton, P., 2010. Biome-BGC version 4.2: Theoretical framework of Biome-BGC. Technical Documentation.

Thornton, P. E., 1998. Description of a numerical simulation model for predicting the dynamics of energy, water, carbon, and nitrogen in a terrestrial ecosystem. Ph.D. thesis, University of Montana, Missoula.

Thornton, P. E., Law, B. E., Gholz, H. L., Clark, K. L., Falge, E., Ellsworth, D. S., Goldstein, A. H., Monson, R. K., Hollinger, D., Falk, M., Chen, J., Sparks, J. P., 2002. Modeling and measuring the effects of disturbance history and climate on carbon and water budgets in evergreen needleleaf forests. Agricultural and Forest Meteorology 113, 185–222.

Thornton, P. E., Rosenbloom, N. A., 2005. Ecosystem model spin-up: Estimating steady state conditions in a coupled terrestrial carbon and nitrogen cycle model. Ecological Modelling 189, 25–48.

Tiktak, A., Bouten, W., 1990. Soil hydrological system characterization of the two ACIFORN stands using monitoring data and the soil hydrological model "SWIF". Lab. of Physical Geography and Soil Science, University of Amsterdam, The Netherlands.

Tiktak, A., Bouten, W., 1994. Soil water dynamics and long-term water balances of a Douglas fir stand in the Netherlands. Journal of Hydrology 156, 265–283.

Trusilova, K., Trembath, J., Churkina, G., 2009. Parameter estimation and validation of the terrestrial ecosystem model BIOME-BGC using eddy-covariance flux measurements. Tech. rep., Max Planck Institute for Biogeochemistry, Germany.

Turner, J., 1981. Nutrient cycling in an age sequence of western Washington Douglas-fir stands. Annals of Botany 48 (2), 159–169.

Turner, J., Long, J. N., 1975. Accumulation of organic matter in a series of Douglas-fir stands. Canadian Journal of Forest Research 5 (4), 681–690.

Ueyama, M., Ichii, K., Hirata, R., Takagi, K., Asanuma, J., Machimura, T., Nakai, Y., Ohta, T., Saigusa, N., Takahashi, Y., Hirano, T., 2010. Simulating carbon and water cycles of larch forests in East Asia by the BIOME-BGC model with AsiaFlux data. Biogeosciences 7 (3), 959–977.

van der Tol, C., Verhoef, W., Timmermans, J., Verhoef, A., Su, Z., 2009. An integrated model of soil-canopy spectral radiances, photosynthesis, fluorescence, temperature and energy balance. Biogeosciences 6 (12), 3109–3129.

van Oijen, M., Cameron, D. R., Butterbach-Bahl, K., Farahbakhshazad, N., Jansson, P. E., Kiese, R., Rahn, K. H., Werner, C., Yeluripati, J. B., 2011. A Bayesian framework for model calibration, comparison and analysis: Application to four models for the biogeochemistry of a Norway spruce forest. Agricultural and Forest Meteorology 151 (12), 1609–1621.

van Oijen, M., Reyer, C., Bohn, F. J., Cameron, D. R., Deckmyn, G., Flechsig, M., Hrknen, S., Hartig, F., Huth, A., Kiviste, A., Lasch, P., Mkel, A., Mette, T., Minunno, F., Rammer, W., 2013. Bayesian calibration, comparison and averaging of six forest models, using data from Scots pine stands across Europe. Forest Ecology and Management 289, 255–268.

van Oijen, M., Rougier, J., Smith, R., 2005. Bayesian calibration of process-based forest models: bridging the gap between models and data. Tree Physiology 25 (7), 915–927.

van Oijen, M., Thomson, A., 2010. Toward bayesian uncertainty quantification for forestry models used in the United Kingdom Greenhouse Gas Inventory for land use, land use change, and forestry. Climatic Change 103 (1), 55–67.

van Wijk, M. T., Bouten, W., Verstraten, J. M., 2002. Comparison of different modelling strategies for simulating gas exchange of a Douglas-fir forest. Ecological Modelling 158 (12), 63–81.

van Wijk, M. T., Dekker, S. C., Bouten, W., Bosveld, F. C., Kohsiek, W., Kramer, K., Mohren, G. M. J., 2000. Modeling daily gas exchange of a Douglas-fir forest: comparison of three stomatal conductance models with and without a soil water stress function. Tree Physiology 20 (2), 115–122.

van Wijk, M. T., Dekker, S. C., Bouten, W., Kohsiek, W., Mohren, G. M. J., 2001. Simulation of carbon and water budgets of a Douglas-fir forest. Forest Ecology and Management 145 (3), 229–241.

Verma, M., Friedl, M. A., Richardson, A. D., Kiely, G., Cescatti, A., Law, B. E., Wohlfahrt, G., Gielen, B., Roupsard, O., Moors, E. J., Toscano, P., Vaccari, F. P., Gianelle, D., Bohrer, G., Varlagin, A., Buchmann, N., van Gorsel, E., Montagnani, L., Propastin, P., 2013. Remote sensing of annual terrestrial gross primary productivity from MODIS: an assessment using the FLUXNET la thuile dataset. Biogeosciences Discuss. 10 (7), 11627–11669.

Vogt, K. A., Vogt, D. J., Gower, S. T., Grier, C. C., 1990. Carbon and nitrogen interactions for forest ecosystems. Proceedings, Above- and Below-ground Interactions in Forest Trees in Acidied Soils. Tech. rep., Air Pollution Research Report Series, No. 32, Environmental Research Programme of the Commission of the European Communities.

Vrugt, J. A., 2016. Markov chain Monte Carlo simulation using the DREAM software package: Theory, concepts, and MATLAB implementation. Environmental Modelling & Software 75, 273–316.

Vrugt, J. A., ter Braak, C. J. F., Clark, M. P., Hyman, J. M., Robinson, B. A., 2008. Treatment of input uncertainty in hydrologic modeling: Doing hydrology backward with Markov chain Monte Carlo simulation. Water Resources Research 44 (12).

Vrugt, J. A., ter Braak, C. J. F., Diks, C. G. H., Robinson, B. A., Hyman, J. M., Higdon, D., 2009. Accelerating Markov chain Monte Carlo simulation by differential evolution with self-adaptive randomized subspace sampling. International Journal of Nonlinear Sciences and Numerical Simulation 10 (3), 273–290.

Wang, H., Jia, G., Fu, C., Feng, J., Zhao, T., Ma, Z., 2010. Deriving maximal light use efficiency from coordinated flux measurements and satellite data for regional gross primary production modeling. Remote Sensing of Environment 114 (10), 2248–2258.

Wang, L., Ibrom, A., Korhonen, J. F. J., Frumau, K. F. A., Wu, J., Pihlatie, M., Schjoerring, J. K., 2013. Interactions between leaf nitrogen status and longevity in relation to N cycling in three contrasting European forest canopies. Biogeosciences 10 (2), 999–1011.

Wang, Y. P., Leuning, R., Cleugh, H. A., Coppin, P. A., 2001. Parameter estimation in surface exchange models using nonlinear inversion: how many parameters can we estimate and which measurements are most useful? Global Change Biology 7 (5), 495–510.

Warren, C. R., Ethier, G. J., Livingston, N. J., Grant, N. J., Turpin, D. H., Harrison, D. L., Black, T. A., 2003. Transfer conductance in second growth Douglas-fir (*Pseudotsuga menziesii* (Mirb.) Franco) canopies. Plant, Cell & Environment 26 (8), 1215–1227.

White, M., Thornton, P., Running, S., Nemani, R., 2000. Parameterization and sensitivity snalysis of the BIOME-BGC terrestrial ecosystem model: Net primary production controls. Earth Interactions 4 (3), 1–85.

Whittaker, R. H., Niering, W. A., 1968. Vegetation of the Santa Catalina Mountains, Arizona: IV. Limestone and acid soils. Journal of Ecology 56 (2), 523–544.

Whittaker, R. H., Niering, W. A., 1975. Vegetation of the Santa Catalina Mountains, Arizona. V. Biomass, production, and diversity along the elevation gradient. Ecology 56 (4), 771–790.

Xenakis, G., Ray, D., Mencuccini, M., 2008. Sensitivity and uncertainty analysis from a coupled 3-PG and soil organic matter decomposition model. Ecological Modelling 219 (1-2), 1–16.

Yan, M., Li, Z., Tian, X., Chen, E., Zhang, W., Guo, Y., Li, C., 2014. Simulation of carbon flux of forest ecosystem by BIOME-BGC and MODIS-PSN models. In: 2014 IEEE Geoscience and Remote Sensing Symposium. pp. 1065–1068.

Biography

Rahul Raj was born on 15th April 1981 in Patna, a capital of state Bihar, India. In 2006, he received his first MSc degree in Physics from Patna University, Patna, India. He received his second MSc degree in Geo-information Science and Earth Observation (specialization - Geoinformatics) in 2009 from International Institute for Geo-Information Science and Earth Observation (ITC), The Netherlands and Indian Institute of Remote Sensing (IIRS), India under a joint MSc program. He subsequently worked at IIRS, India as a research fellow on "National Carbon Project (NCP)", which was initiated as a major integrated project under ISRO (Indian Space Research Organization)-GBP(Geosphere Biosphere Programme) in 2007 with major goals on assessment of carbon pools, fluxes and net carbon balance for terrestrial biosphere in India. He was responsible for measurement and analysis of carbon dioxide flux data, forest and agriculture inventories, and development of programme in R language to generate by-products (e.g., evaporative fraction images, leaf area index map) using RS and GIS data. In the last quarter of 2011, he began to pursue the present PhD research, after receiving the scholarship from Erasmus Mundus, from the Department of Earth Observation Science, Faculty of Geo-Information Science and Earth Observation of the University of Twente, The Netherlands. His research interests include the application of mathematical and statistical approach, such as Bayesian statistics, to understand the prediction uncertainty associated with the process-based simulators and flux tower data. During the PhD research, the research outputs were published in peer reviewed ISI journals, and presented in international conferences. This dissertation is the output of his PhD research.

Author's Publications

Published ISI Journal Articles

Raj, R., Hamm, N.A.S., and Kant, Y., 2013. Analyzing the effect of different aggregation approaches on remotely sensed data. International Journal of Remote Sensing, 34 (14), 4900-4916.

Raj, R., Hamm, N. A. S., van der Tol, C., Stein, A., 2014. Variance-based sensitivity analysis of BIOME-BGC for gross and net primary production. Ecological Modelling 292, 26-36.

Timmermans, W., Van der Tol, C., Timmermans, J., Ucer, M., Chen, X., Alonso, L., Moreno, J., Carrara, A., Lopez, R., de la Cruz Tercero, F., Corcoles, H., de Miguel, E., Sanchez, J.G., Prez, I., Franch, B., Munoz, J.-C., Skokovic, D., Sobrino, J., Soria, G., MacArthur, A., Vescovo, L., Reusen, I., Andreu, A., Burkart, A., Cilia, C., Contreras, S., Corbari, C., Calleja, J., Guzinski, R., Hellmann, C., Herrmann, I., Kerr, G., Lazar, A.-L., Leutner, B., Mendiguren, G., Nasilowska, S., Nieto, H., Pachego-Labrador, J., Pulanekar, S., **Raj, R.**, Schikling, A., Siegmann, B., von Bueren, S., Su, Z., 2014. An overview of the regional experiments for land-atmosphere exchanges 2012 (REFLEX 2012) campaign. Acta Geophysica, 1-20.

Raj, R., Hamm, N. A. S., van der Tol, C., Stein, A., 2016. Uncertainty analysis of gross primary production partitioned from net ecosystem exchange measurements. Biogeosciences 13 (5), 1409-1422.

Article under review

Raj, R., Hamm, N. A. S., van der Tol, C., Stein, A., Bayesian integration of flux tower data into process-based simulator for quantifying uncertainty in simulated output. Geoscientific Model Development Discussions, 1-32, doi:10.5194/gmd-2016-216.

Conference presentations

Raj, R., Hamm, N.A.S., van der Tol, C., and Stein, A. (2013) Variance-based sensitivity analysis of BIOME-BGC for gross primary production: poster. Presented at European Space Agency Living Planet Symposium, 9-13 September, 2013, Edinburgh, United Kingdom.

Raj, R., Hamm, N.A.S., van der Tol, C., and Stein, A. (2015) Uncertainty analysis of GPP separated from NEE measurements at Speulderbos forest, The Netherlands: poster. Presented at European Geosciences Union general assembly, 12-17 April, 2015, Vienna, Austria.

ITC dissertations

A complete list of ITC dissertations is online on the ITC website:

https://www.itc.nl/Pub/research_programme/Research-review-and-output/PhD-Graduates

This dissertation has number 293.

ITC

UNIVERSITY OF TWENTE.

ISBN 978-90-365-4235-7
DOI 10.3990/1.9789036542357
Dissertation number: 293